PARACELLULAR EPITHELIAL TRANSPORT MAXIMIZES ENERGY EFFICIENCY IN THE KIDNEY

By

Lei Pei

Submitted to the graduate degree program in Molecular and Integrative Physiology and the Graduate Faculty of the University of Kansas in partial fulfillment of the requirements for the degree of Doctor of Philosophy

Date Defended: June 9th 2016

The Dissertation Committee for Lei Pei certifies that this is the approved version of the following dissertation:

PARACELLULAR EPITHELIAL TRANSPORT MAXIMIZES ENERGY EFFICIENCY IN THE KIDNEY

_____

Alan S. L. Yu, M.B., B.Chir, Chair

Date approved: June 14th 2016

Abstract

Claudins are tight junction transmembrane proteins that act as paracellular ion channels. The proximal renal tubule reabsorbs 70% of glomerulus-filtered Na^+. Of this Na^+, up to 1/3 is reabsorbed passively via the paracellular pathway. Claudin-2 has been shown to mediate paracellular sodium reabsorption in the proximal tubule of the kidney. Claudin-2 null mice are reported to have markedly decreased proximal tubule Na^+, Cl^- and fluid reabsorption, but they have no apparent disturbance in overall Na^+ balance.

We investigated whether we can uncover the salt-wasting phenotype of claudin-2 knockout mice by challenging them with Na^+ depletion. Even during profound dietary sodium depletion, claudin-2 null mice demonstrated the ability to conserve sodium to the same extent as wild-type mice. We investigated how the Na^+ wasted from the proximal tubule was compensated in other segments of the renal tubule. We performed immunoblot on transcellular Na^+ transporters Na-H antiporter 3, Na-K-2Cl cotransporter, NaCl cotransporter and epithelial Na^+ channel. We found no upregulation of the protein abundance of any of these transcellular transporters. To test whether there was functional upregulation of transcellular Na^+ transport distally, diuretic challenge tests were performed. The natriuresis 4 hours after intraperitoneal furosemide (but not after hydrochlorothiazide or benzamil) was 40% higher in claudin-2 null mice than in WT mice, indicating that the site of compensation was the thick ascending limb. We concluded that claudin-2 null mice are able to conserve sodium to the same extent as wild-type mice, even under extreme conditions, due to upregulation of transcellular Na-K-2Cl transport activity in the thick ascending limb of Henle.

We therefore hypothesized that the shifting of sodium transport to transcellular pathways would lead to increased whole kidney oxygen consumption. Indeed we found that the kidneys of claudin-2 null mice have markedly increased oxygen consumption despite normal sodium reabsorption, and consequently have medullary hypoxia. Furthermore, when subjected to bilateral

renal ischemia-reperfusion injury, kidneys of claudin-2 null mice exhibited more severe tubular injury.

In summary, our findings suggest a more important reason for the existence of the paracellular transport pathway, namely that it evolved to enhance the efficiency of energy and oxygen utilization by the renal tubule epithelium. Our research demonstrates that claudin-2 is a key paracellular pathway for passive Na^+ absorption in the proximal tubule that reduces the overall energy expenditure by the kidneys. This dissertation sheds light on a fundamental metabolic process and thereby provides insight on the process that may have broader significance for epithelial tissues.

Acknowledgements

This dissertation would have been impossible without the support of so many people whom I met over these last 5 years, but also people from way before who have inspired me towards a scientific career. I feel generously blessed to have met all these people and be given this opportunity that has shaped me as a person.

Firstly, I would like to take this opportunity and thank Dr. Yu for his belief in my abilities and also supporting me in every possible way, to pursue this dissertation work and to pursue my future career as a physician scientist. Thank you for giving me the chance to grow both personally and professionally.

Secondly, I want to thank all my committee members – Dr. Blanco, Dr. Wallace, Dr. Hagenbuch, and Dr. Rao – for your time and valuable suggestions throughout the duration of this work and for always looking out for the best for me. I sincerely appreciate the time and efforts you have invested in me.

I want to thank all the members in Dr. Yu's Lab who have worked with me: Dr. Jiahua Li, Dr. Min Zhuo, Dr. Madhumitha Rajagopal, Dr. Igor Boulatnikov, Dr. Morten Engelund, Joshua Curry, Patrick McAnulty, Lynn Magenheimer, Kayleigh Peterson, and Ashima Chadha. For their friendship and support throughout. Especially Madhumitha, Kayleigh, Jiahua and Min, for guiding me initially when I was new to the lab and teaching me how to carry out various methods, designing experiments, interpreting results and troubleshooting. I also want to thank Lynn Magenheimer, Joshua Curry, and Patrick McAnulty for helping me managing the mouse colony and assisting me with some of the animal experiments.

I also want to thank our collaborators Dr. William Welch and Dr. Glenn Solis from Georgetown University for performing the oxygen consumption assay and measuring intrarenal oxygen content,

and Dr. Alicia McDonough, Dr. Mien Nguyen and Dr. Nikhil Kamat for performing the immunoblots for the different transporters.

I want to thank Dr. Rao, Sydney Webb, Shixin Tao, Dr. Sally Salah, Dr. Dong Zheng and Dr. Qingqing Wei for the endless discussions and suggestions to help me learn ischemic reperfusion surgery, and Dr. Timothy Fields for helping me with the histological grading of the tubular injury. I want to thank every person in the Kidney Institute for all the support and help at work and outside work.

I want to take this opportunity to thank Dr. Michael Werle and the IGPBS for accepting me into the PhD program. I also want to thank Dr. Lane Christenson, Dr. Michael Wolfe and Dr. Gustavo Blanco for their guidance throughout my PhD journey and making sure that I finish my PhD on time smoothly. Further, I want to acknowledge the Physiology Department for supporting my PhD journey throughout. I want to specially thank the administrative staff in the Integrated Administrative Support Core, Ann Franken and Bobbi Stidham, and in the Physiology Department, Shari Standiferd, for helping me with all the administrative stuff throughout the PhD. I also want to thank the Physiology Society for giving me opportunities to hang out with friends in the Physiology department and discuss about science in a relaxed environment.

I want to thank all my friends at KUMC who have inevitably formed my family here, for their support through my trials and tribulations during this dissertation work, by never making me feel that I am away from home.

Last but not the least, I want to thank my parents for their unconditional love and support; especially my father Xianyi Pei, for inculcating my love for biology and medicine back in my school days and my mother Shihua Cao, for sowing in me the values of sincerity, commitment and hard work. I want to especially thank my husband Michael Schaefer for all the support for in life and

being a great “English Teacher”; and my sister-in-law Kimberley Schaefer, my parents-in-law Paul Schaefer and Mary Schaefer for being an endless source of encouragement and inspiration.

Lei Pei

Table of Contents

List of figures and tables

Chapter I

Chapter II

Chapter III

Chapter IV

Abbreviations

BUN	Blood Urea Nitrogen
GFR	Glomerular filtration rate
GLUT1	Glucose transporter 1
EPO	Erythropoietin
ENaC	Epithelial Na Channel
HIF-1α	Hypoxia induced factor-1 alpha
IP	Intraperitoneal
IRI	Renal ischemia-reperfusion injury
KIM1	Kidney Injury Molecule
MDCKI	Madin–Darby canine kidney type I
MDCKII	Madin–Darby canine kidney type II
MDA	Malondialdehyde
NKCC2	Na-K-Cl cotransporter
NCC	Na-Cl cotransporter
Nrf2	Nuclear factor erythroid 2–related factor 2
pNa/pCl	Na/Cl permeability ratio
PCR	Polymerase chain reaction
PBS	Phosphate-buffered saline

PAH	Para-aminohippuric acid
PNa	Plasma Na^+ concentration
RT-PCR	Reverse transcription polymerase chain reaction
RBF	Renal blood flow
QO_2	Oxygen consumption
TER	Transepithelial resistance
T_{Na}	Na^+ reabsorption
TRF	Transferrin
TALH	Thick ascending limb of Henle
UNa	Na^+ concentration
UNaV	Urine Na^+ excretion
VEGF	Vascular endothelial growth factor

Chapter I Introduction

1.1 Claudins mediate epithelial paracellular transport

1.1.1 Paracellular transport through tight junctions between epithelial cells

Epithelia are sheets of cells that separate body compartments of different compositions and function as physical and chemical barriers. Epithelia have two functions: 1) to protect the tissues underneath from physical trauma, toxins and invasion by pathogens; and 2) to absorb nutrients and excrete waste by transporting molecules through the epithelia (Lommel 2003).

For almost a century, it was believed that epithelial cells were attached to each other by an impermeable seal that was referred to as the "terminal bar." The understanding of how ions selectively cross epithelia originates with Hans Ussing's work. Ussing addressed the question of how sodium ions were moved in a directional fashion across the epithelium of frog skin, resulting in a steady-state electrical potential across the epithelium (Ussing and Zerahn 1951, Koefoed-Johnsen and Ussing 1958). As a first conceptual breakthrough, the "two membrane model" was first used to explain transepithelial transport. This model demonstrated that the apical and basal membrane surfaces had different conductance properties, namely, that Na^+ enters the cell across the apical membrane down its concentration gradient (later shown to occur through Na^+ channels) but was transported in an energy-dependent fashion out the basolateral surface (later shown to occur via the Na^+-K^+-ATPase). When transcellular transport was inhibited, they observed that there was still directional transport of ions through the epithelium. This led to the conclusion that Cl^- ions must be following Na^+ in a passive fashion through the tight junction coupled to the electrical gradient generated by active Na^+ transport (Ussing & Windhager, 1964). This was the beginning of the understanding of how transcellular and paracellular transport are physiologically coupled (**Fig.1.1**).

1.1.2. Claudins in tight junctions regulate paracellular permeability

After measuring permeability and permselectivity of various epithelia from different organs (Crone and Christensen 1981, Powell 1981), it turned out that transepithelial resistance differs by

several orders of magnitude between “tight” and “leaky” epithelia. For example, the transepithelial resistance of the epithelium of the toad urinary bladder is 300,000 Ω•cm^2 compared with the mammalian proximal tubule with only about 6 Ω•cm^2 (Powell 1981, Van Itallie, Rogan et al. 2006). The leakiness of the epithelia is believed to be determined by the tight junctions which are believed to have ionic charge selectivity. The introduction of electron microscopy in the 1950s led to the description of the intercellular junctional complex and the tight junctions (Farquhar and Palade 1963). Shortly thereafter it became apparent (particularly in leaky epithelia) that the so-called "tight" junctions actually constitute a paracellular pathway that exhibits passive permeability to small ions (Whittembury and Rawlins 1971).

Tight junctions form the continuous intercellular barrier between epithelial cells, which is required to separate tissue spaces and regulate selective movement of solutes across the epithelium. The tight junction has a surprisingly complex protein composition compared to other cell junctions and is composed of more than 40 proteins. These proteins that constitute the multi-molecular tight junction complex can be divided into three groups: 1) integral tight junction proteins that bridge the apical intercellular space and form a regulated permeability barrier; 2) tight junction plaque proteins that serve as links between the integral tight junction proteins and the actin cytoskeleton and as adapters for the recruitment of cytosolic molecules that are involved in cell signaling; 3) a variety of cytosolic and nuclear proteins, including regulatory proteins, tumor suppressors, and transcriptional and posttranscriptional factors that interact either directly or indirectly with tight junction plaque proteins to coordinate various functions such as the regulation of paracellular solute permeability, cell proliferation, cell polarity, and tumor suppression (Schneeberger and Lynch 2004). Among these proteins, the claudin family is reportedly critical in regulating paracellular permeability by influencing pore size, electrical resistance, and ion permeability preference. Claudins are encoded by a family of 28 genes in mammals (Mineta, Yamamoto et al. 2011). They range from 20 to 27 kDa and have four transmembrane helices: a short internal amino-terminal sequence (2–6 residues), two extracellular domains (loop 1 is 49–

52 residues and loop 2 is 16–33 residues), and a longer and more variable cytoplasmic tail (21–63 residues) (Suzuki, Nishizawa et al. 2014). Permeability and selectivity are influenced by the number and position of charged amino acid residues on the first extracellular loop of claudins (Colegio, Van Itallie et al. 2002). Amino acid mutations on the first extracellular loop lead to changes in both transepithelial electrical resistance (Uhlen, Oksvold et al. 2010) and charge selectivity (Colegio, Van Itallie et al. 2002).

Knocking out claudins in mice can induce either barrier function or pore function defects. Knocking out claudin-1 (Ladwein, Pape et al. 2005), claudin-5 (Nitta, Hata et al. 2003) or claudin-15 (Tamura, Kitano et al. 2008) caused defects in barrier function of the tight junctions. However, deleting claudin-16 (Himmerkus, Shan et al. 2008) and claudin-19 (Hou, Renigunta et al. 2008) genes led to impaired ion permeability of the renal tubule epithelium.

The majority of claudin family members are expressed in the kidney, and most are localized to renal epithelial cells (Kiuchi-Saishin, Gotoh et al. 2002). The locations of each claudin isoform are diverse. **Figure 1.2** illustrates the distribution of several claudins in a nephron. Claudin-2 is expressed in the proximal tubule and the early thin descending limb (Enck, Berger et al. 2001).

1.2 Renal Proximal Tubules affect the metabolic balance of the human body

1.2.1 Physiological role of renal proximal tubule

Proximal tubules reabsorb all glomerulus-filtered glucose, amino acids and about 60% of Na^+, K^+, and Cl^-. Proximal tubules are important because various serious inherited or acquired kidney disorders such as Fanconi disease, renal tubular acidosis, and phosphate wasting syndromes are associated with the disruption of the function of transporters in proximal tubule cells (Nakhoul and Batuman 2011). Approximately 3% to 7% of hospitalized patients and 25% to 30% of ICU patients develop acute kidney injury. Although all the nephron segments may be injured during acute kidney injury, the most common renal segment susceptible to acute kidney injury from ischemia, sepsis, or other nephrotoxins is the proximal tubule, especially the S3

segment of the proximal tubule located in the outer stripe of the medulla. Understanding the exact mechanism of solute and water transport in proximal tubules can assist in the development of appropriate therapeutics for these inherited and acquired renal diseases.

1.2.2 Paracellular transport is important in handling Na^+, Cl^-, and water in renal proximal tubules.

In early proximal tubules, Na^+ is reabsorbed transcellularly with $HCO3^-$ (Kokko 1973), and isosmotic water reabsorption follows. These phenomena generate a lumen-negative electrical potential across the tubule. Meanwhile, the lumen-to-plasma concentration gradient in late proximal tubules is high in Cl^- and low in $HCO3^-$ as fluid flows down to the later proximal tubule (Bomsztyk 1986). Paracellular tight junctions in the early proximal tubules are permeable to Cl^-. This negative lumen potential drives paracellular Cl^- reabsorption (Andreoli, Schafer et al. 1979). Enhanced Cl^- reabsorption generates a slightly lumen-positive transepithelial potential in mid to late proximal tubules. Thus, Na^+ is reabsorbed in mid-to-late proximal tubules, driven by the positive electrical gradient (Barratt, Rector et al. 1974) (**Fig. 1.3**).

1.2.3 The paracellular permeability of proximal tubules is believed to be determined by claudins in tight junctions

Tight junctions form intercellular barriers that selectively regulate solute movement. Among the various protein components that were discovered in tight junctions, the claudin family plays a key role in regulating paracellular permeability. Permeability and selectivity are influenced by the number and position of charged amino acid residues on the first extracellular loop of claudins (Colegio, Van Itallie et al. 2002, Yamazaki, Okawa et al. 2008).

The claudin isoforms are expressed in various organs in the body, such as the kidneys, the intestines and brain ventricles. The majority of the claudin family members are expressed in the kidney, and most are localized to the renal epithelial cells (Kiuchi-Saishin, Gotoh et al. 2002).

Claudin isoforms have diverse locations. **Figure 1.2** illustrates the distribution of several claudins in a nephron. The pattern of claudin expression in different segments of the renal tubule is important for the particular ion permeability of each tubular segment. For example, *in vitro* studies show that claudin-7, which is expressed in the distal convoluted tubule and the collecting duct, mediates Cl^- permeability (Tatum, Zhang et al. 2007).Claudin-7 knockout mice exhibited renal salt wasting and chronic dehydration (Tatum, Zhang et al. 2010). Claudin-16 and claudin-19 expressed in the thin and thick ascending limb were found to work synergistically to mediate cation permeability (Konrad, Schaller et al. 2006, Angelow, El-Husseini et al. 2007, Hou, Renigunta et al. 2008). It was observed that mutations of claudin-16 and/or claudin-19 in both human and mice resulted in Mg^{2+} and Ca^{2+} wasting (Weber, Schneider et al. 2001, Himmerkus, Shan et al. 2008).

1.3 Investigation of the functional role of claudin-2

1.3.1 Characterization of the function of claudin-2 *in vitro*

The hallmark discovery of claudin-2 function occurred when researchers found that the transepithelial resistance of Madin–Darby canine kidney type I (MDCKI) cells, a high-resistance cell line, when transfected with claudin-2, dropped to the level of Madin–Darby canine kidney type II (MDCKII) cells, a leaky cell line that shares the same components with the MDCKI cell line, except that MDCKII endogenously expresses claudin-2 (Furuse, Furuse et al. 2001). Later studies showed that the transfection of claudin-2 into high-resistance Madin–Darby canine kidney type C7 (MDCK-C7) cells induces paracellular channels with a permeability preference for cations such as K^+ and Na^+ over anions such as Cl^- and Br^-(Amasheh, Meiri et al. 2002); these results indicate that claudin-2 forms leaky and cation-selective pores.

1.3.2 Characterization of the function of claudin-2 *in vivo*

The first claudin-2 null mice were characterized by Muto et al (Muto, Hata et al. 2010). In

isolated perfused proximal tubule S2 segments from these mice, there was a 2.5-fold increase in transepithelial resistance, a decrease in Na^+/Cl^- permeability ratio (pNa/pCl), and a 37% decrease in net Na^+ reabsorption, demonstrating that claudin-2 plays a major role in paracellular Na^+ transport in the proximal tubule (Muto, Hata et al. 2010). Schnermann et al subsequently confirmed that these mice have a 23% reduction in proximal fluid reabsorption (Schnermann, Huang et al. 2013). Although it was predicted that these mice would exhibit urinary NaCl wasting, this was not observed in metabolic balance studies on a normal diet, raising the question of what role, if any, claudin-2 plays in normal physiology.

1.4 Paracellular transport saves energy

Why is paracellular transport necessary for renal transepithelial transport? Can transcellular transport by itself accommodate all solutes and water? These questions led us to consider one key difference between paracellular transport and transcellular transport: the consumption of energy. All transcellular transport processes in nephrons are driven by the potential energy generated by the Na-K-ATPase on the basolateral membrane of renal tubule cells. Each cycle of the pump hydrolyzes 1 ATP molecule while transporting $3Na^+$ out of the cell and $2K^+$ into the cell. Therefore, consumption of 1 ATP molecule can transport $3Na^+$ from the lumen to the blood (Horisberger 2004, Skou 2004). In the 1960s, researchers measured the energy cost of tubular reabsorption in mammals, and the kidney was calculated to reabsorb $25Na^+$ to $29Na^+$ per O_2 molecule consumed(Kiil, Aukland et al. 1961, Torelli, Milla et al. 1966) If we assume that the mitochondria generate 6 ATP molecules from 1 O_2 molecule, the kidney must therefore reabsorb 4 Na^+ to 5 Na^+ per ATP molecule, which is more than 3 Na^+ per 1 ATP molecule that we predicted. One possible reason for the lower-than-expected energy consumption of Na^+ transport is the existence of paracellular transport. A portion of the solute is believed to be transported driven by electrical and chemical gradients created by transcellular transport. The ratio of O_2 consumed per Na^+ reabsorbed reportedly increases during carbonic anhydrase inhibition (Mathisen, Monclair et

al. 1980, Weinstein, Klose et al. 1984). These findings suggest that when HCO_3^- reabsorption was inhibited in the proximal tubule, water was also not reabsorbed. Thus, the concentration gradient for Cl^- could not be generated in the early proximal tubule, and this led to impaired paracellular Cl^- and Na^+ reabsorption. As a result, more Na^+ was reabsorbed through the transcellular pathway and in turn more O_2 was consumed.

Based on this hypothesis, depletion of paracellular transport in the kidney may increase the workload of transcellular transporters. The kidney would consume more energy and consequently more O_2 than normal kidneys. To the best of our knowledge, evidence is lacking on the effect of the direct inhibition of paracellular transport in the proximal tubule on oxygen consumption efficiency. This idea has not been tested yet *in vivo*. Moreover, no study has reported on the extent of effect on total kidney O_2 consumption if the paracellular pathway in the proximal tubule is knocked out and whether it has any physiological significance. Thus, we will explore these issues by studying claudin-2 KO mice. The ability to ablate paracellular Na^+ transport in the proximal tubule by gene targeting of claudin-2 in mice afforded us a unique opportunity to test this directly.

1.5 Significance and purpose of this dissertation

Researchers have found a variety of *in vitro* evidence showing that claudins play a critical role in reabsorption of ions (Coyne, Gambling et al. 2003, Alexandre, Lu et al. 2005, Hou, Renigunta et al. 2008, Amasheh, Milatz et al. 2009, Borovac, Barker et al. 2012, Krug, Gunzel et al. 2012). However, the *in vivo* characterization is not thoroughly-studied, especially for the claudins that mediate Na^+ or Cl^- reabsorption, such as claudin-2, claudin-7 and claudin-10a. The salt wasting phenotypes of these claudin knockout mice are usually absent or mild (Muto, Hata et al. 2010, Tatum, Zhang et al. 2010). One important factor that needs to be taken into consideration

is that there are so many Na^+ transporters along the renal tubule. Some examples are: Na-H antiporter 3 (NHE3) in the proximal tubules, Na-K-2Cl cotransporter (NKCC2) in the thick ascending limb, NaCl cotransporter in the distal convoluted tubules, and epithelial Na^+ channel (ENaC) in the cortical collecting duct. Na^+/K^+-ATPase, which is present in the basolateral membrane, creates a concentration gradient for sodium to flow into the cell through apical transporters. As apical transporter activity increases, so too does Na^+/K^+-ATPase activity in order to maintain the low intracellular Na^+ environment. These transporters play a significant role in the regulation of Na^+ reabsorption in renal tubules. It has been shown that when one transporter is dysfunctional, other transporters will compensate for it (Brooks, Sorensen et al. 2001). Whether there is any compensation by other Na^+ transporters in claudin-null mice has never been investigated. In this dissertation, we performed a series of experiments to uncover the mystery behind the absence of the salt-wasting phenotype in claudin-2 null mice. We studied whether other Na^+ transporters could compensate and prevent the salt wasting phenotype in claudin-2 null mice. In addition we further investigated the fundamental significance of paracellular transport. We are the first to prove that paracellular transport evolved to make ion transport more energy-efficient. It utilizes the gradient that was created by transcellular transport and mediates ion transport without directly consuming oxygen. Without paracellular transport, the tissue will be more susceptible to ischemic insult.

1.6 Figures

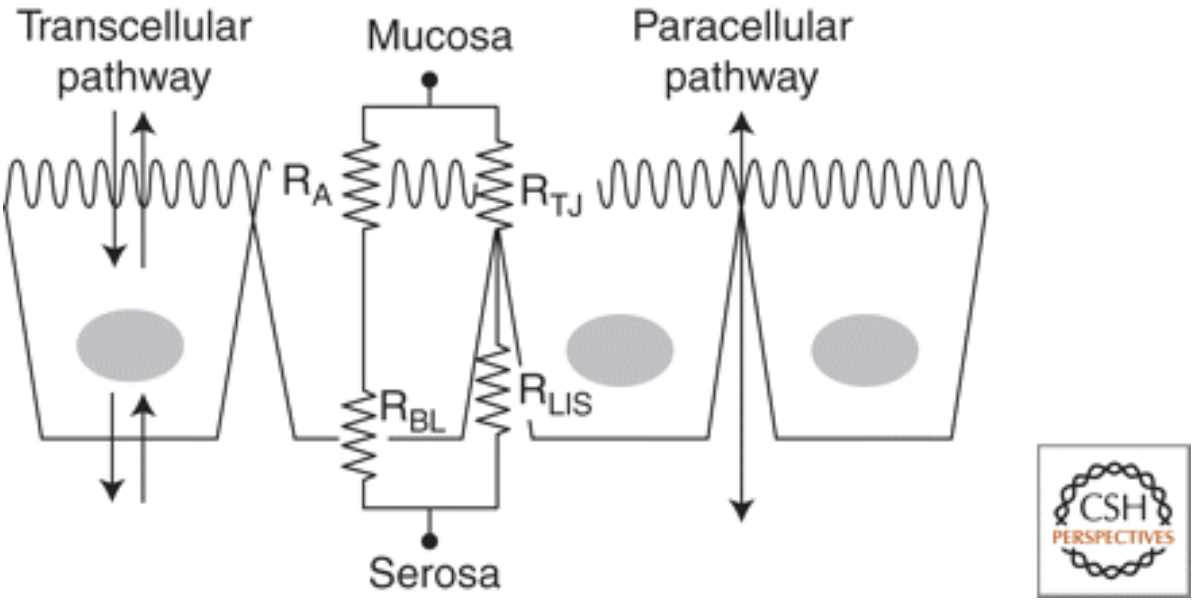

Figure 1.1 Electrical circuit model of paracellular resistances across transcellular and paracellular pathways of an epithelial cell monolayer. Transcellular transport is controlled by transporters in the apical and basolateral surfaces. The resistance of these series elements is typically much higher than that of the parallel elements of the paracellular pathway. Thus, the overall resistance of an epithelium is defined by R_{TJ}, which is defined by the composition of claudins in the tight junctions (Anderson and Van Itallie 2009). R_{TJ}: resistance of tight junction; R_{BL}: basolateral cell membrane resistance; R_{LIS} : Resistance of Lateral Intercellular Space; R_A : apical cell membrane resistance.

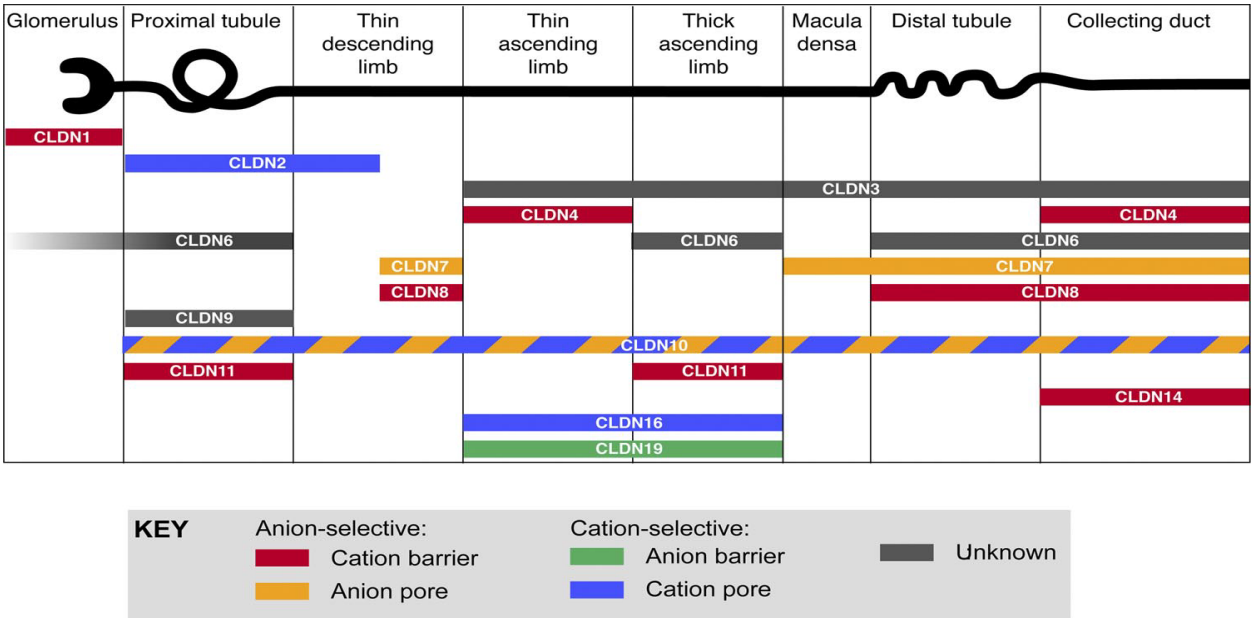

Figure 1.2 Distribution and putative function of claudin proteins in mouse nephron segments. Summary of the segment-specific expression patterns of claudins in mouse nephrons. In the thin descending limb of Henle, some, but not all, aquaporin 1-positive tubules were positive for claudin-2 (CLDN-2). Similarly, from the thin ascending limb of Henle to the collecting duct, claudin-3 was detected in some, but not all, marker-positive tubules. These findings may be consistent with previous reports that the distal tubules, as well as the collecting tubules, are composed of several functionally distinct segments. In other cases, claudins were detected in all of the respective marker-positive tubules (Angelow, Ahlstrom et al. 2008).

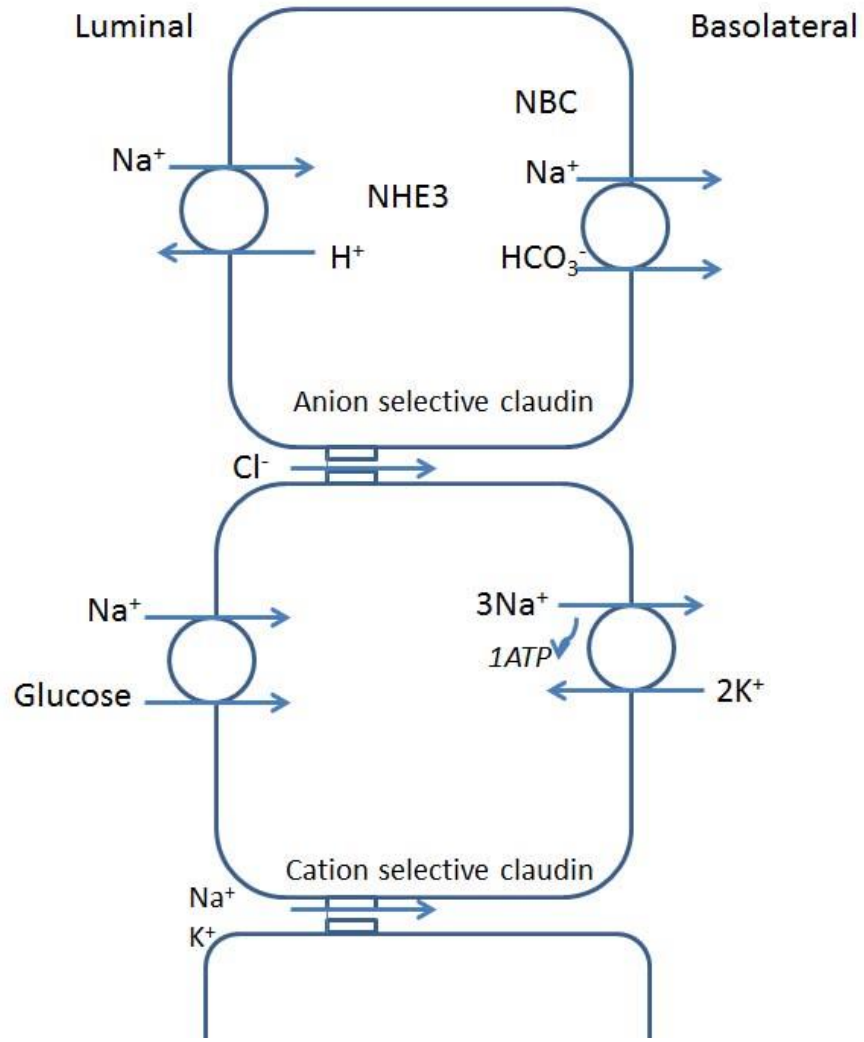

Figure 1.3 Transepithelial Na^+–Cl^- transport in the proximal tubule. In early renal proximal tubules, Na^+ is actively transported into proximal tubule cells by the Na^+–H^+ antiporter and then exits the basolateral membrane through the Na^+–$HCO3^-$ cotransporter. This phenomenon leads to increased Cl^- gradient and thus drives paracellular Cl^- reabsorption through claudin-10a pores. The Cl^- reabsorption generates a positive lumen potential and drives paracellular Na^+ and K^+ reabsorption through cation-selective claudin-2.

Chapter II General characterization of claudin-2 null mice model

2.1 Introduction

After we purchased claudin-2 null mice, we bred them with C57BL/6J mice to generate different genotypes. We then performed a Southern blot to confirm the absence of the claudin-2 gene in the knockout mouse genome. Also, we used RT-PCR, western blot and immunofluorescence to confirm the absence of claudin-2 mRNA and protein expression. We characterized the claudin-2 expression and localization in heterozygous mice to see whether there was any lyonization. Muto *et al* reported that although isolated claudin-2 null proximal tubules revealed less permeability to Na^+, there was no change in urinary Na^+ excretion unless they challenged the mice with a high salt saline infusion (Muto, Hata et al. 2010). We performed a similar experiment to confirm this result.

2.2 Methods and Materials

Animal source and breeding scheme

Mice - in which the single coding exon of claudin-2 on the X chromosome was replaced by a βGeo/Puro cassette by homologous recombination (**Fig. 2.1**) and maintained on a B6;129F2 segregating background (B6;129S5-Cldn2tm1Lex/Mmcd) - were purchased from Mutant Mouse Regional Resource Centers. These chimeric mice were bred with C57BL/6J mice to generate F1 heterozygous animals. Their progeny were then intercrossed to generate F2 heterozygous mice Cldn2 [+/-]. Given that the resulting F2 Cldn2 [+/-] mice have a mixed background, we bred the Cldn2 [+/-] mice with Cldn2[+/Y] mice containing a pure C57BL/6 background in order to generate hemizygous Cldn2[-/Y] and WT [+/Y]. Then we bred claudin-2 heterozygous mice Cldn2 [+/-] with claudin-2 hemizygous mice Cldn2[-/Y] to generate claudin-2 homozygous mice Cldn2[-/-]. **Figure 2.2** shows the schematic of our breeding strategy that produced the generation of hemizygous male KO mice, homozygous female KO mice, and heterozygous female mice.

Southern Blotting

Genomic DNA from claudin-2 WT and KO kidney was extracted using phenol and chloroform and purified with 70% ethanol. The extracted genomic DNA was digested with EcoR1 at 37° overnight. We separated the digested DNA samples in a 0.5X Tris/Borate/EDTA (TBE) gel at 20 volts for 8 hours in 1X TBE buffer. The targeted DNA was transferred to a nitrocellulose membrane (Boehringer-Mannheim cat#:1417240) via electrophoretic transfer (Genie Blotter), denatured by NaOH and fixed by UV crosslinker. A 3' external probe and a 5' external probe were labeled with [α^{32}P] dCTP using the High Prime DNA labeling kit (Roche 11585584001). The membrane was hybridized with α^{32}P labeled DNA probe at 42°C overnight. We washed the membrane with 2X SSC/ 0.1% SDS for 15 minutes at room temperature twice, and then switched the washing buffer to 0.5X SSC/ 0.1% SDS for 15 minutes at 65°C once. The radioactive signal from the membrane was absorbed for 24 hours by a storage phosphor screen and then scanned by a typhoon scanner. A 5' external probe was produced via PCR of mice genomic DNA using the primers:

Forward: 5'-GAGTACTGTGTAAGGTACAYG-3'

Reverse: 5'-CATAGTGCTAAGAATGCAG-3'

A 3' external probe was produced via PCR of mice genomic DNA using the primers:

Forward: 5-CATCTGGATGAGCAGATTTG-3'

Reverse: 5'-GAACTGACCTGAGAGTCTTG-3'

Immunoblotting

The preparation of the whole kidney lysates was described in previous studies (Nguyen, Yang et al. 2012). Briefly, one whole kidney of each mouse was minced and suspended in 2 ml isolation buffer (5% sorbitol, 0.5 mM disodium EDTA, and 5 mM histidine-imidazole buffer, pH = 7.5, with the addition of 167 mM PMSF, 9 μg/ml aprotinin, and 5 μl/ml phosphatase inhibitor cocktail [Sigma]). Each sample was homogenized for 5 min at a low-speed setting with an Ultra-Turrax T25 (IKA-Labortechnik) and then centrifuged at 2,000 g for 10 min. Supernatants were retained, and the pellets were rehomogenized in another 2 ml of isolation buffer, recentrifuged, and the resulting supernatants were pooled with the first supernatants.

Equal amounts of the supernatant proteins from the kidney lysates were boiled at 60℃ for 20 minutes and loaded to 10% acrylamide gels (Bio-Rad) for electrophoresis. After that, the proteins were transferred to polyvinyl di-fluoride (PVDF) membranes. Non-specific binding was blocked by gently agitating the membranes in 5% non-fat milk and 0.1% Tween in PBS (PBST) for 1 hour at room temperature. Blots were subsequently incubated in 5% bovine serum albumin (BSA) containing 0.1% Tween with the designated primary antibody (**Table 2.1**) overnight at 4°C with gentle agitation. After PBST washes, the blot was then incubated with the appropriate horseradish peroxidase-conjugated secondary antibody for 1 hour at room temperature with gentle agitation. After PBST washes, the blots were incubated with Pierce™ ECL Western Blotting Substrate (Thermoscientific).

Equal loading of WT and KO kidney protein lysates represented the same percentage of a whole kidney since there was no difference in kidney weight between WT and KO mice (**Fig. 2.3**). The immunoblot signals were quantitated with the Odyssey Infrared Imaging System (Li-COR). All comparisons were performed on samples run on the same membrane.

Immunofluorescence staining

In a separate set of WT and claudin-2 KO mice, kidneys were perfusion-fixed via the heart with 4% paraformaldehyde in PBS. The fixed tissues were cryoprotected by overnight incubation with 30% sucrose in 1X Phosphate-buffered saline (PBS), embedded in Tissue-Tek O.C.T. compound (Sakura Finetek, Torrance, CA), and frozen on dry ice. Cryosections (10 μm) from WT and KO animals were sliced and transferred to the same Superfrost Plus-charged glass slide (Fisher) for direct side-by-side processing and viewing. For immunofluorescent labeling, the sections were rehydrated and antigen-retrieved via immersing the slides in 1X antigen decloaker solution and steaming the slides in a pressure cooker for 5 minutes. After that, the slides were washed and blocked with 1% BSA/5% goat serum/PBS for 1 hour at room temperature before antibody incubation. All antibodies (see **Table 2.2**) were diluted in 1% BSA/5% goat serum/PBS. The blocked kidney sections were incubated with primary and secondary antibodies at room temperature for 1 hour each. Between each incubation, the sections were washed with 1XPBS 5 minutes for 3 times. After that, the sections were mounted in Prolong Anti-fade containing DAPI (Invitrogen) and air dried overnight.

RNA extraction and quantitative real-time PCR

RNA was extracted from tissue homogenate with TRI Reagent (Sigma-Aldrich) and purified using an RNeasy mini kit (Qiagen). First-strand cDNA was synthesized using iScript Reverse Transcription Supermix for RT-PCR (Bio-rad). Quantitative real-time PCR was performed using a CFX96 Touch™ Real-Time PCR Detection System and iTaq™ Universal SYBR® Green Supermix (Bio-rad) with the primers indicated in **Table 2.3**. Expression levels were normalized to β-actin levels.

Blood and urine studies

Mouse whole blood was collected through cardiac puncture. The blood was left undisturbed at room temperature for 30 minutes to allow it to clot and the clot was removed by centrifuging at 1,000 x g for 10 minutes in a refrigerated centrifuge. Serum potassium was measured via flame photometer (BWB Technologies). Na^+ concentration was measured with a sodium ion-sensitive microelectrode and urine volume was measured by urine weight.

NaCl hypertonic saline challenge experiment

Mice were given 40 mL/kg bodyweight of a 2% (weight/volume) sterile NaCl solution via intraperitoneal injection. After the injection, the mice were housed in metabolic cages individually for 4 hours to collect urine. Urine Na^+ excretion was calculated as "urine Na^+ concentration X urine volume." Na^+ concentration was measured with a Na^+ ion-sensitive microelectrode and urine volume was measured by urine weight.

Low potassium diet metabolic study

Mice were placed in metabolic cages for 10 days and fed custom purified rodent diets (Teklad, Harlan Laboratories). A control diet containing 0.8% potassium (TD.120258) was provided for the first 5 days and then switched to a potassium-deficient diet containing 0.006% potassium (TD.120260) for the next 5 days. Urine was collected daily except on the first day after the switch to the potassium-deficient diet, when urine was collected every 8 hours. This was done to capture transient changes in urine K^+ excretion rate prior to attainment of a new steady state.

Study approval

All animal experiments were performed in accordance with NIH guidelines on the use of laboratory animals as well as by the Institutional Animal Care and Use Committee at the University of Kansas Medical Center.

Data analysis

Data are expressed as means ± standard error of the means (SEM). To compare means between two groups we used two-way, unpaired Student's t-tests, with p-values of <0.05 considered significant.

2.3 Results

In order to produce claudin-2 null mice with a pure C57BL/6J background, first generation claudin-2 heterozygous mice were bred to C57BL/6J mice for more than 10 generations. Their growth rate, appearance, activity and behavior were normal. Because the claudin-2 gene is on the X chromosome, we used male hemizygous mice Cldn2[-/Y] as the KO mice and compared them to their male wild-type littermates Cldn2[+/Y] for matched controls (WT). Southern blot confirmed the disruption of the claudin-2 gene in claudin-2 KO mice (**Fig. 2.4**). Quantitative RT-PCR and Western blotting confirmed the absence of claudin-2 in hemizygous KO Cldn2[-/Y] mice (**Fig. 2.5 A and B**). There was an intermediate level of expression of claudin-2 in heterozygous female Cldn2[+/-] mice. Immunofluorescence confirmed that claudin-2 was expressed and localized in tight junctions in WT mouse kidney proximal tubules in a continuous distribution but were absent from the KO kidneys. Heterozygous kidneys showed a discontinuous distribution of claudin-2 in only some of the proximal tubule cells, presumably due to lyonization (**Fig. 2.5C**).

The intraperitoneal injection of mice with a hypertonic (2%) saline solution resulted in a higher urine Na^+ excretion in claudin-2 KO mice (**Fig. 2.6**). To investigate whether other paracellular transport pathways were upregulated to compensate for the lack of claudin-2, we performed quantitative real-time PCR for other claudins expressed in the proximal tubule (claudin-10a, -17), the thick ascending limb (claudin-10b, -16 and -19) and the distal tubule (claudin-4, -8). We found no difference in the expression (**Figure 2.7 and 2.8B**) or localization (**Fig. 2.8A**) of any of these claudins between KO and WT mice. To investigate whether claudin-2 depletion has any influence on renal potassium handling, we performed a 10-day metabolic study to measure serum K^+ levels at the baseline and during a low potassium diet. No difference was detected in serum K^+ levels between the claudin-2 WT and KO mice (**Fig. 2.9**). Age-matched adult (8 weeks old) claudin-2 WT and KO mice were placed in metabolic cages and were fed a control diet with normal sodium content (0.3% sodium, 0.8% potassium) for 5 days. Urine collected daily showed no significant difference in the urine potassium/creatinine (K/Cr) concentration ratio between the WT and KO mice (**Fig. 2.10**). After the 5-day acclimatization period, the mice were switched to a matched potassium-deficient diet (0.006% potassium) and urine K^+ was monitored 8 hourly for the first 24 hours, and daily thereafter. Any inability of the KO mice to maximally conserve K^+ would have manifested itself as a transiently higher K^+ excretion rate as compared to WT mice, in which K^+ excretion rate returns to a steady-state within a few days. We did not find any difference in urine K^+ excretion rates between WT and KO mice.

2.4 Discussion

Claudin-2 null mice were born with expected Mendelian ratios. There was no overt phenotype of claudin-2 null mice at the baseline; they grew and bred normally. This observation was consistent with what has been previously reported (Muto, Hata et al. 2010). We confirmed that the claudin-2 gene was disrupted in the claudin-2 null mice genome. We also confirmed the

absence of claudin-2 mRNA and protein expression in KO and intermediate claudin-2 expression in heterozygous mice. Claudin-2 is also known to mediate K^+ permeability *in vitro* (Amasheh, Meiri et al. 2002). Around 60% of the K^+ is believed to be transported via claudin-2 between proximal tubule cells. Therefore we expected to see an increased urinary potassium excretion in claudin-2 null mice. However, we found no change in the serum or urine K^+ levels of claudin-2 null mice. One possibility for our finding is that the increased expression and/or activity of K^+ transporters - such as H^+-K^+-ATPase (Kone and Higham 1998) - or the decreased expression and/or activity of K^+ channels - such as Maxi-K^+ channel (Najjar, Zhou et al. 2005, Rieg, Vallon et al. 2007) - compensated for the impaired K^+ reabsorption from the proximal tubule. This hypothesis can be further explored in future studies.

Consistent with what Muto *et al.* found, hypertonic saline injection led to more natriuresis in claudin-2 null mice. Saline loading is known to decrease proximal tubule Na^+ and fluid reabsorption by affecting peritubular oncotic and hydrostatic pressure and hence the balance of Starling forces in the proximal tubule (Ichikawa and Brenner 1979). If this is mediated in part by claudin-2, then claudin-2 KO mice should have decreased and not increased saline-induced natriuresis.

Our interpretation of this experiment, however, differs from that of Muto *et al.* The finding that saline-induced natriuresis was greater in claudin-2 KO than WT mice suggests that natriuresis was not mediated by changes in paracellular Na^+ transport. Brenner, Troy and Daugharty showed that saline-induced volume expansion reduced peritubular oncotic pressure thus shifting the balance of Starling forces to inhibit proximal tubule fluid reabsorption (Brenner, Troy et al. 1971). To the extent that proximal tubule water reabsorption is primarily transcellular and mediated by aquaporins, we predicted that saline expansion should inhibit primarily transcellular transport in the proximal tubule, which should be similar in claudin-2 KO and WT mice. How then to explain the observation that natriuresis is paradoxically increased in KO mice?

Saline loading, by decreasing proximal tubule Na^+ reabsorption, increases Na^+ delivery to the loop of Henle, where absolute and fractional Na^+ reabsorption are increased. This is likely mediated by increased flow. In addition, because in this experiment hypertonic saline was used, the vasopressin release may also contribute to increased salt reabsorption by stimulating the activities of distal transcellular transporters such as the Na-K-Cl cotransporter (NKCC2) on the ascending limb of loop of Henle (TALH). Claudin-2 null mice exhibited no salt wasting phenotype at the baseline because the defect in proximal tubule Na^+ reabsorption was compensated by the increased activity of distal transporters such as NKCC2. If that is the case, we postulate that, in claudin-2 null mice, the activity of NKCC2 was already maximally stimulated. Thus, KO mice are unable to further increase Na^+ transport in the thick ascending limb of loop of Henle in order to mitigate an even greater Na^+ load delivered from the proximal tubule with hypertonic saline expansion. Hence KO mice exhibit greater diuresis to saline than WT mice. In the future studies, we need to further investigate whether there is any upregulation of expression and/or activity of distal renal transcellular transporters.

2.6 Figures and tables

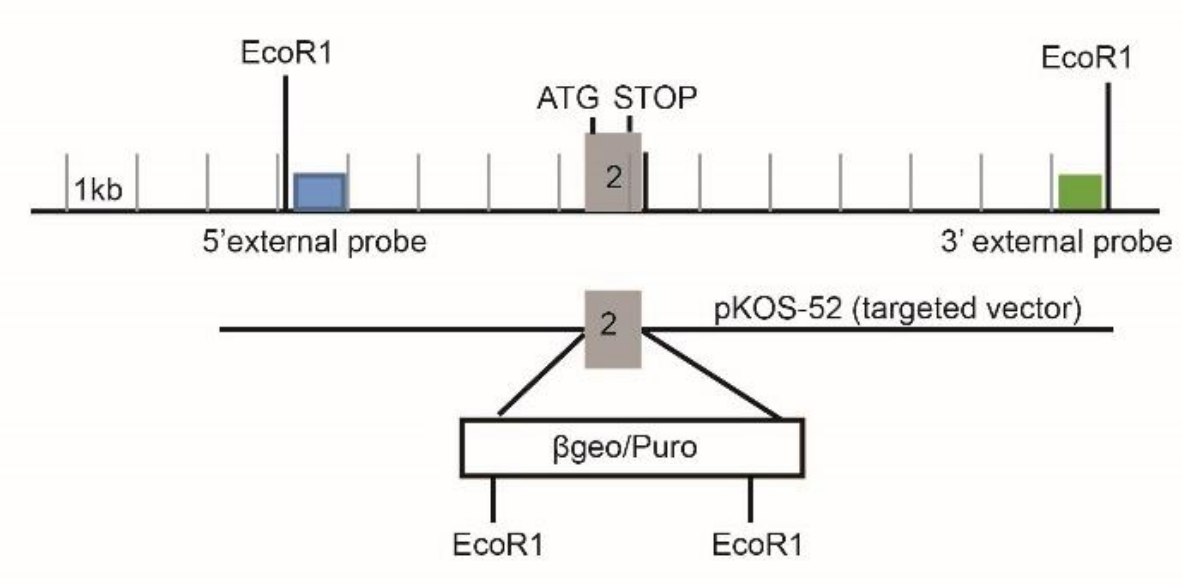

Figure 2.1 Generation of claudin-2 knockout mice: Diagram of targeting strategy. The grey bar indicates the single coding exon of the mouse claudin-2 gene. The targeting vector contains a βGeo/Puro cassette designed to replace all of the coding region and part of the 3'-UTR. The 5' external probe is indicated by the green bar and the 3' external probe by the blue bar. From http://mmrc.mouse biology.org (Lexicon Genetics MEM726N1)

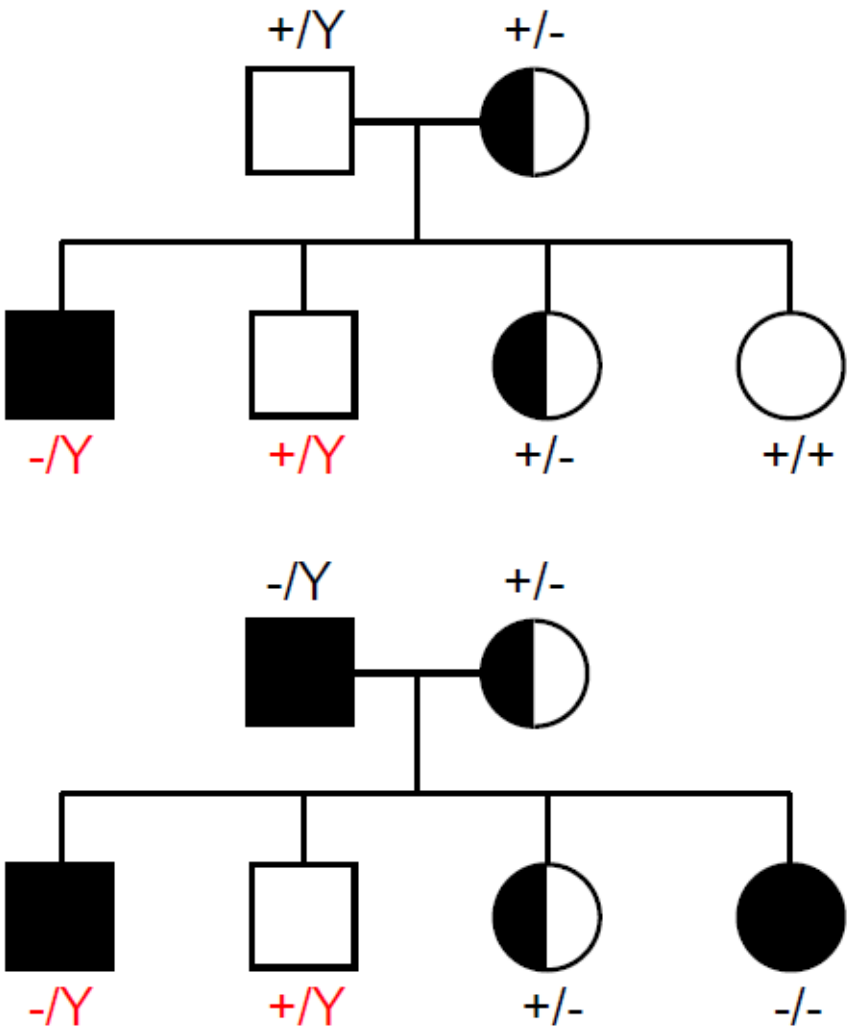

Figure 2.2 Two breeding strategies used to generate the matched WT [+/Y] and KO [-/Y] littermates (red labels) used for the experiments described. Genotypes refer to alleles at the claudin-2 locus on the X chromosome. Fully shaded symbols are mice that are claudin-2 knockouts, partially shaded symbols represent heterozygotes.

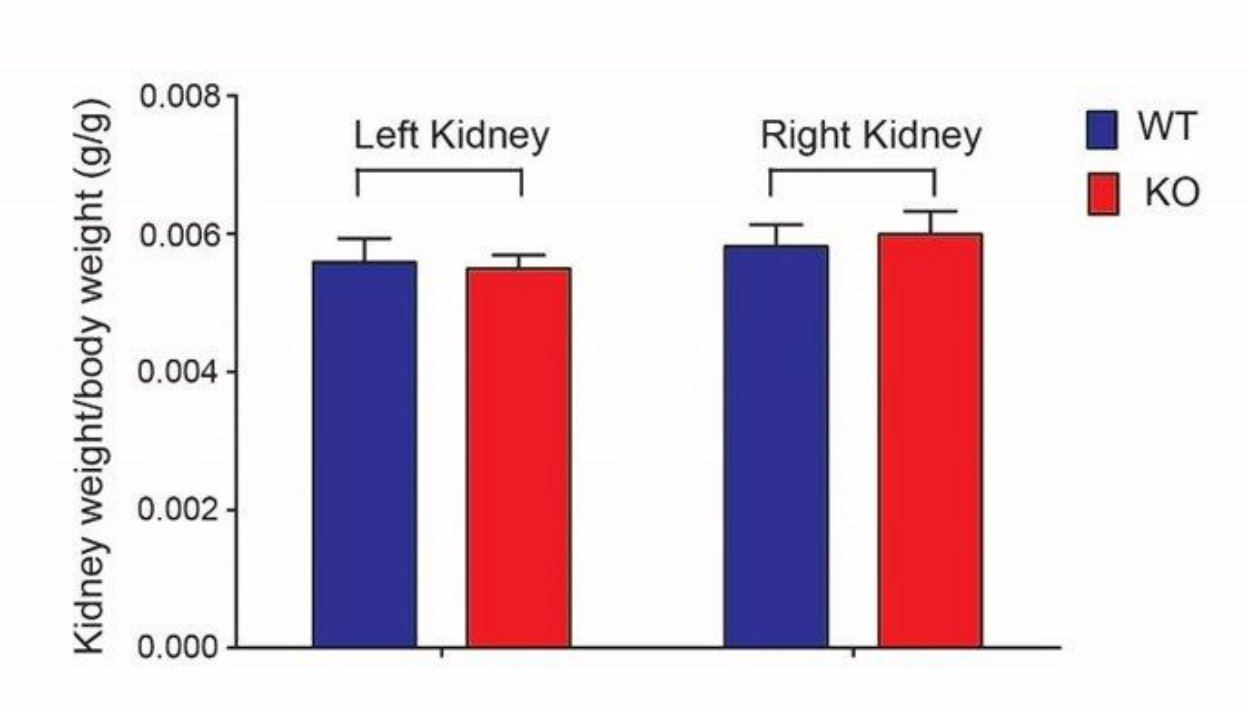

Figure 2.3 Kidney weight of claudin-2 WT and KO mice. Kidney weight is represented as the ratio between left or right kidney weight and body weight.

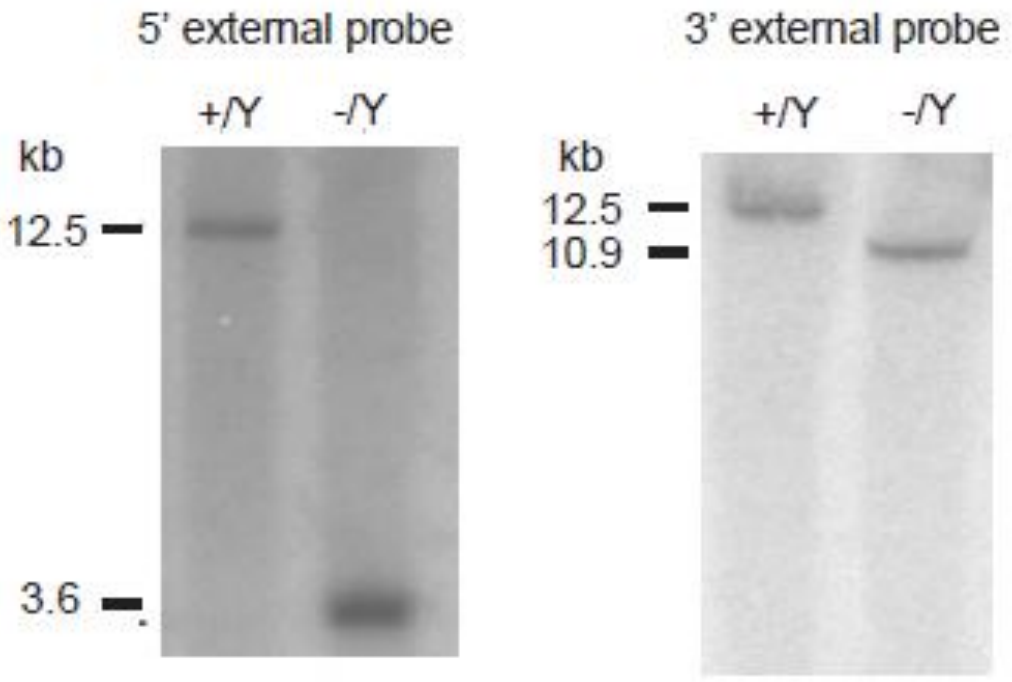

Figure 2.4 Southern blot of EcoR1-digested genomic DNA from wild-type (+/Y) and hemizygous (-/Y) mice indicated correct targeting. Blotting using the 5' external probe indicated in A. should yield a 12.5 kb or a 3.6 kb band from the wild-type and targeted allele, respectively. Blotting with the 3' external probe should yield a 12.5 kb or a 10.9 kb band from the wild-type and targeted allele, respectively.

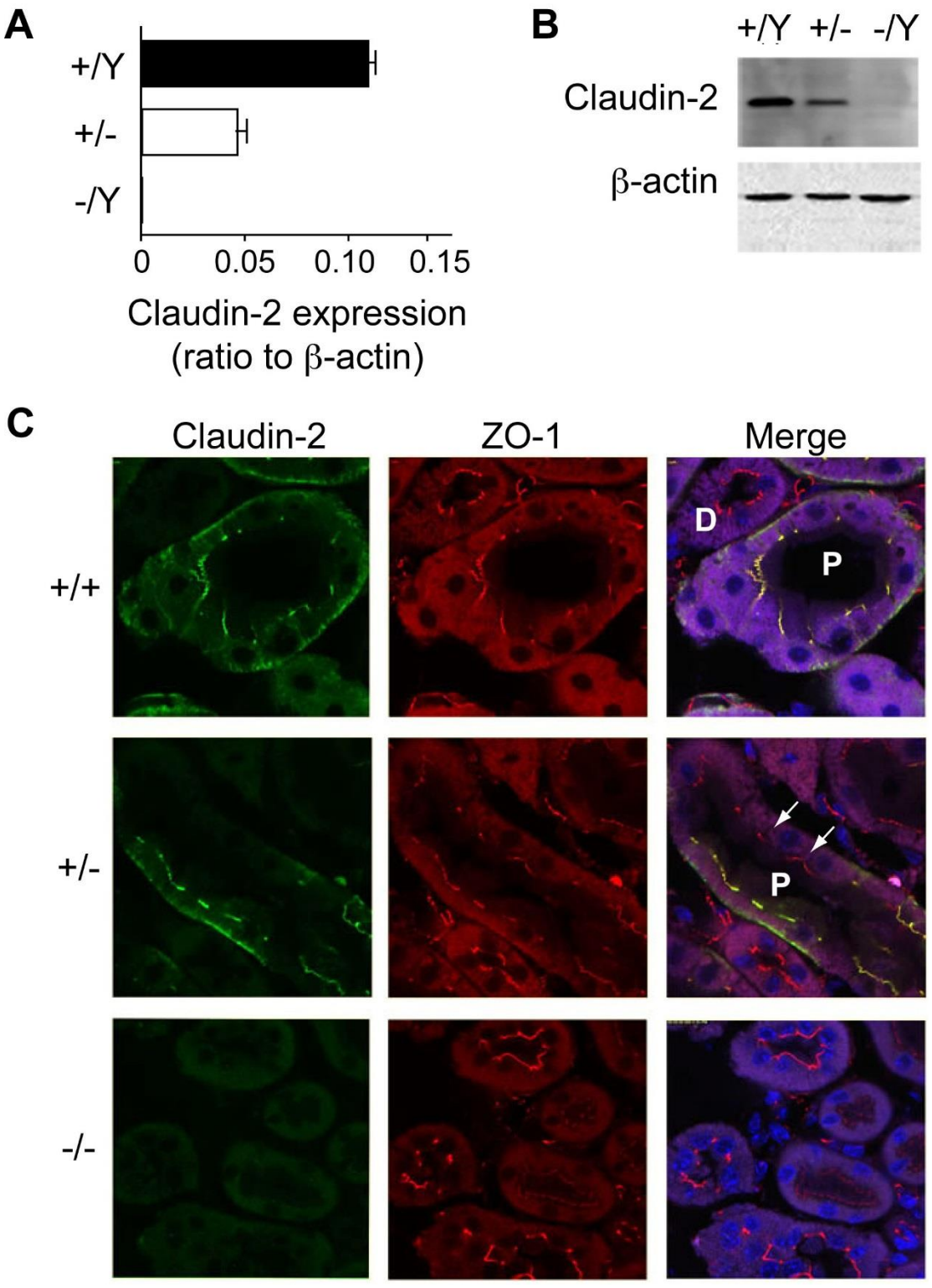

For Legend, see next page

Figure 2.5 mRNA and protein expression of claudin-2 in claudin-2 KO mice. A. Quantification of whole kidney mRNA levels of claudin-2 relative to β-actin in claudin-2 hemizygous KO [-/Y], heterozygous [+/-] and WT [+/Y] mice (n = 6 per group). B. Western blot of the whole kidney lysates probed with mouse anti-claudin-2 antibody showing bands at the expected size for claudin-2 in heterozygous [+/-] and WT [+/Y] mice. The lower panel shows an immunoblot for β-actin as a loading control. C. Immunolocalization of claudin-2. Mouse kidney frozen sections were double-stained with claudin-2 antibody (Zhang, Gillihan et al. 2013)and antibody to ZO-1 (Simon, Lu et al. 1999) a marker of the tight junction. Note localization of claudin-2 in WT to the tight junctions of proximal tubules (P) but not to distal tubules (D), as well as faint basolateral staining. In heterozygous mice, proximal tubule staining is heterogeneous with claudin-2 absent from some cells (arrows) but present in others due to lyonization. Magnification of the microscope: 40X.

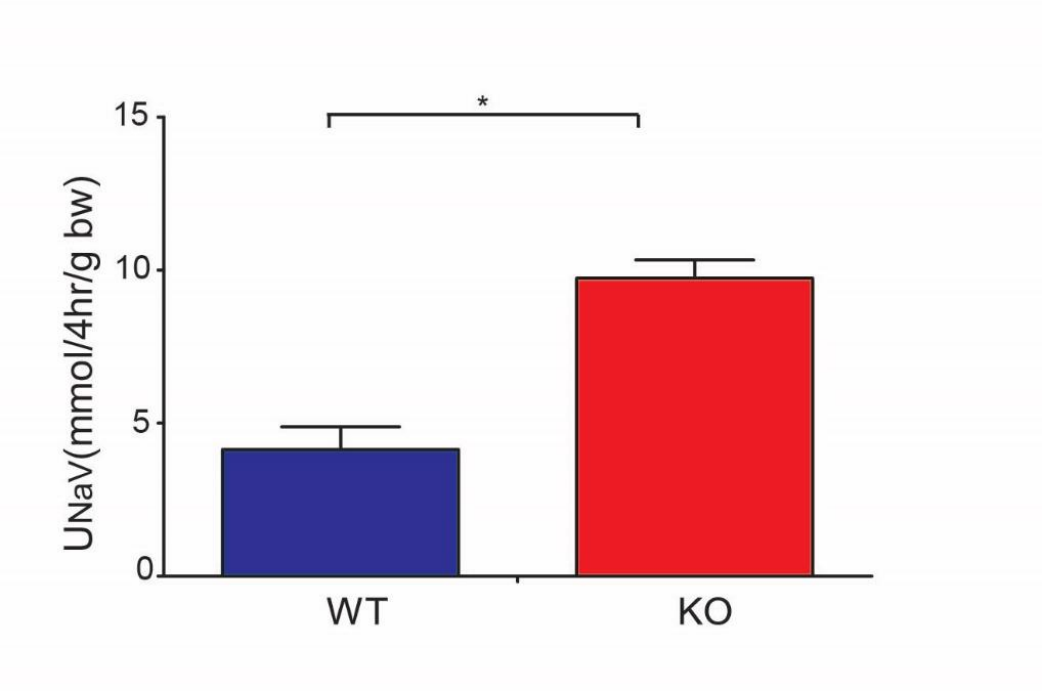

Figure 2.6 Hypertonic saline challenge test in claudin-2 WT and KO mice. Mice were given 40 mL/kg bw of 2% (w/v) NaCl intraperitoneally and urine collected over the subsequent 4 hours. Urine Na^+ excretion (UNaV) was greater in KO mice than WT. *$p < 0.01$ bw: body weight; w/v: weight/volume.

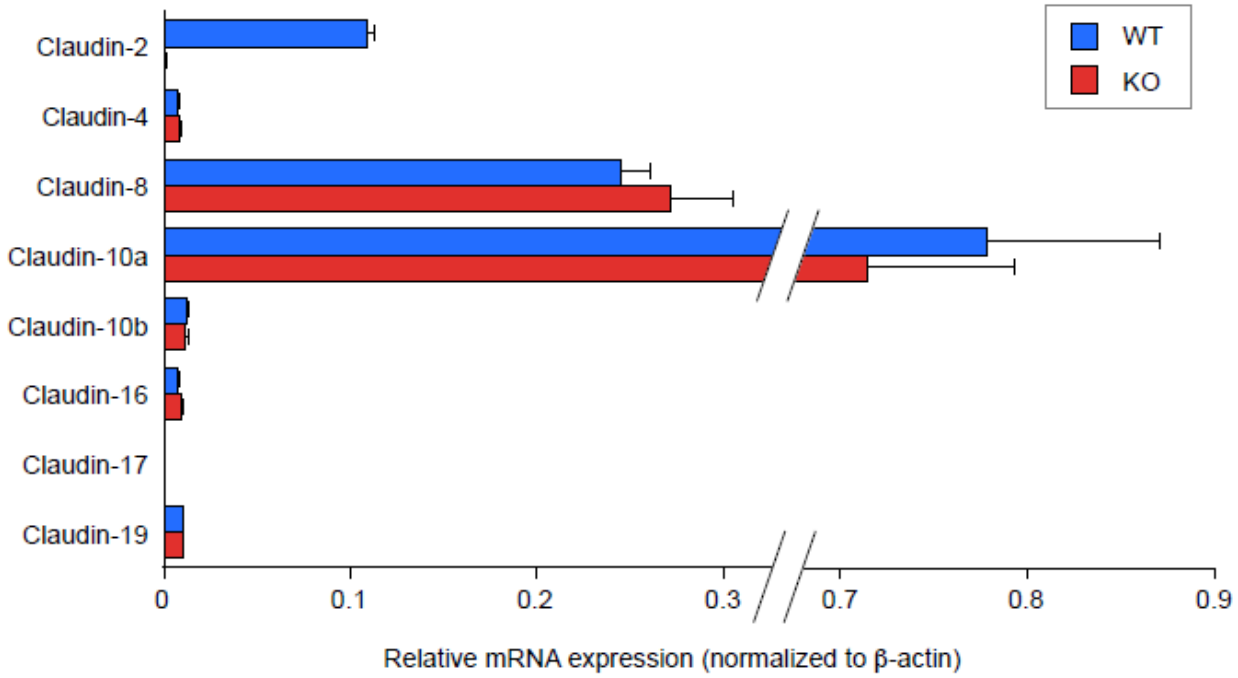

Figure 2.7 Claudin mRNA expression in claudin-2 WT and KO mouse kidneys, quantitated by real-time RT-PCR and normalized to the level of β-actin by the ΔCt method (n = 6 per group).

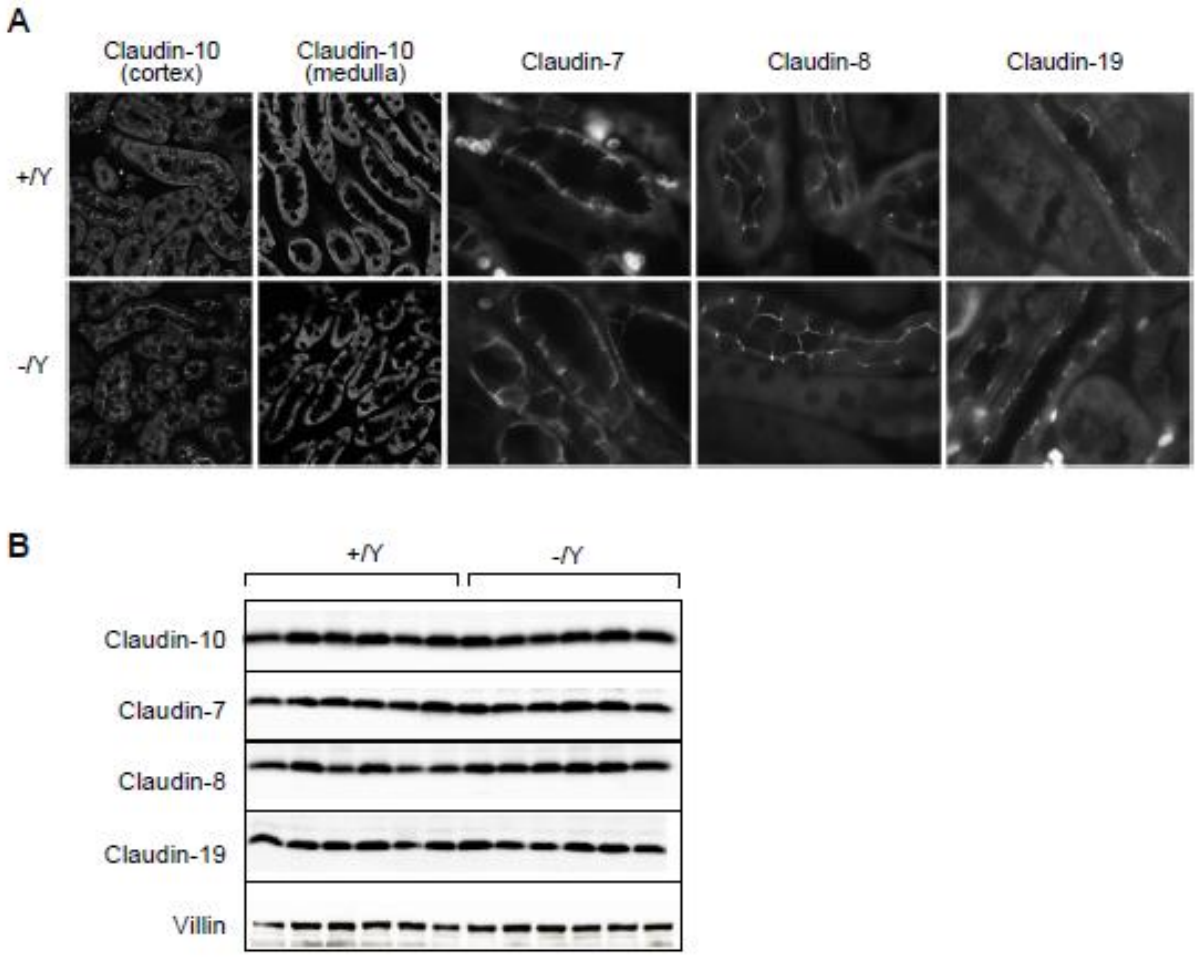

Figure 2.8 Localization and protein expression of claudin isoforms in the Cldn2[+/Y] and Cldn2[-/Y] mice. A. Immunolocalization of claudin isoforms. Mouse kidney frozen sections were stained with claudin-10, claudin-7, claudin-8, and claudin-19 antibodies. B. Western blot of whole kidney lysates probed with rabbitanti-claudin-10, claudin-7, claudin-8 and claudin-19 antibodies showing bands at the expected sizes. The lower panel shows an immunoblot for villin as a loading control. Magnification of the images: claudin-10 staining: 20X; claudin-7, claudin-8 and claudin-19: 40X.

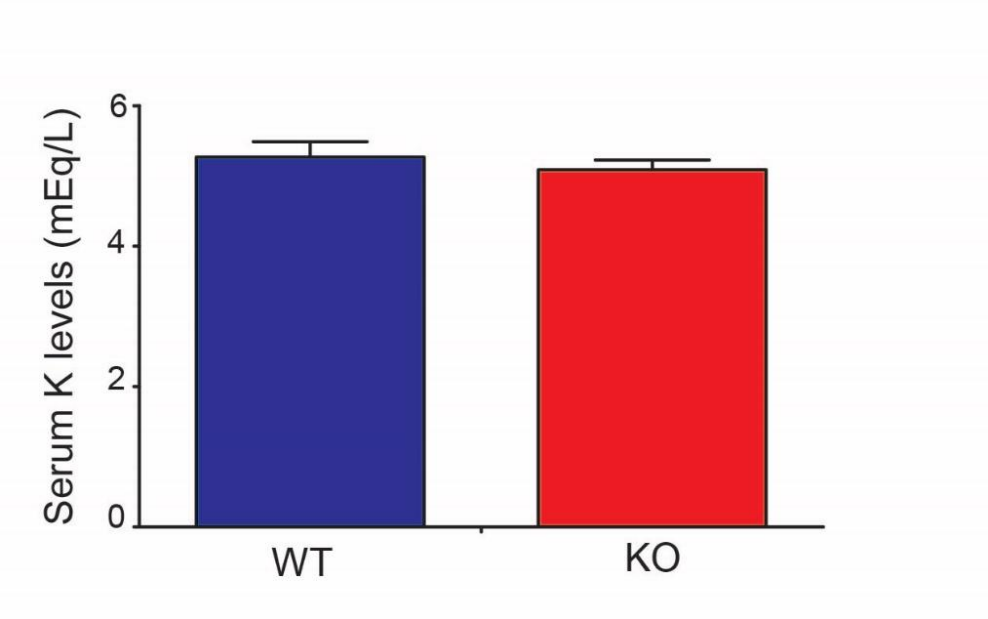

Figure 2.9 Serum potassium (K) concentration in claudin-2 WT and KO mice. In mEq/L (n=6 mice per group, p=ns)

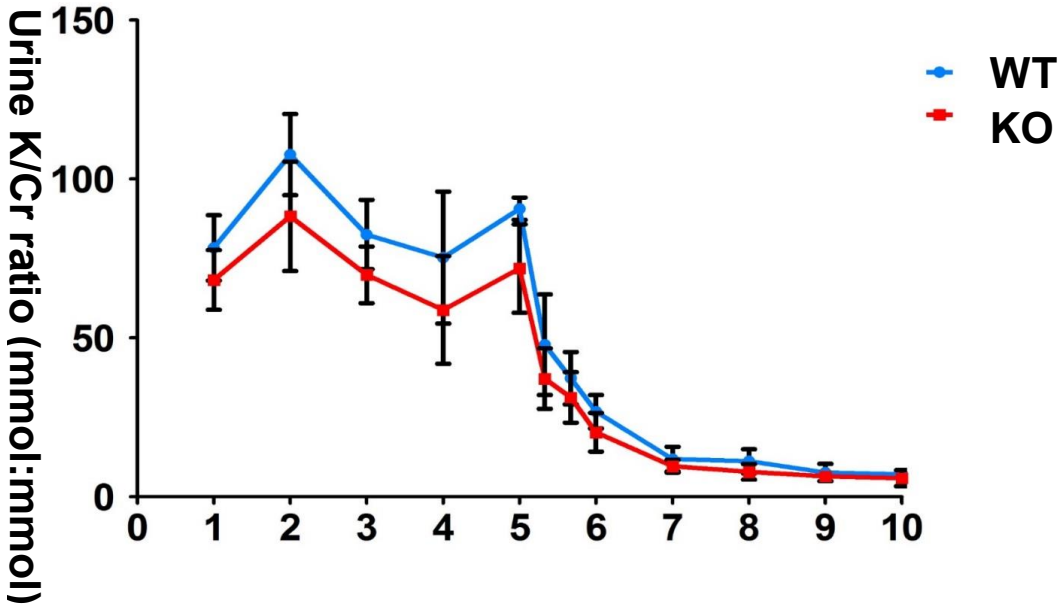

Figure 2.10 Effect of dietary potassium depletion on claudin-2 potassium handling. Urine potassium excretion rate, expressed as the ratio of potassium to creatinine concentration (mean ± S.E.M., n = 6 per group), is shown in mice on a normal (0.8%) potassium diet (Day 1 to Day 5) followed by a potassium-deficient (0.01%) diet (Day 6 to Day 10). *$p < 0.05$ by paired t-test (n = 7-9 per group). bw, body weight.

Antibody Target	Apparent Mobility (kDa)	Protein (µg/lane)*	Primary antibody supplier (cat. no.)	Primary antibody host	Primary antibody dilution	Incubation time	Ref
Claudin-2	23	10	ThermoFisher Scientific (cat# 5600)	Mu	1:2000	O/N	
Claudin-7	23	15	ThermoFisher Scientific (cat# 9100)	Rb	1:1000	O/N	
Claudin-8	23	15	ThermoFisher Scientific (cat# 2600)	Rb	1:500	O/N	
Claudin-10	21	15	ThermoFisher Scientific (cat# 8400)	Rb	1:250	O/N	
Claudin19	23	15	Alan Yu (Univ. of Kansas)	Rb	1:1000	O/N	(Angelow, El-Husseini et al. 2007)
β-actin	42	15	Sigma-Aldrich (#A2066)	Rb	1:1000	O/N	
Villin	90	15	Santa Cruz (#28283)	Rb	1:500	O/N	
Renin	37	30	AnaSpec (#54373)	Rb	1:500	O/N	

Table 2.1: Primary antibodies used for immunoblotting. O/N: Overnight; Mu: mouse; Rb: Rabbit.

Antibody Target	**Primary antibody supplier (cat. no.)**	**Primary antibody host**	**Primary antibody dilution**	**Incubation time**	**Ref**
Claudin-2	ThermoFisher Scientific (#585600)	Mu	1:500	O/N	
ZO-1	ThermoFisher Scientific, anti-ZO-1 Alexa Fluor® 594 conjugate (# 339194)	Mu	1:1000	O/N	
Claudin-7	ThermoFisher Scientific (#599100)	Rb	1:500	O/N	
Claudin-8	ThermoFisher Scientific (#602600)	Rb	1:200	O/N	
Claudin-10	ThermoFisher Scientific (#618400)	Rb	1:100	O/N	
Claudin-19	Alan Yu (Univ. of Kansas)	Rb	1:1000	O/N	(Angelow, El-Husseini et al. 2007)

Table 2.2: Primary antibodies used for immunofluorescence. O/N: Overnight; Mu: mouse; Rb: Rabbit.

β-Actin Forward	5'-CTA AGG CCA ACC GTG AAA AG-3'
β-Actin Reverse	5'-ACC AGA GGC ATA CAG GGACA-3'
Claudin 2 Forward	5'-TGGCGTCCAACTGGTGGGCT-3'
Claudin 2 Reverse	5'-ACCGCCGTCACAATGCTGGC-3'
Claudin 2 genotype WT Forward	5’-CAGGCTCCGAAGATACTTC-3'
Claudin 2 genotype WT Reverse	5’-GTAGAAGTCCCGAAGGATG-3'
Claudin 2 genotype KO Reverse	5’-CCCTAGGAATGCTCGTCAAGA-3'
Claudin 4 Forward	5'-TGGGGACAGGCAAACCCGGA-3'
Claudin 4 Reverse	5'-CTTGCCGGCCGTAAGGAGCC-3'
Claudin 8 Forward	5'-TCCCTGTCAGCTGGGTTGCCA-3'
Claudin 8 Reverse	5'-GCTCGCGCTTTAGGGCCACA-3'
Claudin 10b Forward	5'-GAT CTG CGT TAC CGA TTC CA-3'
Claudin 10b Reverse	5'-GCA GCG ATC ATT AGT CCT CTA C-3'
Claudin 16 Forward	5'-GCA AGA GGG ATG TGA GGA AA-3'
Claudin 16 Reverse	5'-CTA TGG GCC TCT GTT GCT ATT-3'
Claudin 17 Forward	5'-GAC TCC TAC ACA TTC TGC ATCT-3'
Claudin 17 Reverse	5'-CCA GCG ATC TGT AAG GGA TAAA-3'
Claudin 19 Forward	5'-GAA GGA AGA GTG TGG GAG AAAC-3'
Claudin 19 Reverse	5'-GAG CCT TCA GCC TTG AGA TTAG-3'

Table 2.3: Oligonucleotide primers that were used for genomic DNA or quantitative RT-PCR.

Chapter III Claudin-2 and Salt and Water Balance

3.1 Abstract

Claudin-2 null mice were reported to exhibit markedly decreased renal proximal tubule Na^+, Cl^- and fluid reabsorption. Yet they have no apparent disturbance in overall Na^+ balance. We hypothesize that the *in vivo* role of claudin-2 might be to maximally conserve urinary Na^+ under conditions of extreme Na^+ depletion. To test this idea, claudin-2 null mice were placed on a very low sodium (0.01%) diet, and Na^+ excretion rate was monitored at eight-hour intervals. Surprisingly, claudin-2 null mice were able to maximally conserve Na^+ to the same extent as their wild-type littermates, pointing to the existence of a very effective compensatory mechanism. Quantitative RT-PCR analysis showed no compensatory changes in other claudin isoforms. Immunoblotting for a panel of transcellular Na^+ transporters showed a 23% decrease in the abundance of Na-H antiporter 3, only borderline increases in phosphorylated NaCl cotransporter and the γ subunit of the epithelial Na^+ channel, and no change in total or phosphorylated Na-K-2Cl cotransporter. To test whether there was compensatory functional upregulation of transcellular Na^+ transport activity distally, diuretic challenge tests were performed. The natriuresis of the mice 4 hours after intraperitoneal injection of furosemide (but not after hydrochlorothiazide or benzamil) was 40% higher in claudin-2 null mice than WT.

3.2 Introduction

Muto *et al.* reported that claudin-2 KO renal proximal tubules exhibited much lower permeability to Na^+ than those of WT mice (Muto, Hata et al. 2010). It was expected that claudin-2 KO mice would exhibit salt wasting phenotypes such as increased urinary Na^+ excretion, dehydration and hypotension. However, no salt wasting phenotype was observed at the baseline. One of the most likely explanations for this observation is that the impaired Na^+ reabsorption is compensated by paracellular or transcellular transporters in distal tubules. Two kinds of transporters are likely to play a role in this compensation process. First, many other claudin isoforms are expressed along the renal tubules. Some of them, such as claudin-10 (Van Itallie,

Rogan et al. 2006), claudin-7 (Tatum, Zhang et al. 2010) and claudin-4 (Van Itallie, Rahner et al. 2001) have been reported to be involved in NaCl transport in renal tubules. It is possible that other claudin isoforms compensated for the impaired Na^+ reabsorption mediated by claudin-2. Second, several transcellular transporters from the renal tubule were reported to play an important role in the regulation of Na^+ reabsorption in renal tubules. The major transcellular Na^+ transporters in the renal tubules are: Na-H antiporter 3 (NHE3) in the proximal tubules, Na-K-2Cl cotransporter (NKCC2) in the thick ascending limb (**Fig. 3.1A**), NaCl cotransporter in the distal convoluted tubules (**Fig. 3.1B**), and epithelial Na^+ channel (ENaC) in the cortical collecting duct (**Fig. 3.1C**). Also, each Na^+ that is actively transported into the renal tubular cell is pumped back to the blood via Na-K-ATPase across the basolateral membrane (**Fig. 3.1**). As described in Chapter II, we discovered that there was no compensation from other claudin isoforms (**Fig. 2.7, 2.8**). Therefore the question is whether the transcellular transporters were upregulated, thereby compensating for the defect of salt reabsorption in the proximal tubule. We approached this problem in two ways. First, we aimed to unmask the salt wasting phenotype by challenging the mice with salt depletion. Our rationale was that, under extreme conditions, the compensation effect is not enough to obscure the salt wasting phenotype in claudin-2 null mice. As a result, we should see increased urinary Na^+ excretion. Second, we aimed to investigate whether the expression or activity of the transcellular transporters was upregulated. We measured the protein expression of transcellular transporters in claudin-2 null mice using immunoblots with antibodies against total and phosphorylated NHE3, NKCC2, NCC and α, β, γ subunits of ENaC, and the Na^+/K^+ ATPase We also performed a diuretic challenge test to investigate whether there was any functional upregulation of these transcellular transporters. The rationale behind the diuretic challenge test was to determine whether the activity of these transcellular transporters was increased without upregulating the actual amount of the protein. By inhibiting specific transcellular Na^+ transporters through specific diuretics, we were able to find out which transporter had higher activity in claudin-

2 null mice by comparing the sodium excretion in the urine of WT and KO mice (Madala Halagappa, Tiwari et al. 2008, Tiwari, Li et al. 2009).

3.3 Methods and Materials

Immunoblotting

The preparation of the whole-kidney lysates has been described in previous studies (Nguyen, Yang et al. 2012). Briefly, one whole kidney of each mouse was diced and suspended in 2 ml of isolation buffer (5% sorbitol, 0.5 mM disodium EDTA, and 5 mM histidine-imidazole buffer, pH = 7.5, with the addition of 167 mM PMSF, 9 µg/ml aprotinin, and 5 µl/ml phosphatase inhibitor cocktail [Sigma]). Each sample was homogenized for 5 min at a low-speed setting with an Ultra-Turrax T25 (IKA-Labortechnik) and then centrifuged at 2,000 g for 10 min. Supernatants were retained, and the pellets were rehomogenized in another 2 ml of isolation buffer, recentrifuged, and the resulting supernatants were pooled with the first supernatants.

Equal amounts of the supernatant proteins from the protein lysates were boiled at 60˚C for 20 minutes and loaded to 10% acrylamide gels (Bio-Rad) for electrophoresis. After that, the proteins were transferred to polyvinyl di-fluoride (PVDF) membranes. Non-specific binding was blocked by gently agitating the membranes in 5% non-fat milk and 0.1% Tween in PBS (PBST) for 1 hour at room temperature. Blots were subsequently incubated in 5% bovine serum albumin (BSA) containing 0.1% Tween with the designated primary antibody (**Table 3.2**) overnight at 4°C with gentle agitation. After PBST washes, the blot was then incubated with the appropriate horseradish peroxidase-conjugated secondary antibody for 1 hour at room temperature with gentle agitation. After PBST washes, the blots were incubated with Pierce™ ECL Western Blotting Substrate (Thermoscientific).

Equal loading of WT and KO kidney protein lysates represented the same percentage of a whole kidney since there is no difference in kidney weight between WT and KO mice (**Fig. 2.3**).

The immunoblot signals were quantitated with the Odyssey Infrared Imaging System (Li-COR). All comparisons were performed on samples run on the same membrane.

Diuretic challenge experiment

The protocol was modified from that described by the group of Ecelbarger (Madala Halagappa, Tiwari et al. 2008, Tiwari, Li et al. 2009). As shown in **Figure 3.2**, 10 weeks old mice were acclimatized for five days in metabolic cages, then administered single intraperitoneal injections of the following three diuretics and their matching vehicle according to the following schedule: 25 mg/kg bodyweight furosemide (day 2), 1.4 mg/kg bodyweight benzamil (day 9) and 25 mg/kg bodyweight hydrochlorothiazide (day 16). Immediately after each injection of diuretic or vehicle, a 4-hour collection of urine was performed. Urine Na^+ concentration was measured as before. Furosemide (Sigma), benzamil (Sigma), hydrochlorothiazide (HCTZ, from Sigma were dissolved in 10% DMSO/1XPBS and had been filter sterilized before use.

Low sodium diet study

Eight week-old mice were placed in metabolic cages for 9 days and placed on custom purified rodent diets (Teklad, Harlan Laboratories). A control diet containing 0.3% sodium (TD.120258) was provided for the first five days and then switched to a sodium-deficient diet containing 0.01% sodium (TD.120259) for the next four days. Urine was collected daily except on the first day after switching to the sodium-deficient diet, when urine was collected every eight hours. This was done to capture transient changes in urine Na^+ excretion rate prior to attainment of a new steady state.

Blood and urine studies

Mouse whole blood was collected through cardiac puncture. The blood was left undisturbed at room temperature for 30 minutes to allow it to clot and the clot was removed by centrifuging at 1,000 x g for 10 minutes in a refrigerated centrifuge. Aldosterone was measured via aldosterone EIA Kit – Monoclonal kit (Cayman Chemical Company). Na^+ concentration was measured with a sodium ion-sensitive microelectrode and urine volume was measured by urine weight.

Study approval

All animal experiments were performed in accordance with NIH guidelines on the use of laboratory animals and were approved by the Institutional Animal Care and Use Committees at the University of Kansas Medical Center.

Data analysis

Data are expressed as means ± standard error of the means (SEM). To compare means between two groups we used two-way, unpaired Student's t-tests, with p-values of <0.05 considered significant. ANOVA was used to test for differences in the diuretic challenge experiment.

3.4 Results

3.4.1 Absence of salt wasting phenotype when claudin-2 null mice were treated with a low salt diet.

Age-matched adult claudin-2 WT and KO mice were placed in metabolic cages and were fed a control diet with normal sodium content (0.3% sodium, 0.8% potassium) for five days. Urine collected daily showed no significant difference in the urine Na^+/creatinine concentration ratio between the WT and KO mice (**Fig. 3.3**). After the five-day acclimatization period, the mice were switched to a matched sodium-deficient diet (<0.01% sodium). Then urine Na^+ was monitored every 8 hours for the first 24 hours and daily thereafter. If the KO mice had a defect in their ability

to maximally conserve Na^+, this should have manifested as a transiently higher Na^+ excretion rate compared to WT, which would return to a steady-state within a few days. To our surprise, we found no difference whatsoever (**Fig. 3.3**)**.** Like WT mice, claudin-2 KO mice were able to fully suppress urinary Na^+ excretion by more than 90%. There was also no difference in the blood pressure (BP), as measured by tail-cuff using volume-pressure recording, or in body weights (**Fig. 3.4**). This suggests that salt wasting in the proximal tubule was completely compensated by increased Na^+ reabsorption elsewhere in the tubule.

3.4.2 Compensatory increase in Na^+ reabsorption in the thick ascending limb of claudin-2 KO mice

To investigate whether there was upregulation in the expression of transcellular Na^+ transporters, we immunoblotted whole-kidney lysates for major renal tubule transcellular Na^+ transport proteins. The protein abundance of total and activated (phosphorylated or cleaved, as appropriate) forms of Na^+-K^+-ATPase, NCC, NKCC2, and ENaC α, β and γ subunits and Na^+-/K^+-ATPase was not different between WT and KO mice. Total NHE3 showed a 23% reduction, and phosphorylated NHE3 showed a 27% reduction in claudin-2 KO kidneys (**Fig. 3.5**). But no difference in protein abundance was detected through immunofluorescence staining (**Fig. 3.6**).

To confirm whether there was a functional increase in the activity of NKCC2 in claudin-2 KO mice, and to test for increased activity of transcellular Na^+ transporters in other nephron segments, we performed a diuretic challenge experiment. Mice were given single intraperitoneal injections of vehicle or diuretic on consecutive days and urine was collected for 4 hours after each injection to determine Na^+ excretion rate**.** This was repeated weekly in the same set of mice with three different diuretics: furosemide, a NKCC2 blocker; hydrochlorothiazide (HCTZ), a NCC blocker; and benzamil, an ENaC blocker. WT mice responded to all three diuretics with a brisk natriuresis, compared to vehicle injection. KO mice had a 40% greater natriuresis in response to furosemide than WT mice (**Fig. 3.7**), indicating that increased activity of the Na-K-2Cl cotransporter, NKCC2,

in the thick ascending limb of Henle was the primary mechanism for compensation. The diuretic response to HCTZ and benzamil was also modestly increased but the difference was not statistically significant (**Fig. 3.8**).

3.5 Discussion

Our results show that claudin-2 KO mice compensate for loss of paracellular Na^+ reabsorption in the proximal tubule by upregulating thick ascending limb transcellular transport. The mechanism of upregulated NKCC2 activity remains to be determined. Because there was no change in expression of the major paracellular and transcellular transport proteins in claudin-2 KO mice, but there was increased natriuresis in response to furosemide, we attribute the compensatory increase in Na^+ reabsorption to a change in the functional activity of NKCC2.

Studies done more than 40 years ago either by free flow micropuncture with saline expansion (Landwehr, Klose et al. 1967), or by tubule microperfusion at varying flow rates (Morgan and Berliner 1969), clearly showed that the loop of Henle increases Na^+ reabsorption in response to the delivered load. More recently, the Cowley and Garvin labs have shown that increase in flow to the thick ascending limb increases generation of superoxide and secondarily reduces bioavailability of nitric oxide, both of which can stimulate NKCC2 activity (Ortiz and Garvin 2002, Juncos and Garvin 2005, Abe, O'Connor et al. 2006, Cabral and Garvin 2011, Hong and Garvin 2012).

An alternative mechanism can be postulated by which high tubular flow rates could increase thick ascending limb Na^+ reabsorption, even in the absence of any change in the surface density and activity of NKCC2. Burg proposed a model in which, if the capacity for Na^+ reabsorption in the thick ascending limb is sufficiently large that it is not rate-limiting, luminal Na^+ concentration will be lowered until it reaches a limiting concentration or "static head" (Burg 1982). In this scenario, increases in tubular flow rate would simply shift the point at which the static head is attained

distally along the thick ascending limb, so that the rate of Na^+ reabsorption in the thick ascending limb will always be equal to the difference between the product of the flow rate and the Na^+ concentration difference between plasma and the lumen at the static head (i.e., Na^+ reabsorption will be proportional to the flow rate).

We also found a small decrease in the protein abundance of NHE3 in the claudin-2 KO kidney. Schnermann et al. reported that claudin-2 KO mice had an approximate 23% reduction in single-nephron GFR, which was attributed to tubuloglomerular feedback (Schnermann, Huang et al. 2013). It is conceivable that the reduced delivery of Na^+ to the proximal tubule might signal to downregulate NHE3, as a mechanism to maintain glomerulotubular balance. However, our data (**Table 4.1**) and that of Muto et al. (Muto, Hata et al. 2010) show no difference in the whole kidney GFR between claudin-2 KO and WT, so at this point we are not able to explain this finding. Alternatively, the increased delivery of salt from the proximal tubule to the macula densa could suppress renin secretion from the juxtaglomerular apparatus, and reduce angiotensin II levels, thereby reducing NHE3 expression. Our analysis of the renin-angiotensin-aldosterone axis revealed that claudin-2 KO mice have a slight reduction in tissue renin expression in the kidney, but normal serum aldosterone levels (**Fig. 3.9**), so it is unclear whether this is the cause.

The finding that NKCC2 activity was increased in claudin-2 null mice also provided evidence as to why natriuresis was paradoxically increased in KO mice (**Fig. 2.6**) after a 2% NaCl challenge. Saline loading, by decreasing proximal tubule Na^+ reabsorption, increases Na^+ delivery to the loop of Henle, where absolute and fractional Na^+ reabsorption are increased, likely mediated by increased flow. In addition, because in this experiment hypertonic saline was used, vasopressin release may also contribute by stimulating NKCC2 activity. As we have shown, our claudin-2 KO mice are already compensating for decreased proximal tubule Na^+ reabsorption at baseline by increased NKCC2 activity. We postulate that this is already maximally stimulated. Thus, KO mice are unable to further increase thick ascending limb Na^+ transport to mitigate an even greater Na^+

load delivered from the proximal tubule with hypertonic saline expansion. Hence KO mice exhibit greater diuresis to hypertonic saline than WT mice.

3.6 Figures and tables

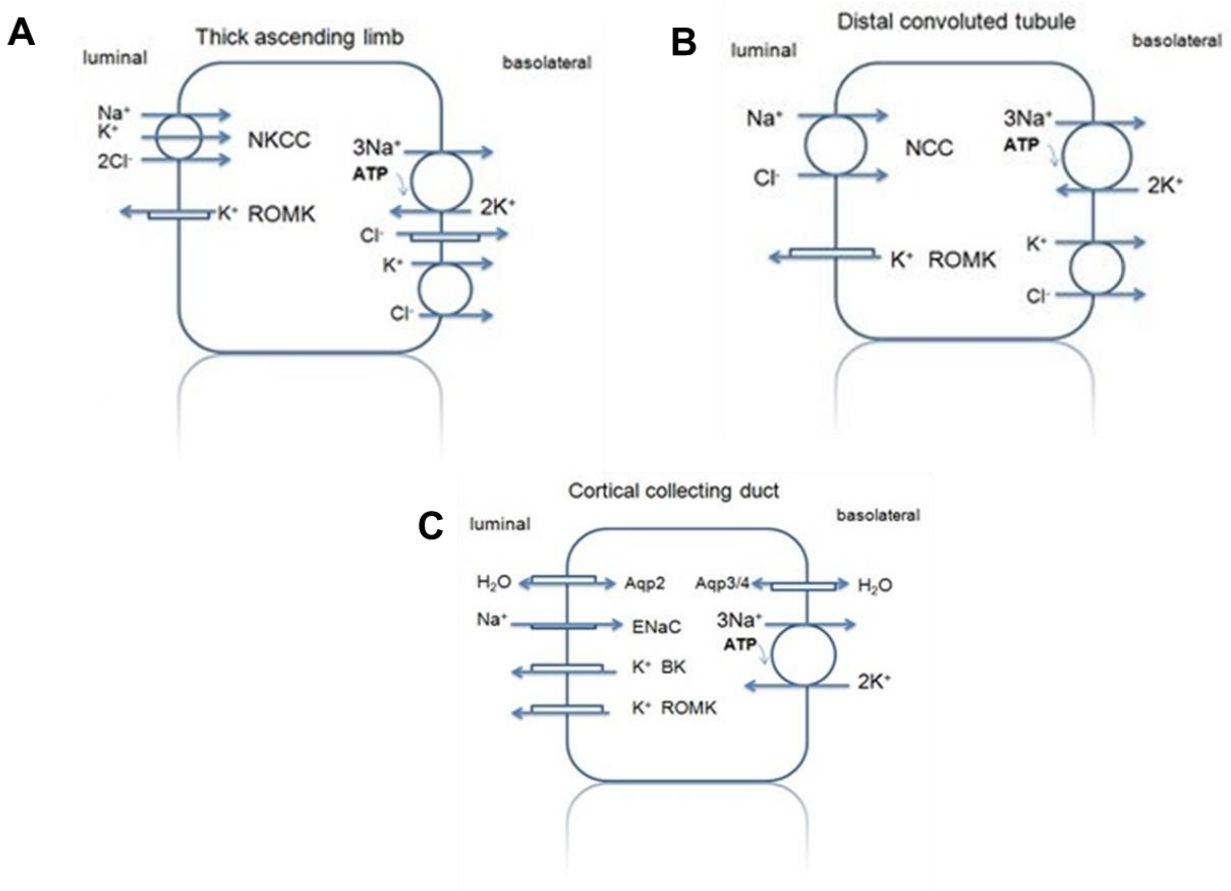

Figure 3.1 Transport pathway for Na^+-Cl^- in the distal nephron. A. Thick ascending limb of Henle cells (TALH). NKCC: Na-K-2Cl cotransporter. B. Distal convoluted tubule (DCT) cells. NCC, thiazide-sensitive Na^+-Cl^- cotransporter. C. Cortical collecting duct (CCD) cells. BK: Maxi K^+ channel; ROMK: renal outer medullary potassium channel.

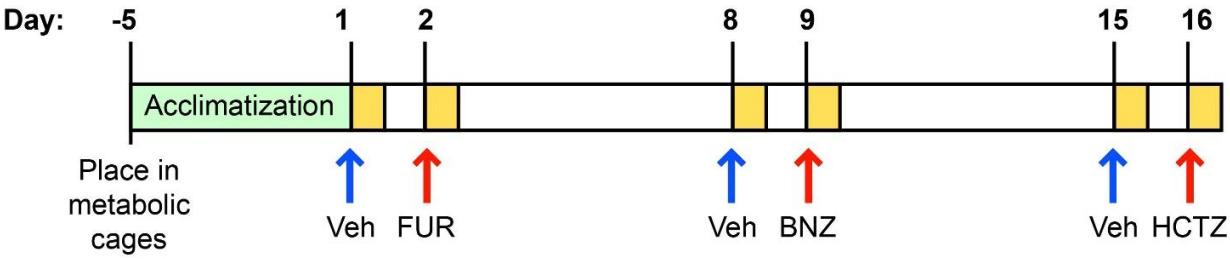

Figure 3.2 Timeline of the diuretic challenge experiment. Yellow boxes denote 4-hour urine collection. Blue arrows indicate i.p. injection of the appropriate vehicle (Veh), either saline or methanol. Red arrows indicate i.p. injection of diuretic. Veh: Vehicle; FUR: furosemide; BNZ: benzamil; HCTZ: hydrochlorothiazide. i.p: intraperitoneal.

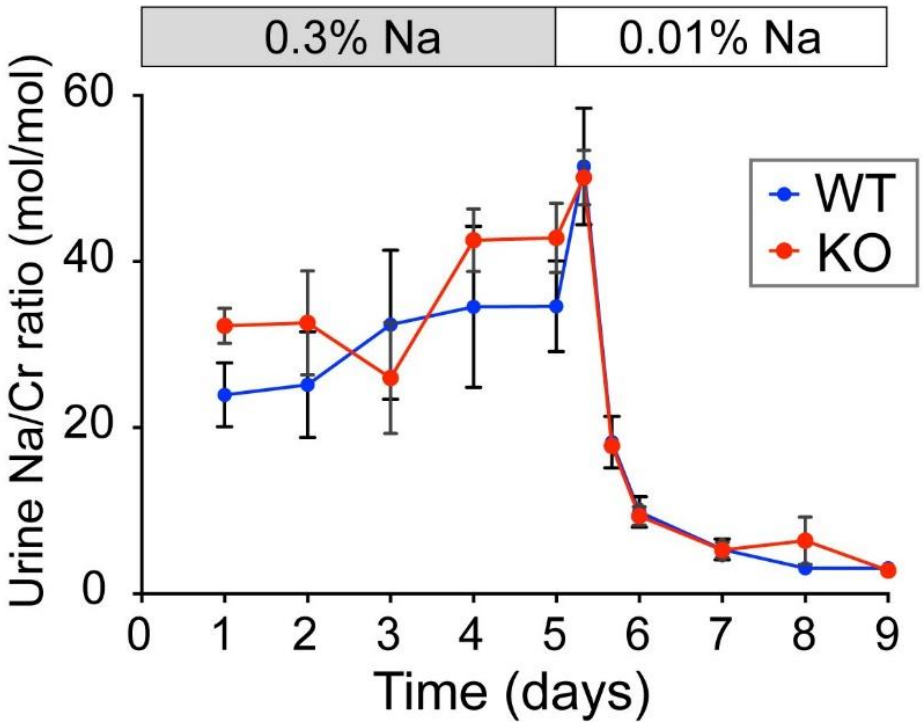

Figure 3.3 Effect of dietary Na^+ depletion on claudin-2 salt handling. Urine Na^+ excretion rate, expressed as the ratio of Na^+ to creatinine concentration (mean ± S.E.M.), is shown in mice on a normal (0.3%) sodium diet (Day 1 to Day 5) followed by a sodium-deficient (0.01%) diet (Day 6 to Day 9). *$p < 0.05$ by paired t-test ($n = 5$ per group).

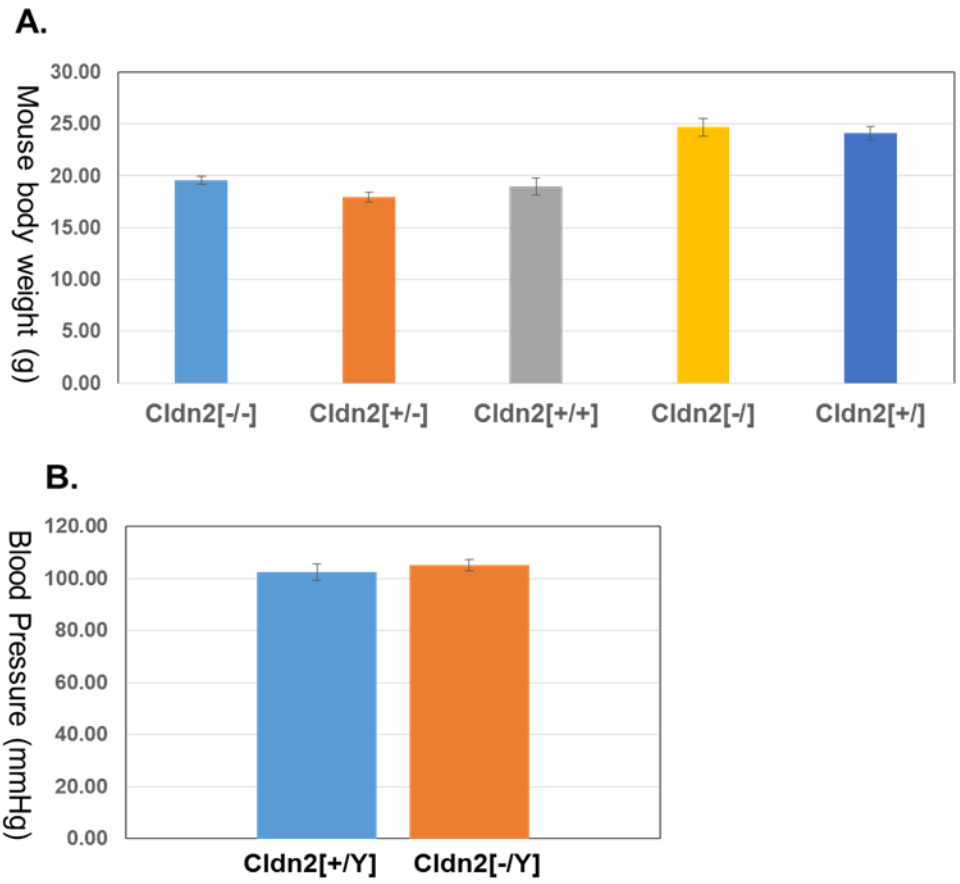

Figure 3.4 Body weight and blood pressure between WT and KO. A. Body weights of claudin-2 homozygous female (Cldn2[-/-]), heterozygous female (Cldn2[+/-]), WT female (Cldn2[+/+]), KO male (Cldn2[-/Y]) and WT male (Cldn2[+/Y]). Results are presented as mean ± S.E.M. n=7-9 per group. B. Tail-cuff blood pressure measurements. Results are presented as mean ± S.E.M, n=5 per group.

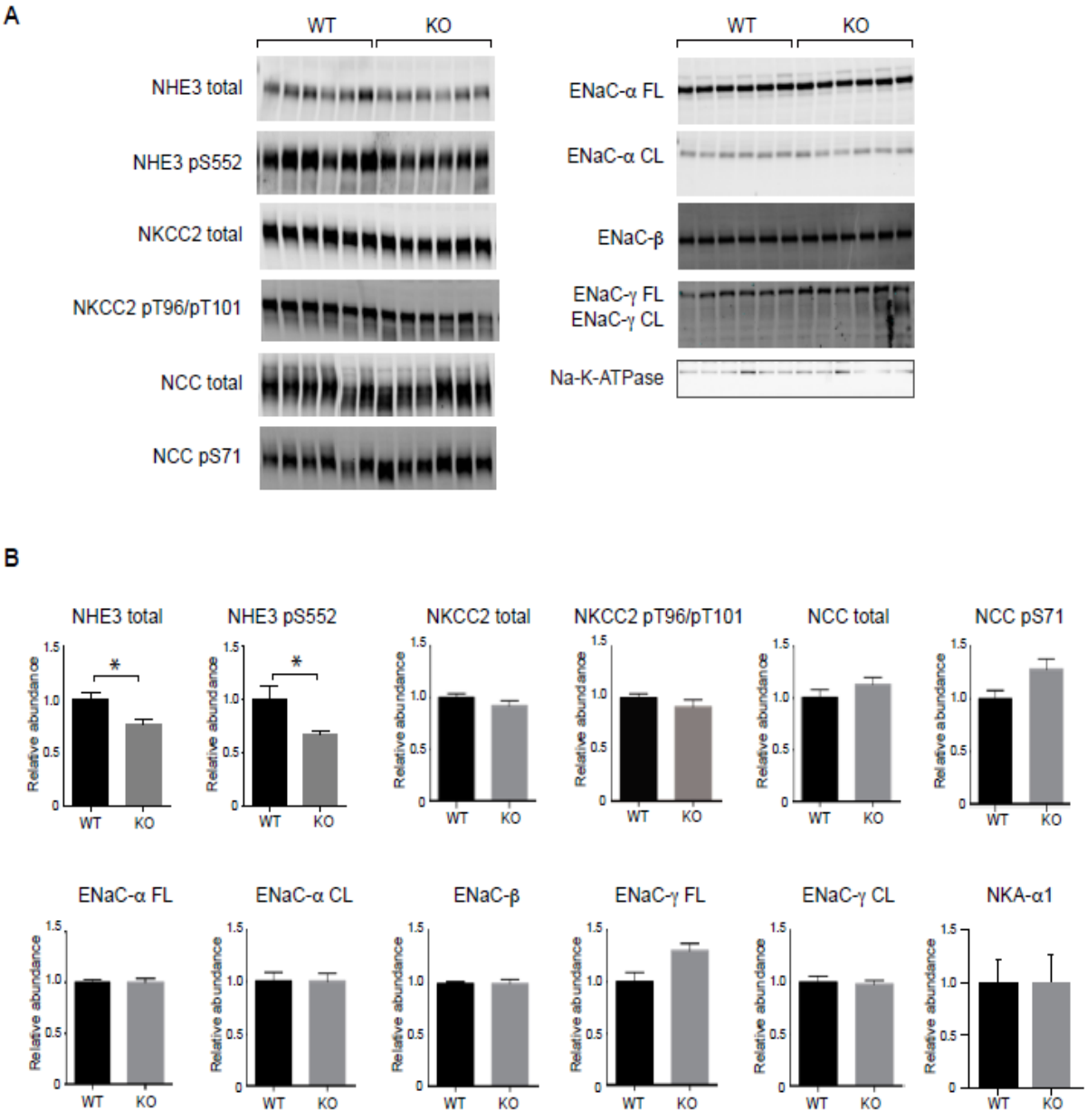

For Legend, see next page

Figure 3.5 Expression of renal transcellular Na^+ transport proteins. A. Immunoblots of whole kidney lysates with antibodies to total or phosphorylated Na-H exchanger (NHE3), thiazide-sensitive electroneutral NaCl cotransporter (NCC), apical Na-K-2Cl cotransporter (NKCC2), 3 subunits of the epithelial Na^+ channel (ENaC-α, -β and -γ) and Na-K-ATPase α1 subunit (NKA-α1. FL: full-length; CL: cleaved. B. Results of quantitation of the immunoblot band densities as a measure of protein abundance which are displayed as individual records with mean ± SEM.*$p < 0.05$.

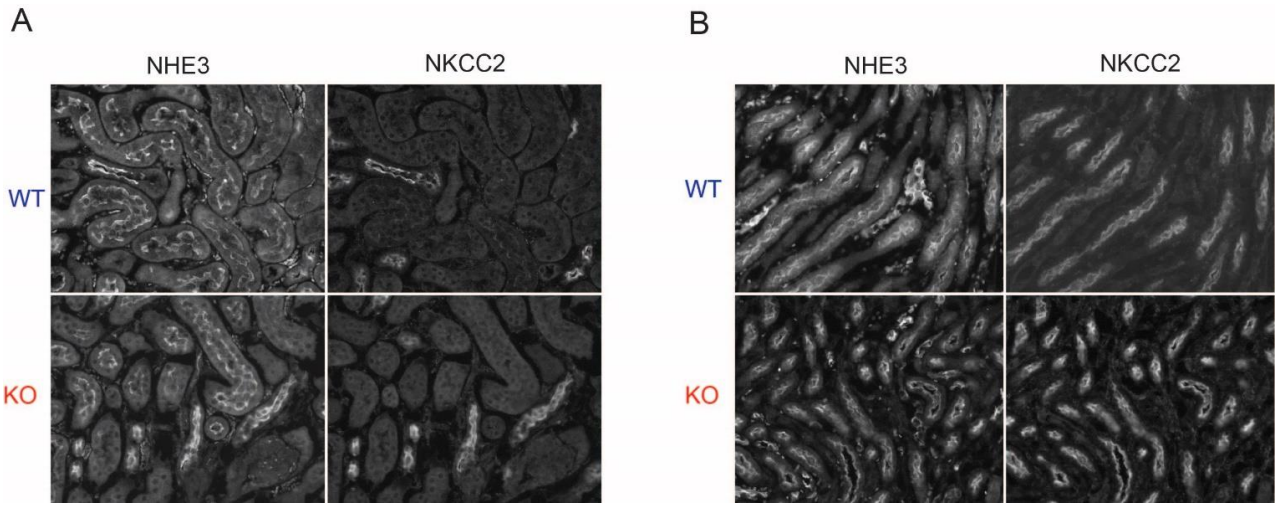

Figure 3.6 Immunofluorescence staining of Na/H exchanger-3 (NHE3) antigen in the renal cortex and medulla. Claudin-2 WT and KO kidneys were perfusion-fixed and cryosections stained for NHE3 or NKCC2. Representative pictures of cortex (A) and medulla (B) showed similar NHE3 expression between WT and KO, both in tubules that do not express NKCC2 (PT S1 and S2 in cortex, S3 and thin descending limbs in medulla), and in tubules that coexpress NKCC2 (cortical and medullary thick ascending limb). Images are representative of findings from 3 mice per group. Magnification of the images: 20X.

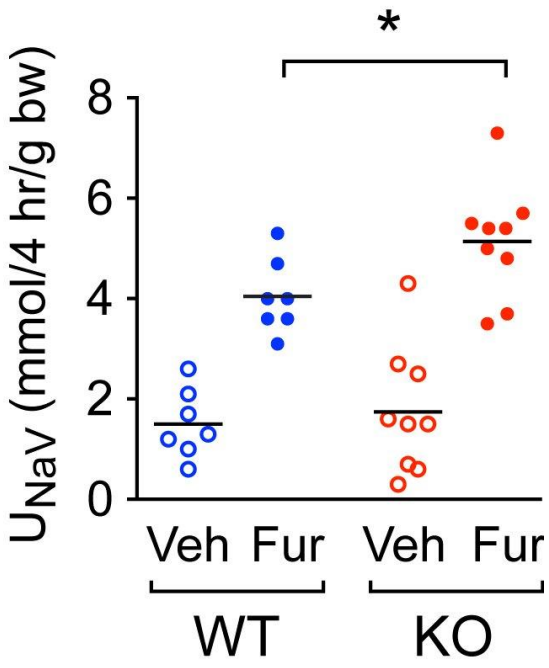

Figure 3.7. Compensatory increase in the activity of NKCC2 in claudin-2 KO mice, as determined by diuretic challenge. Mice were administered vehicle (Veh) I.P. on the 1st day and furosemide 25 mg/kg bw (Fur) on the 2nd day. Urine Na^+ excretion during 4 hours after Fur was greater in KO mice than WT. *$p < 0.05$ by paired t-test (n = 7-9 per group). bw: body weight; I.P: Intraperitoneal; Fur: furosemide. Circles represent individual measurements and horizontal lines indicate the group means.

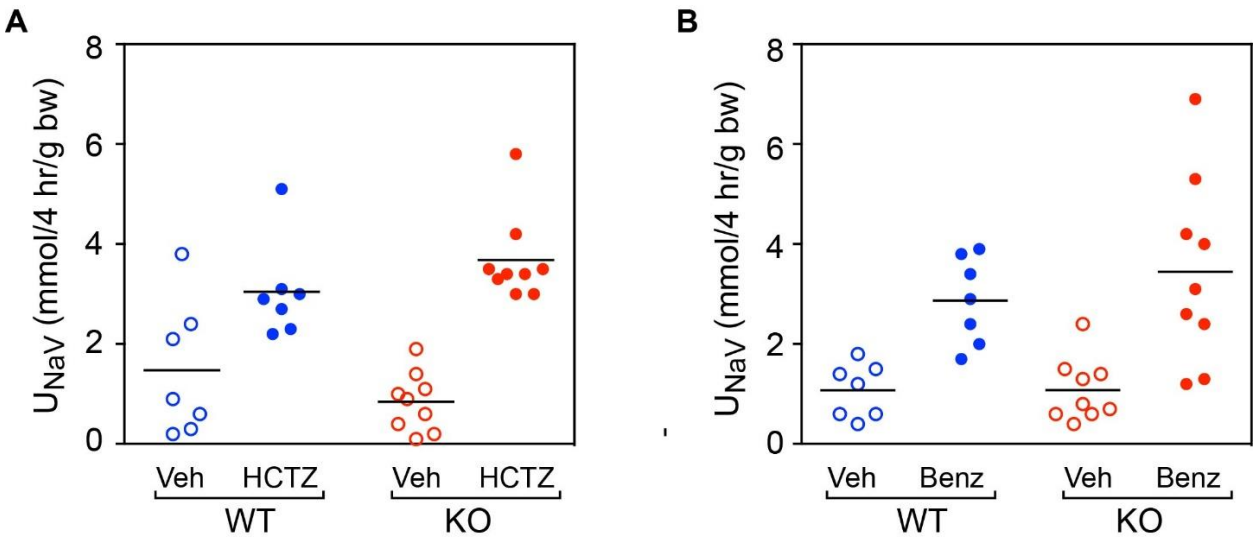

Figure 3.8 Absence of compensatory increase in the activity of NCC and ENaC in claudin-2 KO mice, as determined by diuretic challenge. NCC and ENaC activity in WT and KO mice were assessed by measuring the natriuretic response over 4hr after a single i.p. bolus of hydrochlorothiazide (HCTZ , an NCC blocker, 25 mg/kg) or benzamil (Benz, an ENaC blocker, 1.4 mg/kg), or matching vehicle (Veh) (n = 8 per group). Circles represent individual measurements and horizontal lines indicate the group means. I.P: Intraperitoneal.

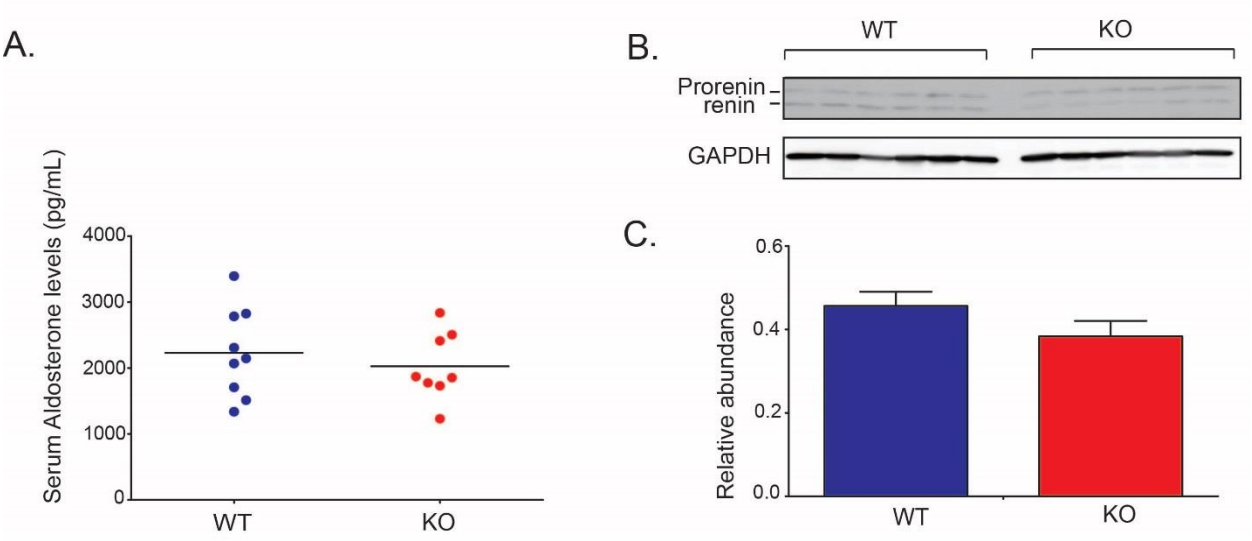

Figure 3.9 Renin and aldosterone levels in claudin-2 WT and KO mice. A. Serum aldosterone levels (p = NS). B. Upper panel: Western blot of the whole kidney lysates probed with a renin antibody, showing distinct bands for prorenin and renin. Lower panel: Immunoblot for GAPDH as a loading control. C. Quantitation of the blots depicted in B. Relative protein abundance (renin + prorenin)/GAPDH is presented as mean ±S.E.M. (p = 0.04).

Antibody Target	Apparent Mobility (kDa)	Protein (µg/lane)	Primary antibody supplier (cat. no.)	Primary antibody host	Primary antibody dilution	Incubation time	Ref
ENaC-α	90 (full length), 25 (cleaved)	40, 20	Johannes Loffing (Univ. of Zurich)	Rb	1:5000	O/N	(Duc, Farman et al. 1994)
ENaC-β	100	30, 10	Johannes Loffing (Univ. of Zurich)	Rb	1:15000	O/N	(Duc, Farman et al. 1994)
ENaC-γ	80-60	40, 20	Lawrence Palmer (Cornell University)	Rb	1:5000	O/N	(Ergonul, Frindt et al. 2006)
NCC	150	40, 20	Alicia McDonough (USC Keck)	Rb	1:5000	O/N	(Nguyen, Lee et al. 2013)
NCC pS71	150	40, 20	Johannes Loffing (Univ. of Zurich)	Rb	1:5000	2 hrs	(Picard, Trompf et al. 2014)
NHE3	83	40, 20	Millipore	Rb	1:1000	O/N	
NHE3 pS552	85	40,20	Santa Cruz	Mu	1:1000	2 hrs	
NKCC	150	20, 10	Christopher Lytle "T4" (Univ. of California at Riverside)	Mu	1:6000	O/N	(Lytle, Xu et al. 1995)
NKCC2pT 96/pT101	150	20, 10	Biff Forbush "R5" (Yale University)	Rb	1:2000	2 hrs	(Flemmer, Gimenez et al. 2002)

Table 3.1 Primary antibodies used for immunoblotting. O/N: Overnight; Rb: rabbit; Mu: mouse

Antibody Target	Primary antibody supplier (cat. no.)	Primary antibody host	Primary antibody dilution	Incubation time
NHE-3	Alicia McDonough (USC Keck)	Rb	1:1000	Overnight

Table 3.2 Primary antibodies used for immunofluorescence. Rb: rabbit.

Chapter IV Claudin-2 null mice exhibit less oxygen consumption efficiency, medullary hypoxia and more susceptibility to acute kidney injury

4.1 Abstract

We found that claudin-2 null mice were able to conserve sodium to the same extent as wild-type mice, even during profound dietary sodium depletion, due to upregulation of the transcellular Na-K-2Cl transporter activity in the thick ascending limb of Henle. Given that transcellular transport has the capacity to fully compensate for loss of paracellular Na^+ reabsorption in the proximal tubule, this raises the fundamental question: What then, if any, is the teleological purpose of paracellular transport in the proximal tubule? Paracellular transport exploits the potential energy from pre-existing transepithelial electrochemical gradients, set up by transcellular transport, to drive transport by passive diffusion without any additional ATP. We therefore hypothesized that the primary purpose of paracellular Na^+ transport is to exploit transtubular electrochemical gradients to drive passive Na^+ reabsorption, and hence to enhance the efficiency of overall renal oxygen consumption. To test this, we determined the ratio between whole kidney Na^+ reabsorption (T_{Na} = GFR X PNa) and oxygen consumption (QO_2 = RBF X A-VO_2) in anesthetized WT (n=8) and claudin-2 null mice (n=9). T_{Na}/QO_2 (mol/mol) in claudin-2 deficient mice was significantly lower than in WT. Renal O_2 extraction was also higher in KO mice. These data show that the efficient utilization of oxygen to reabsorb Na^+ in the kidney is reduced in mice deficient of claudin-2. We then measured O_2 content in the cortex and medulla of claudin-2 null mice and we found that claudin-2 null mice had medullary hypoxia that can be reversed by treatment with furosemide. Furthermore, when subjected to bilateral renal ischemia-reperfusion injury, kidneys of claudin-2 null mice exhibited more severe tubular injury, and this injury could be partially ameliorated by pretreatment with furosemide. Our results indicate that paracellular transport in the proximal tubule is required for efficient utilization of oxygen in the service of sodium transport. Moreover, it suggests that paracellular permeability may have evolved as a general strategy in epithelial tissues to maximize energy efficiency.

4.2 Introduction

Claudin-2 KO mice have impaired salt reabsorption in the proximal tubule. The salt wasted from the proximal tubule was compensated by increased NKCC2 activity in the thick ascending loop of Henle. Transmembrane transport proteins are notable for their heterogeneity (being encoded by ~1000 distinct genes) (Fagerberg, Jonasson et al. 2010, Uhlen, Oksvold et al. 2010) and substrate specificity, and regulation over a remarkable dynamic range by means of gene transcription, translation, protein stability, and trafficking. Given the vast capabilities and flexibility of transcellular transport, a fundamental and highly significant question in biology is: Why did epithelia evolve the capability for paracellular transport?

The kidney has certain features that make it a particularly good organ system in which to answer this fundamental question (McDonough 2012). Although the kidneys receive 25% of cardiac output, the oxygen tension in kidney tissue is low, ranging from 10 mm Hg in the inner medulla to 40 mm Hg in the cortex (Lubbers and Baumgartl 1997). Moreover, unlike all other organs, the kidney cannot enhance its oxygenation simply by increasing renal blood flow. Increasing renal blood flow does indeed increase oxygen delivery; however, it also increases glomerular filtration rate (GFR) and hence tubule salt transport in parallel through glomerulotubular balance, and so it simultaneously increases energy demand and hence oxygen consumption. Thus, under normal conditions the kidney medulla cannot help but live persistently "on the edge of hypoxia." In this rather tenuous situation, the efficiency with which oxygen is utilized by the kidney becomes a critical determinant of kidney oxygen tension. Renal oxygen consumption is determined primarily by the energy required to drive tubular sodium reabsorption (Brodwall 1964), which should be theoretically predictable. Transcellular transport of Na^+ is dependent on the potential energy generated by the Na^+/ K^+-ATPase, which uses one molecule of ATP to directly drive the transport of three Na^+ ions. Ninety-five percent of ATP in the kidney is generated by aerobic respiration (Soltoff 1986), which produces six molecules of ATP for each molecule of O_2 consumed. Thus, the ratio of suprabasal renal oxygen consumption (QO_2) to Na^+ reabsorption (T_{Na}) is predicted to be 1:18 (mol: mol). Alternative pathways for basolateral Na^+

efflux that are indirectly driven by the Na-K-ATPase, such as the electrogenic Na-bicarbonate cotransporter in the proximal tubules, can increase T_{Na} modestly. However, experimentally measured values of QO_2/T_{Na} are in the range of 1:25 to 1:29 (Kiil, Aukland et al. 1961, Thurau 1961, Knox, Fleming et al. 1966), indicating that the kidney uses oxygen much more efficiently than expected.

One explanation that has been proposed for this enhanced efficiency of oxygen usage is that the proximal tubule leverages the excess free energy in solute gradients established by active transcellular transport to drive additional, paracellular reabsorption of Na^+, Cl^-, and other solutes in a purely passive manner (i.e., not requiring additional energy expenditure) (Neumann and Rector 1976, Berry, Warnock et al. 1978). Transcellular reabsorption of Na^+ in the early proximal tubule is coupled largely to either $HCO3^-$ or organic solutes (with a small amount of Cl^- reabsorbed by Cl-base exchange). This, together with near-isosmotic water reabsorption, produces a luminal fluid that, by the time it reaches the late proximal tubule, has relatively high concentrations of Cl^- and low $HCO3^-$. The late proximal tubule is more permeable to Cl^- than $HCO3^-$ (pCl/pHCO3 ranging from 2 to 18 (Schafer, Patlak et al. 1975, Warnock and Burg 1977)). This permits net passive reabsorption of Cl^-, thought to be via paracellular diffusion, and generates a lumen-positive electrical potential (Barratt, Rector et al. 1974). This voltage difference, in turn, provides the driving force for passive reabsorption of Na^+, again presumably via the paracellular pathway. It has been estimated that 32-64% of superficial proximal tubule NaCl reabsorption is passive and paracellular (reviewed in (Moe OW, Berry CA et al. 2000)). It is currently unknown to what extent paracellular transport in the proximal tubule affects renal O_2 utilization *in vivo*, and whether this is physiologically important. The ability to ablate proximal tubule paracellular Na^+ transport by gene targeting of claudin-2 in mice afforded us a unique opportunity to test this directly.

Absence of proximal tubule paracellular reabsorption of NaCl leads to compensatory transcellular Na^+ transport; thus, the NaCl reabsorption by the renal tubule is less efficient. We hypothesize that the balance between Na^+ reabsorption and oxygen consumption will be

disturbed in claudin-2 null mice. Dr. William Welch of Georgetown University conducted a series of experiments to measure the ratio of Na^+ reabsorption to oxygen consumption (T_{Na}: QO_2) and O_2 content in cortex and medulla. We predicted that oxygen consumption efficiency (T_{Na}: QO_2) in claudin-2 null mice is decreased compared to WT.

If, as we expected, there was more oxygen consumption in claudin-2 null kidney, we wanted to further test the hypothesis that the extra energy that was consumed attributes to increased NKCC2 activity. In order to test this hypothesis, we measured the oxygen content in the renal medulla before and after furosemide treatment in WT and claudin-2 null mice. We expected to find that the difference in oxygen content before and after furosemide treat was higher in claudin-2 null mice.

What is the clinical implication of medullary hypoxia in claudin-2 null mice? We first investigated whether claudin-2 null mice suffer from chronic hypoxia by measuring the hypoxia marker HIF-1α and its activation. HIF-1α is a short-lived transcriptional factor that is stable in the nucleus (Wang and Semenza 1993). Its levels are tightly regulated by oxygen concentration via the ubiquitin–proteasome system (Salceda and Caro 1997). It is therefore possible that the mRNA levels of HIF-1α remain unchanged, and the changes in protein levels may not be detected by Western blot. We also used RT-PCR to measure the mRNA levels of other transcripts, such as vascular endothelial growth factor (VEGF), erythropoietin (EPO), glucose transporter 1 (GLUT1), phosphoglycerate kinase (PGK), and transferrin (TRF) that are regulated by HIF-1α. In addition, we measured some oxidative stress markers to test the hypothesis that oxidative stress is caused by renal hypoxia. Peroxisome proliferator-activated receptor gamma coactivator 1-alpha (PGC-1α) is a key regulator of energy metabolism and is highly expressed in kidney tissue. An important role of PGC-1α is to stimulate mitochondrial biogenesis and thereby prevent injury from oxygen depletion. It was reported that PGC-1α was upregulated in tissue hypoxia (Weinberg 2011). For that matter, we also measured the mRNA expression of PGC-1α in the claudin-2 WT and KO kidneys. AMP-activated protein kinase (AMPK) is ubiquitously expressed and functions as an

intracellular fuel sensor by maintaining energy balance. AMPK activation requires phosphorylation at Thr-172 in the activation loop and is regulated by increased cellular AMP and decreased ATP. In other words, the ratio of pAMPK/AMPK will increase in hypoxic tissues. Therefore, we also performed western blots of pAMPK and AMPK in claudin-2 WT and KO mice.

If there is increased oxygen consumption in claudin-2 KO kidneys, we expect claudin-2 null mice to be more susceptible to oxygen/ATP depletion. In order to test this hypothesis, we chose to perform ischemia-reperfusion surgery on claudin-2 WT and KO mice to induce acute kidney injury. We hypothesized that claudin KO mice would show more damage than WT mice. We evaluated the severity of the acute kidney injury in WT and KO mice with three assays: 1) measurement of plasma blood urea nitrogen (BUN) and creatinine, which are indicators of renal function; 2) quantification of mRNA expression and protein expression of kidney injury marker (KIM1), which is a novel biomarker for human renal proximal tubule injury (Han, Bailly et al. 2002); and 3) evaluation of the degree of renal damage in kidneys stained with the Periodic Acid Schiff (PAS) method. The typical renal tubular damage due to ischemia includes severe tubular lysis, loss of brush border, and sloughed debris in tubular lumen space (**Fig. 4.1**). In ischemic acute kidney injury, the most severely injured site is the S3 segment of proximal tubules located at the outer stripe of the outer medulla. Dr. Timothy Fields, a very experienced and professional pathologist who has practiced more than 20 years in renal pathology at the University of Kansas Medical Center, graded the severity of the tubular injury in both WT and KO mice.

4.3 Materials and Methods

Immunoblotting

HIF-1α nuclear and cytosol fractions of claudin-2 WT and KO kidney lysates were prepared with NE-PER nuclear and cytoplasmic extraction reagents (Thermoscientific). Equal amounts of the supernatant proteins from the lysates were boiled at 60˚C for 20 minutes, resolved by

electrophoresis in 10% acrylamide gels (BioRad), and then transferred to polyvinyl di-fluoride (PVDF) membranes. Non-specific binding was blocked by gently agitating the membranes in 5% non-fat milk and 0.1% Tween in PBS (PBST) for 1 hour at room temperature. Blots were subsequently incubated in 5% bovine serum albumin (BSA) containing 0.1% Tween with the designated primary antibody (**Table 4.2**) overnight at 4°C with gentle agitation. After PBST washes, the blot was then incubated with the appropriate horseradish peroxidase-conjugated secondary antibody for 1 hour at room temperature with gentle agitation. After PBST washes, the blots were incubated with Pierce™ ECL Western Blotting Substrate (Thermoscientific).

Equal loading of WT and KO kidney protein lysates represented the same percentage of a whole kidney since there is no difference in kidney weight between WT and KO mice (**Fig. 2.3**). The immunoblot signals were quantitated with the Odyssey Infrared Imaging System (Li-COR). All comparisons were performed on samples run on the same membrane.

Urine MDA assay

Urinary malondialdehyde (MDA) was determined by measurement of thiobarbituric acid reactive substances (TBARS). Aliquots of 500 µl of urine or MDA standards were mixed with 500 µl thiobarbituric acid (1%, pH 1.5) and boiled for 30 minutes. After cooling to room temperature, its absorbance was measured at 540nm with a microplate reader.

\The final concentration of MDA was expressed as the difference between TBARS and the blank in order to diminish the interference of urine chromogens (Zhou, Kato et al. 2006).

Immunohistochemistry staining

In a separate set of WT and claudin-2 KO mice, kidneys were perfusion-fixed via the heart with 4% paraformaldehyde in PBS. The fixed tissues were cryoprotected by overnight incubation with 30% sucrose in PBS, embedded in Tissue-Tek O.C.T. compound (Sakura Finetek, Torrance,

CA) and frozen on dry ice. Cryosections (10 µm) from WT and KO animals were sliced and transferred to the same Superfrost Plus-charged glass slide (Fisher) for direct side-by-side processing and viewing. For immunohistochemistry labeling, the sections were rehydrated and heated in a microwave oven in 0.01 mol/L citrate buffer, pH 6.0 for 10 minutes, and were blocked with 10% goat serum/PBS at room temperature for one hour. Primary antibody (**Table 4.3**) was then added to the sections and incubated overnight at 4°C with 0.2% BSA/PBS. After application of the primary antibody, positive staining was detected using a HRP-conjugated secondary antibody with DAB substrate (Vector Labs, Burlingame, CA, USA) for peroxidase staining. The sections were counterstained with Harris hematoxylin.

RNA extraction and quantitative real-time PCR

RNA was extracted from tissue homogenate with TRI Reagent (Sigma-Aldrich). First-strand cDNA was synthesized using iScript Reverse Transcription Supermix for RT-PCR (Bio-Rad). Quantitative real-time PCR was performed using a CFX96 Touch™ Real-Time PCR Detection System and iTaq™ Universal SYBR® Green Supermix (Bio-Rad) with the primers indicated in **Table 4.4**. Expression levels were normalized to cyclophillin B levels.

Renal oxygen consumption measurement

The ratio of net tubular Na^+ transport to O_2 consumption (T_{Na}: QO_2) in the kidney was determined using previously described techniques (Welch, Baumgartl et al. 2003, Welch, Mendonca et al. 2003, Welch, Blau et al. 2005). Adult mice (~12 weeks old) were anesthetized with isoflurane. The jugular vein, femoral artery, and renal vein were cannulated and urine collected by suprapubic catheter to monitor flow rate (V) and determine Na^+ concentration (UNa). Warmed 0.154 M NaCl/1% albumin (2% body weight) was infused to replace surgical blood loss. To determine the glomerular filtration rate (GFR) and renal blood flow (RBF), ^{14}C-inulin and ^{3}H-para-aminohippuric acid (PAH) were infused. After 30 minutes of equilibration, urine was collected

over two 30-minute periods, blood was sampled at the midpoint of each period for liquid scintillation counting, and clearances were calculated. At the end of the study, blood was drawn from the femoral artery and renal vein for measurement of O_2 (AO_2 and VO_2, respectively) in a blood gas analyzer (i-STAT1, Abbott Labs, Abbott Park, IL, USA) and used to calculate total O_2 content. T_{Na} is the total kidney transport of Na^+, and is equal to filtered Na^+ minus excreted Na^+: T_{Na} = [GFR X plasma Na^+ concentration (PNa)] – Urine Na^+ excretion (UNaV). Renal oxygen consumption (QO_2) was calculated by the renal extraction of O_2 factored by RBF, where the renal extraction of O_2 was calculated by arterial-venous difference. Thus, QO_2 = RBF X [AO_2 –VO_2]. The efficiency of O_2 utilization for the transport of Na^+ (not corrected for basal metabolic rate) was calculated by the ratio of T_{Na}/QO_2.

Measurement of intrarenal oxygen tension

The intrarenal partial pressure of O_2 (pO_2) was measured with a Clark-type O_2 microelectrode (OX-10, Unisense) with tip diameter of 8-12 µm, connected to an ultra-high impedance picoammeter (Unisense, Aarhus, Denmark). Electrodes were inserted into the immobilized kidney of anesthetized mice and advanced to the outer or inner cortex (0.5 – 1.0 µm) or to the outer medulla (1.5 µm). The electrodes were stabilized and pO_2 was recorded for two to four minutes.

Bilateral renal ischemia-reperfusion injury model

Eight to ten week old mice were anesthetized with xylazine (10 mg/kg intraperitoneal) and ketamine (90-120 mg/kg intraperitoneal). The kidneys were exposed through flank incisions and both renal pedicles were occluded with microaneurysm clamps (Fine Science Tools, Foster City, CA). The body temperature was maintained between 36.3°C and 36.5°C using a rectal temperature probe and thermostatically controlled homoeothermic blanket system (Harvard Apparatus) set to 36.5°C. After exactly 23 minutes, the clamps were removed, reperfusion of the

kidneys was confirmed visually, and the mice were sutured up. They were given 0.5 ml of warm sterile 0.9% saline subcutaneously at the end of the operation and before they recovered from anesthesia. Blood was collected immediately before and at 24 hours and 48 hours after the surgery by tail nicking. One kidney from each mouse was harvested for RNA isolation and RT-PCR for Kidney Injury Molecule 1 (KIM-1). The other kidney was fixed with 4% buffered paraformaldehyde and paraffin-embedded sections stained with Periodic Acid Schiff (PAS) for histological scoring. Separate groups of WT and KO mice underwent furosemide pre-treatment before ischemia-reperfusion surgery. In these groups, the mice were administered single intraperitoneal injections of 25 mg/kg bodyweight furosemide in 0.5 mL total volume of saline two hours prior to the start of surgery. Furosemide-treated mice were given 1 ml of saline subcutaneously at the end of surgery.

The method for quantifying acute kidney injury was adapted from that previously reported (Wei and Dong 2012, Zhang, Gillihan et al. 2013). Briefly, kidney images were acquired (Spot v5.0; Diagnostic Instruments, Sterling Heights, MI, USA) from mid-sagittal sections of whole kidneys stained by the PAS method. The total kidney area and areas of tubular necrosis were measured using ImageJ64 (Schneider, Rasband et al. 2012). The acute injury index was calculated by dividing the injured area by the total area.

Data Analysis

Statistical analyses were performed with SPSS Statistics software, version 22 (IBM, NY, USA). Data are expressed as mean ± SEM. Student's two-tailed t-test was used to test differences between means in two-group comparisons. ANOVA was used to test for differences in multi-group experiments. Mixed factor ANOVA was used to test the between-subjects effect of genotype (WT vs. KO) and the within-subjects effect of diuretic (furosemide vs. vehicle) on outer medullary pO_2. Because a significant (genotype x diuretic) interaction was detected, simple effects analysis was then performed to determine the effect of furosemide within each genotype and the effect of

genotype within vehicle- and furosemide-treated conditions. The p value was multiplied by the number of tests performed within each factor to protect against familywise Type I error due to multiple comparisons (an application of Bonferroni's procedure). Similarly, mixed ANOVA followed by simple effects analysis was used to test the effect of genotype on BUN within the time points of 0, 24 and 48 hours, as well as serum creatinine, KIM1 levels and kidney injury score at 48 hours after bilateral renal ischemia-reperfusion injury, as well as the effect of furosemide pretreatment vs. control within the WT mice group and the KO mice group at each time point. P values <0.05 were considered significant.

Study approval

All animal experiments were performed in accordance with NIH guidelines on the use of laboratory animals and were approved by the Institutional Animal Care and Use Committees at the University of Kansas Medical Center, Georgetown University Medical Center, and the University of Southern California.

4.4 Results

4.4.1 Claudin-2 null mice exhibit lower efficiency of oxygen utilization and renal medullary hypoxia

Despite the substantial defect in proximal tubule paracellular Na^+ transport, it is remarkable that claudin-2 KO mice are able to maximally conserve Na^+ even on a severely sodium-restricted diet. We speculated that this might be due to a compensatory increase in the activity of transcellular Na^+ transporters further downstream along the nephron. This raises the obvious question of what physiological role paracellular transport plays. If transcellular transport can completely compensate for paracellular transport, even under the most extreme conditions, does this come with any cost to the organism, or is paracellular transport simply a vestigial process? We hypothesized that paracellular transport in the proximal tubule exists to exploit transtubular

electrochemical gradients to drive passive transport of NaCl and hence to maximize the efficiency with which this tubule segment utilizes O_2 to reabsorb NaCl. Therefore, if the burden of NaCl reabsorption in claudin-2 KO mice is shifted distally, our hypothesis predicts that these mice will have increased renal O_2 consumption.

To test this hypothesis, we determined the ratio between whole kidney Na^+ reabsorption (T_{Na}) and oxygen consumption (QO_2) in anesthetized WT and KO mice. T_{Na} was calculated from the difference between the filtered load of sodium (GFR, determined from inulin clearance, multiplied by PNa) and the renal Na excretion (UNaV). QO_2 was determined from the renal blood flow (assessed by PAH clearance) factored by the arterial-venous O_2 difference. GFR, RBF and mean arterial pressure (MAP) were not different between the groups. T_{Na} was also similar between the WT and KO, whereas QO_2 was 80% higher in KO mice ($p < 0.005$)), resulting in a nearly 40% lower T_{Na}/QO_2 ($p < 0.01$) in KO mice **(Table 4.1 and Fig. 4.2).**

To investigate the effect of this increase in oxygen consumption on intrarenal oxygenation, we measured pO_2 in the outer medulla and cortex with an O_2-sensing microelectrode. In the outer medulla, claudin-2 KO kidneys exhibited a lower pO_2 than WT kidneys ($p = 0.01$) (**Fig. 4.3.B**), whereas in the cortex, claudin-2 KO and WT had similar pO_2 **(Fig. 4.3A).** Based on the results of our previous study that showed increased NKCC2 activity in the thick ascending limb of Henle, we can conclude that this increased activity comes with the price of increased oxygen consumption in the outer medulla. We hypothesized that furosemide treatment would block the extra oxygen utilization by NKCC2 in claudin-2 null mice. After treatment with furosemide, the pO_2 was not changed in the cortex of both genotypes. However, the pO_2 increased in the outer medulla of both genotypes **(Fig. 4.3B)**. As we expected, there was a 2.7-fold greater increase in pO_2 in KO compared to WT mice ($p < 0.005$ by paired t-test) **(Fig. 4.3C)**, so that the pO_2 after furosemide was no longer significantly different between KO and WT animals ($p = 0.068$).

4.4.2 Absence of hypoxia markers in claudin-2 null mice

To investigate whether there is any upregulation in hypoxia markers, we measured nuclear HIF-1α protein expression and mRNA expression of HIF-1α targeted genes. Similar to WT kidneys, we were unable to detect HIF-1α in the claudin-2 null kidney nucleus lysates **(Fig. 4.4B).** There was no difference in the expression of HIF-1α target genes such as EPO, VEGF, GLUT1 and TRF between WT and KO **(Fig. 4.4A)**. There was also no upregulation of oxidative stress markers, PGC-1α and ratio of pAMPK/AMPK in claudin-2 null mice **(Fig. 4.5 and 4.6)**.

4.4.3 Claudin-2 null mice are more susceptible to ischemic injury

Since claudin-2 null mice exhibit lower efficiency of oxygen utilization and renal medullary hypoxia, we hypothesized that claudin-2 null kidneys would be more susceptible to kidney injury from oxygen/ATP depletion. To test this hypothesis, we subjected WT and KO mice to bilateral renal ischemia-reperfusion injury (IRI). As shown in **Figure 4.7**, BUN increased in both WT and KO mice at 24 hours and 48 hours following reperfusion. However, the extent of elevation at both time points was much higher in KO compared to WT mice ($p < 0.005$). We hypothesized that the increased susceptibility of KO mice to ischemic injury was due to increased activity of and hence oxygen consumption by NKCC2, so we tested whether pretreatment with furosemide 2 hours before ischemia could prevent injury. Consistent with this hypothesis, BUN elevation in KO mice at 24 and 48 hours after reperfusion was ameliorated by furosemide ($p < 0.01$), whereas the diuretic had no effect in WT mice. The plasma creatinine concentration was also significantly higher in the KO compared to WT mice at 48 hours following reperfusion (1.45 mg/dl vs 0.33 mg/dl, $p < 0.005$), and was reduced by furosemide pretreatment in KO mice ($p < 0.05$) but not in WT **(Fig. 4.8A).** KIM-1 is a commonly used early marker of kidney injury and correlates positively with the degree of renal damage in both acute and chronic injuries (Han, Bailly et al. 2002, Waanders, van Timmeren et al. 2010). The mRNA level of KIM-1 showed identical trends to that of BUN and creatinine **(Fig. 4.8B),** and KIM-1 protein expression by immunohistochemistry showed consistent findings **(Fig. 4.9).**

Morphological studies at 48 hours showed evidence of tubular injury (e.g., tubular necrosis, sloughed cells, mitotic figures, and luminal casts) that were most readily identified within the S3 segment of the proximal tubule. In WT mice, only a portion of the renal tubules (~50%) in the outer medulla showed morphological features of ischemic injury such as loss of the brush border, flattening of the epithelium, tubular necrosis, and luminal casts, while the renal cortex was almost completely intact. However, in KO mice, almost all the renal tubules (~95%) in the outer medulla exhibited ischemic injury, and tubule injury, especially within proximal tubules, was also observed in parts of the renal cortex **(Fig. 4.10).** We graded the severity of the renal tubular injury by estimating the proportion of the entire kidney area that was involved. The KO kidneys had a larger area of injury compared to WT ($p < 0.005$). Finally, pretreatment with furosemide had no significant effect on the severity of injury in WT mice, but significantly ameliorated the injury in KO mice ($p = 0.018$, **Fig. 4.10 and Fig. 4.11**). These findings suggest that claudin-2 null mice are more susceptible to acute ischemic renal injury because of upregulated NKCC2 activity in the thick ascending limb and hence increased outer medullary oxygen consumption.

4.5. Discussion

The shift in burden of Na^+ reabsorption from the proximal tubule to the thick ascending loop of Henle in claudin-2 KO mice occurs at the expense of increased oxygen consumption. Viewed thermodynamically, the free energy cost of transporting Na^+ uphill is dependent on the transtubular concentration gradient (specifically, it is proportional to the negative logarithm of the concentration gradient (Stephenson, Tewarson et al. 1974)). Because of the large water permeability of the proximal tubule, there is almost no detectable transtubular concentration gradient for Na^+ in this nephron segment (Windhager and Giebisch 1961, Barratt, Rector et al. 1974)), whereas the tubular fluid/plasma Na^+ concentration ratio approaches 0.2 to 0.4 when measured by micropuncture at the end of the thick ascending loop of Henle (Burg and Good 1983). Thus, Na^+ reabsorption in the thick ascending loop of Henle necessarily requires more energy

and hence greater O_2 consumption than the same amount of reabsorption occurring in the proximal tubule.

The consequence of the increased O_2 consumption was that the outer medullas of claudin-2 KO mice were more hypoxic than those of WT mice even at baseline**.** We expected upregulation of chronic hypoxia markers in claudin-2 KO kidneys. However, there was no change in hypoxia-inducible factor-1, indicated by lack of increased HIF-1 protein translocation to the nucleus, and no difference in RNA expression of HIF-1 target genes such as VEGF, EPO, GLUT-1 and PGK between WT and KO. There was also no change in reactive oxygen species, PGC-1α and the ratio of pAMPK/AMPK. Our explanation is that the medullary hypoxia in claudin-2 null mice is relatively mild compared to the hypoxic conditions reported in the previous studies describing upregulation of HIF-1α (Semenza 2000). The small reduction of pO_2 that is observed in our claudin-2 null mice is not big enough to induce HIF1α activation. Nevertheless, this mild hypoxia reflects a serious deficit in the ability of the kidney to reduce O_2 consumption to match delivery. This is demonstrated by our finding that a modest reduction in O_2 delivery, imposed by brief (23 minutes) renal artery clamping, was sufficient to dramatically tip the delicate balance between O_2 delivery and consumption, and greatly increased the susceptibility of the KO mice to ischemic tubule injury. When furosemide was given to claudin-2 KO mice, there was a 2.7-fold greater increase in pO_2 in the outer medulla compared to WT mice. Furosemide pretreatment before ischemic reperfusion injury partially alleviated the injury, presumably by inhibiting NKCC2 and hence increasing pO_2 in the outer medulla. It is conceivable that inherited or acquired variations in the proximal tubule paracellular transport pathway in humans might similarly affect the clinical susceptibility to acute ischemic kidney injury. HIF-1α was reported to be protective in ischemic reperfusion surgery (Jamadarkhana, Chaudhary et al. 2012). Ischemic preconditioning can be a protective factor for the subsequent acute ischemic injury due to pre-upregulated HIF1α activation and the subsequent enhancement of renoprotective gene expression (Goldfarb, Rosenberger et

al. 2006). However, the absence of upregulation of HIF-1α suggests that the severity of the acute kidney injury is not influenced by HIF-1α.

The findings described here may provide insights into the evolutionary purpose of tight junctions. Transport of solutes and water by epithelia plays a critical role in the homeostasis of body fluid compartments in higher organisms and consumes a substantial amount of energy. Why epithelia evolved to have a leaky paracellular pathway is unknown. One possibility is that paracellular transport simply adds to the capacity of transcellular transport. However, this seems to add unnecessary complexity since transcellular transport proteins are so abundant and versatile already. Here we found that the defect in paracellular sodium reabsorption in the proximal tubule of the kidney in claudin-2 null mice can be completely compensated under even the most extreme circumstances that could be encountered *in vivo* (near-zero sodium diet), confirming that the contribution of paracellular transport is dispensable. The results that we report here suggest a more nuanced reason for the existence of a paracellular transport pathway, namely that it evolved to enhance the efficiency of energy and oxygen utilization by the renal tubule epithelium. We show that the cost of losing paracellular transport is increased oxygen consumption, tissue hypoxia, and increased susceptibility to ischemic injury.

4.6 Figures and tables

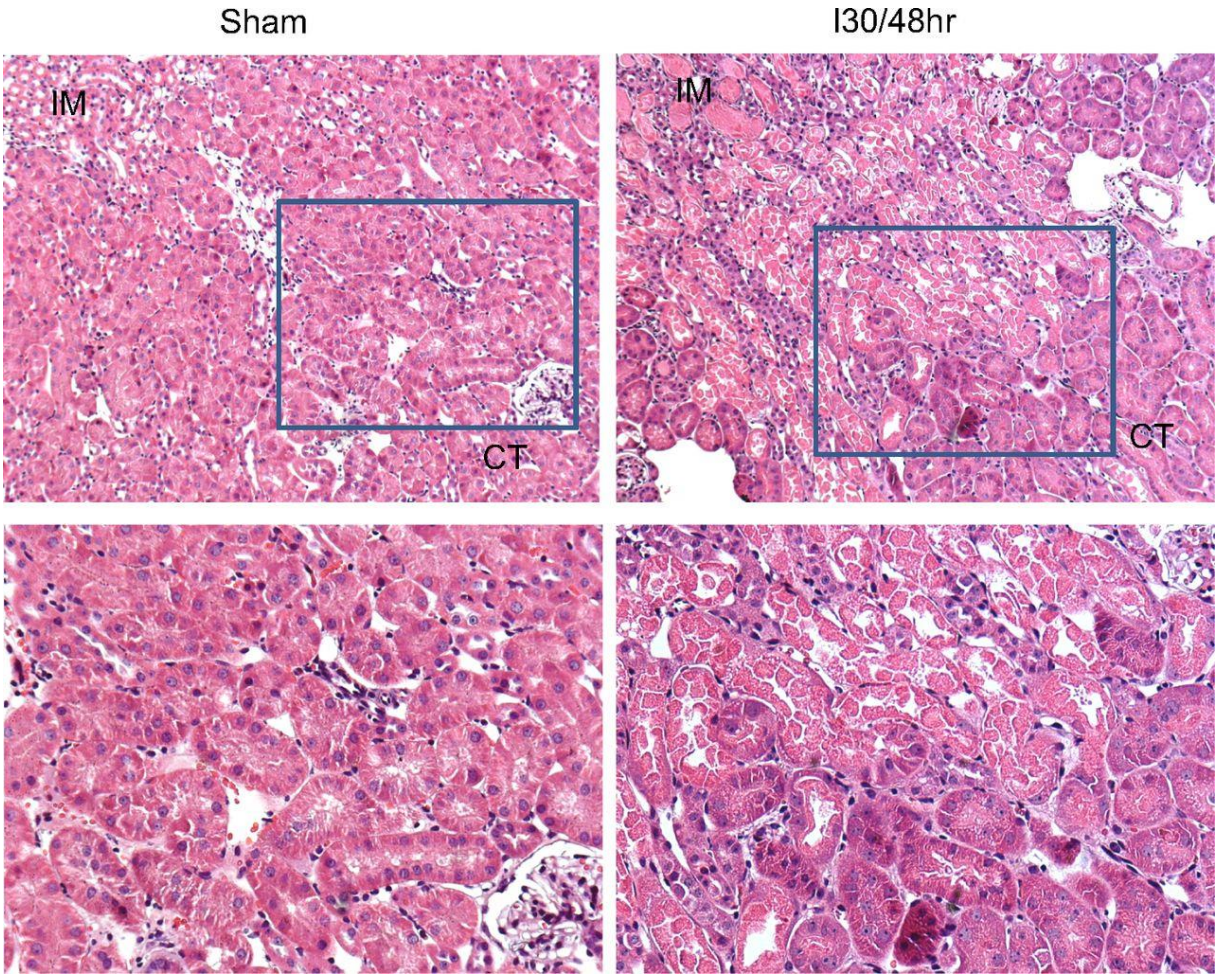

Figure. 4.1 Renal histology after ischemic acute kidney injury. Top: kidney tissues from C57BL/6 mice with 30 min of bilateral renal ischemia and 48 h of reperfusion or sham operation were stained by hematoxylin and eosin. IM, inner medulla. CT, cortex. Bottom: enlarged images of boxed area in the upper panels (Wei and Dong 2012).

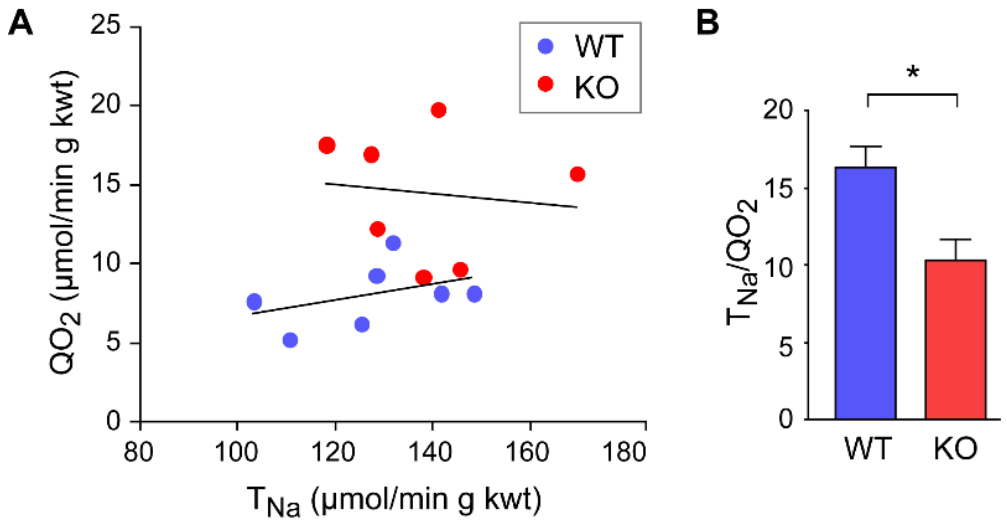

Figure 4.2 Role of claudin-2 in renal O_2 utilization. A. Relationship between T_{Na} and QO_2 in individual claudin-2 WT and KO mice, expressed per gram of kidney weight (g kwt). B. The efficiency of oxygen utilization for renal Na^+ transport, T_{Na}/QO2, calculated from the data in A (n=7 per group). *p < 0.01 by t-test.

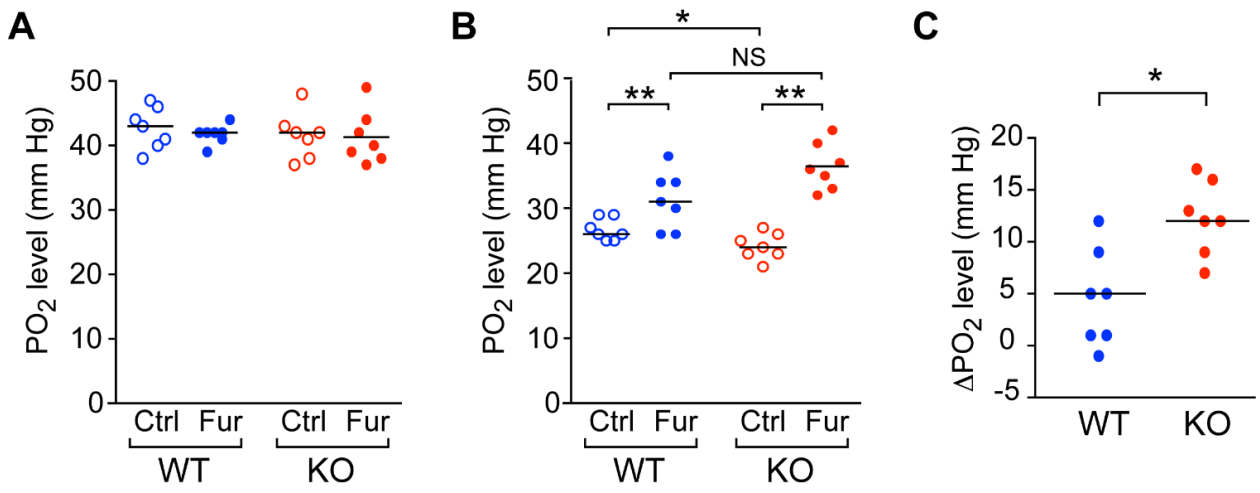

Figure 4.3 Effect of claudin-2 KO on intrarenal pO_2, as measured with O_2-sensing microelectrodes. A, B. pO_2 in kidney cortex (A) and outer medulla (B) at baseline (Ctrl) and after treatment with furosemide (Fur). *p = 0.01, **p < 0.001; NS, non-significant by ANOVA. C. Change in pO_2 (ΔpO_2) in the outer medulla induced by furosemide (n=7 per group). *p < 0.005 by t-test.

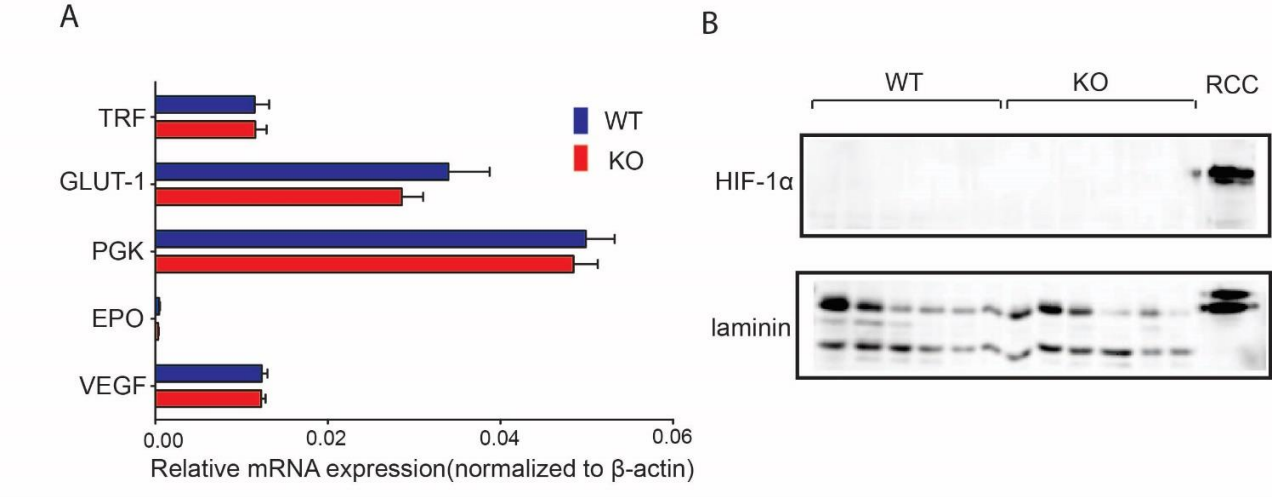

Figure 4.4 Absence of HIF-1α activation in claudin-2 KO kidney. A. Quantification of whole kidney mRNA levels of HIF-1α target genes in claudin-2 WT and KO mice, relative to β-actin. TRF: transferrin; GLUT-1: Glucose transporter 1; PGK: Phosphoglycerate kinase; EPO: erythropoietin; VEGF: vascular endothelial growth factor. The fold change is presented as mean ± S.E.M. B. Western blots of kidney nuclear tissue lysate from WT and KO mice. Upper panel is probed with rabbit-anti-HIF-1α antibody. The last lane contains human renal cell carcinoma lysate (RCC) as a HIF-1α expression control. HIF-1α is absent in both WT and KO kidney at baseline. Lower panel shows the same blot stripped and reprobed with rabbit anti-laminin as a marker for nuclear proteins.

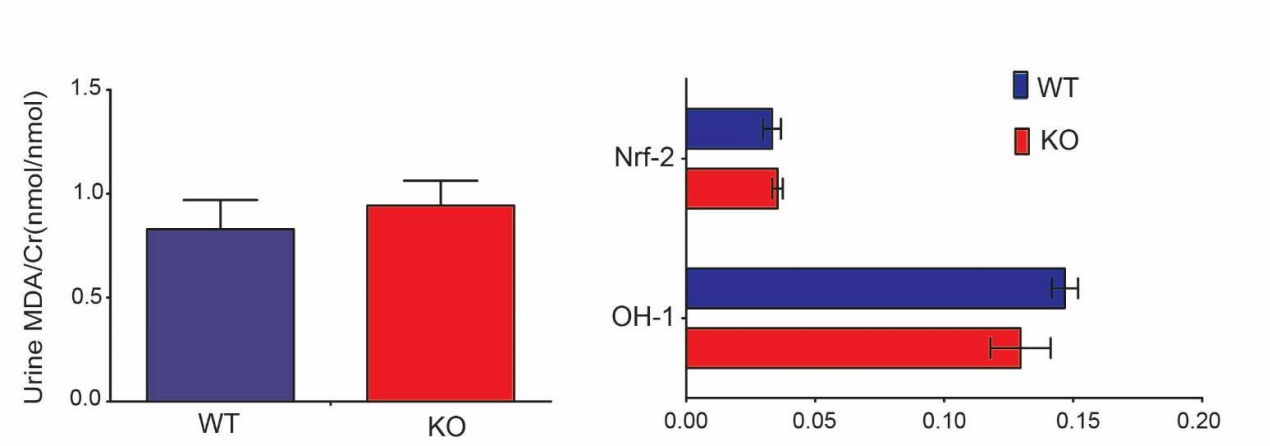

Figure 4.5 Absence of upregulation of oxidative stress markers in claudin-2 KO kidneys compared to WT kidneys at baseline. A. Urinary malondialdehyde (MDA) excretion is expressed as the ratio of urinary MDA concentration to creatinine concentration (mean ± S.E.M.). B. mRNA expression of oxidative stress response genes. Quantification of whole kidney mRNA levels of OH-1 and Nrf2 gene relative to β-actin. OH-1: heme oxygenase 1; Nrf2: nuclear factor, erythroid derived 2. The fold change is presented as mean ± S.E.M.

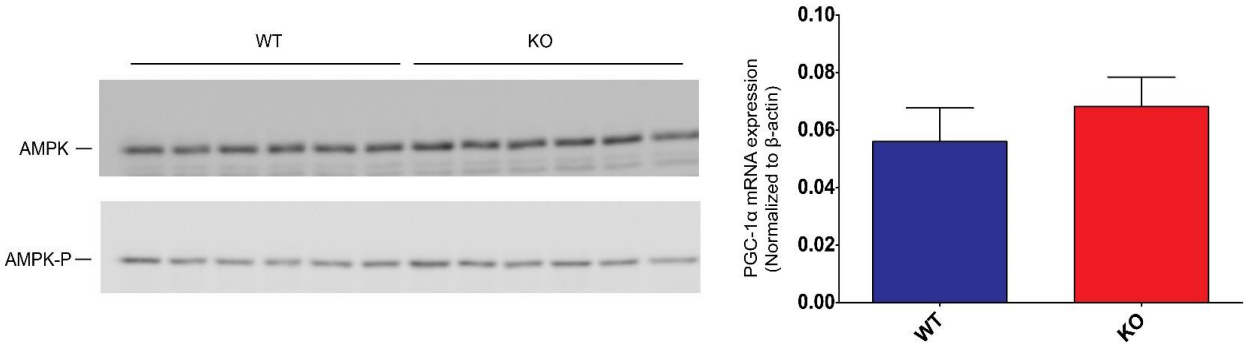

Figure 4.6 Absence of upregulation of mitochondria biogenesis in claudin-2 KO kidneys compared to WT kidneys at baseline. A. Western blots of whole kidney tissue lysate from WT and KO mice. Upper panel was probed with rabbit-anti-pAMPK antibody, lower panel was probed with rabbit-anti-AMPK. B. mRNA expression of peroxisome proliferator-activated receptor gamma coactivator 1-alpha (PGC-1α). Quantification of whole kidney mRNA levels of PGC-1α gene relative to β-actin. The fold change is presented as mean ± S.E.M.

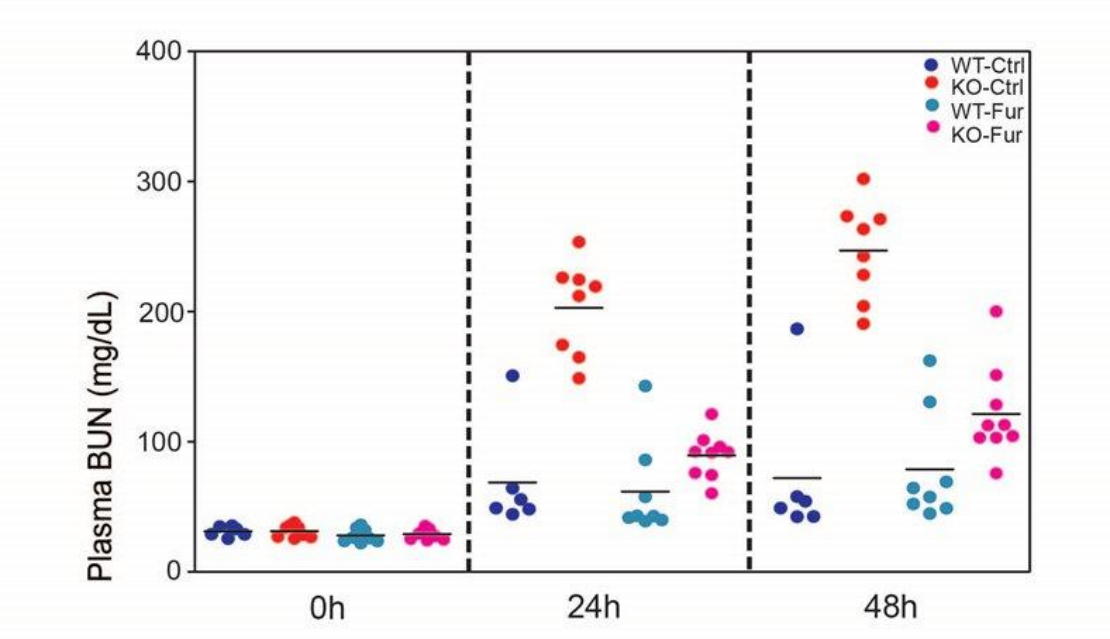

Figure 4.7 Effect of claudin-2 KO on susceptibility to acute renal ischemia: measurement of plasma BUN levels. BUN levels at 0, 24 and 48 hours following bilateral renal IRI in claudin-2 KO and WT littermates, with or without (control) furosemide pretreatment. $p < 0.005$ for KO control vs. WT control, and for KO control vs. KO furosemide; NS, p not significant for WT control vs. WT furosemide, by ANOVA.

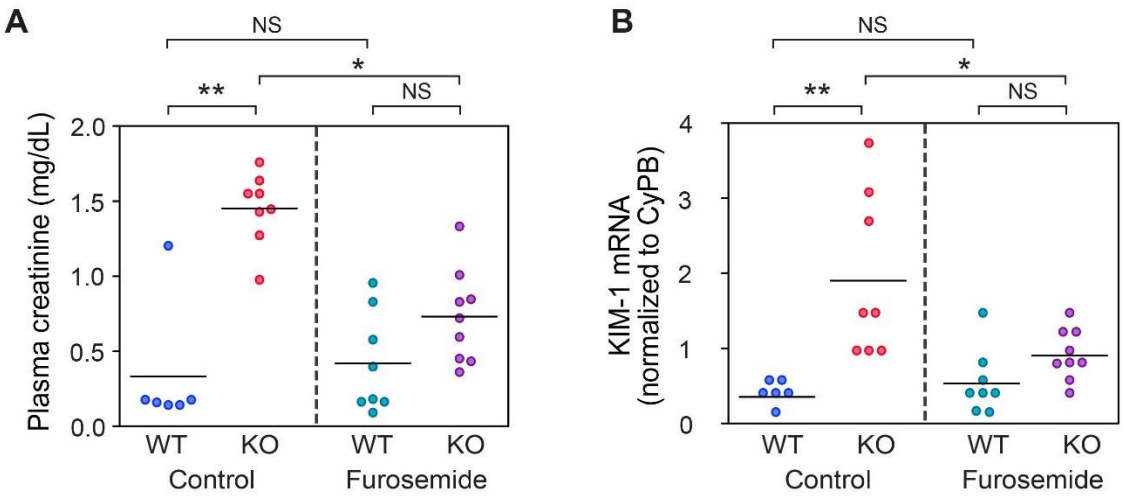

Figure 4.8 Effect of claudin-2 KO on susceptibility to acute renal ischemia: measurement of plasma creatinine and KIM1 mRNA. A. Plasma creatinine levels at 48 hours after IRI. B. KIM-1 mRNA levels in kidneys at 48 hr after IRI (normalized to cyclophilin B). CyPB: cyclophilin B; IRI: ischemic reperfusion injury. *$p < 0.01$; **$p < 0.001$ by t-test ($n = 6–8$ per group).

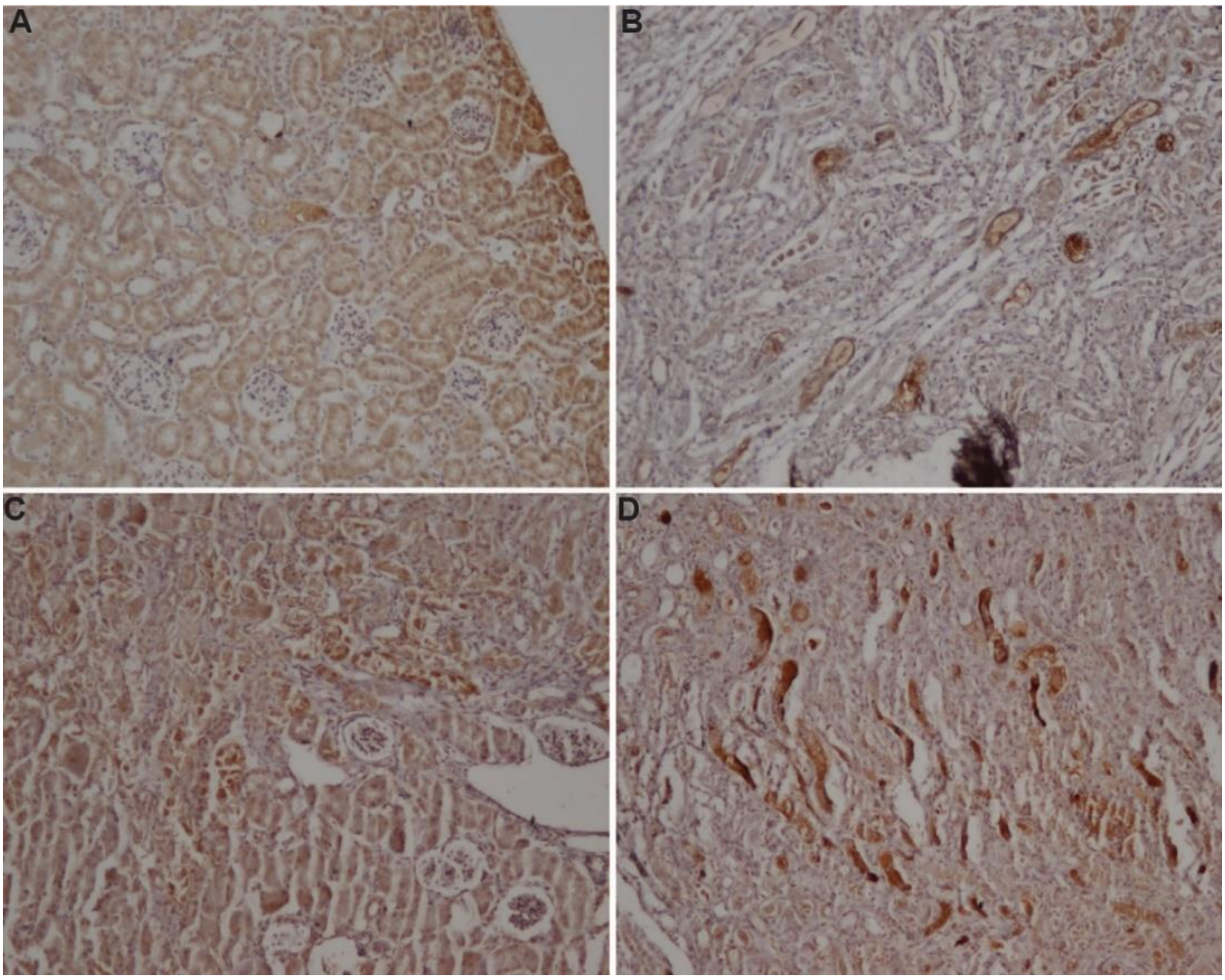

Figure 4.9 Confirmation of kidney injury by KIM-1 protein staining. Representative images are shown of rabbit anti-KIM-1 antibody immunohistochemistry staining of the kidney cortex (A,C) and outer medulla (B,D) from WT(A,B) and KO (C.D) mice 48 hours following IRI. Magnification: 20X.

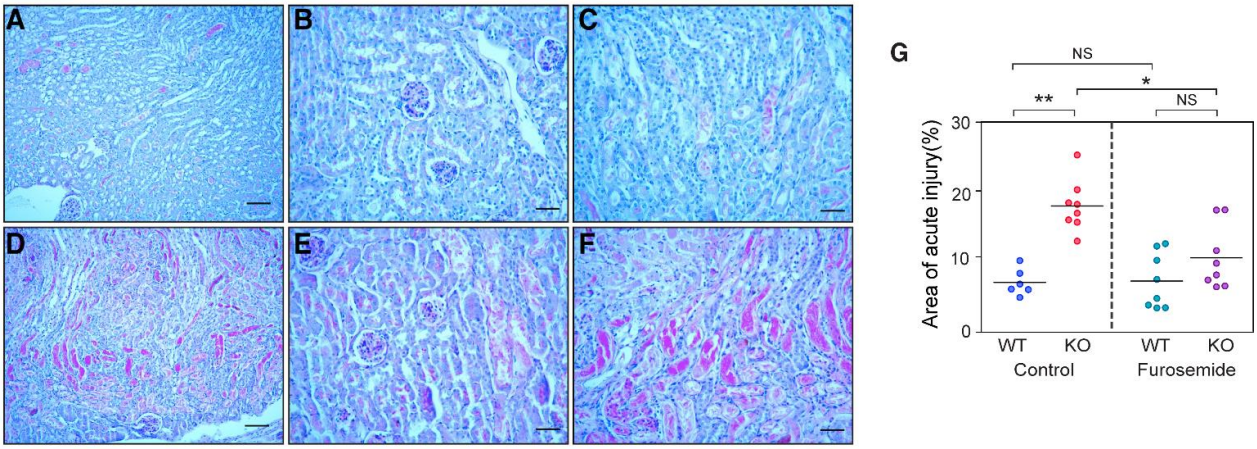

Figure 4.10 Histological analysis of acute kidney injury. Representative images are shown of periodic acid-Schiff (PAS) stained WT (A-C) and KO (D-F) kidneys 48 hrs following IRI. A and D are low power views (100 µm scale bar). B, E are high power views of the cortex, while C, F are high power views of the outer medulla (50 µm scale bar). G. Histological scoring of acute injury, expressed as % of kidney area involved. *$p < 0.001$ by t-test, n = 6-8 per group. Magnification: A and D: 10X; B, C, E and F: 20X.

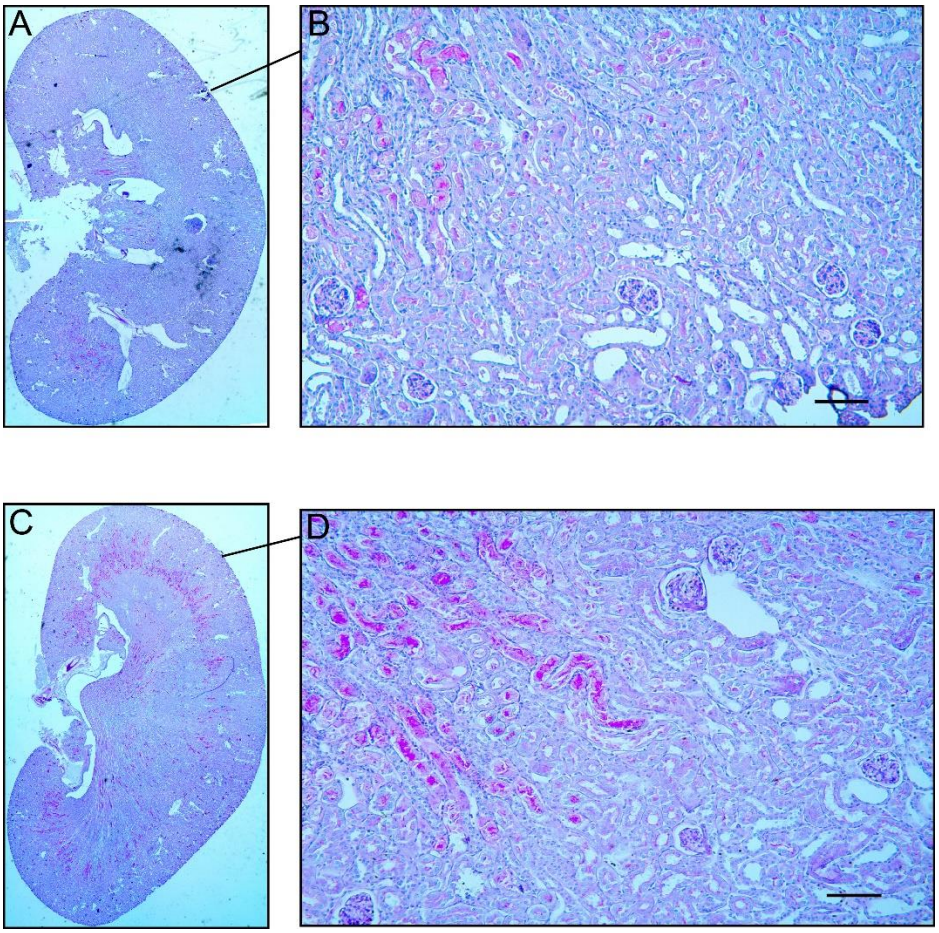

Figure 4.11 Histological analysis of acute kidney injury in mice pretreated with furosemide. Representative images are shown of periodic acid-Schiff (PAS)-staining WT (**A, B**) and KO (**C, D**) kidneys 48 hours following IRI. **A, C** are low power overviews of the whole kidney section. **B, D** are higher power views showing the cortex and outer medulla (100µm scale bar). Please see figure 4.10 for quantitative scoring of the degree of the injury. Magnification: 20X.

	WT (n = 8)	KO (n = 9)	p value
GFR (µl/min/g kw)	846 ± 40	911 ± 38	0.26
RBF (ml/min/g kw)	7.69 ± 0.35	7.72 ± 0.24	0.96
MAP (mm Hg)	101.8 ± 3.3	105.1 ± 2.6	0.45
T_{Na} (µmol/min/g kw)	126.9 ± 6.0	138.2 ± 6.3	0.22
QO2 (µmol/min/g kw)	8.06 ± 0.74	14.50 ± 1.55	0.003
T_{Na}/QO2 (mol/mol kw)	16.36 ± 1.31	10.34 ± 1.33	0.007

Table 4.1 Renal hemodynamics and function in anesthetized mice. GFR, glomerular filtration rate; RBF, renal blood flow; MAP, mean arterial pressure; T_{Na}, net renal Na reabsorption; QO_2, renal oxygen consumption; kw, kidney weight.

Antibody Target	Apparent Mobility (kDa)	Protein (µg/lane)*	Primary antibody supplier (cat. no.)	Primary antibody host	Primary antibody dilution	Incubation time
HIF-1α	150	30	Novus (#NB100-449)	Rb	1:1000	O/N
Lamin A/C	70-28	30	Cell Signaling (#2032)	Rb	1:1000	O/N

Table 4.2 Primary antibodies used for immunoblotting. Rb: rabbit; O/N: overnight.

Antibody Target	**Primary antibody supplier (cat. no.)**	**Primary antibody host**	**Primary antibody dilution**	**Incubation time**
Kim-1	Novus (#NBP1-76701)	Rb	1:500	O/N

Table 4.3 Primary antibodies used for immunohistochemistry. Rb: rabbit; O/N: overnight.

Kim-1 Forward	5'-CAG GAA GAC CCACGACTA TTTC-3'
Kim-1 Reverse	5'-GTG TGT AGA TGT TGG AGG AGTG-3'
Cyclophilin B Forward	5'-CGA GTC GTC TTT GGA CTC TTT-3'
Cyclophilin B Reverse	5'-GCC AAA TCC TTT CTC TCC TGT A-3'
OH-1 Forward	5'-CTC CCT GTG TTT CCT TTC TCT C-3’
OH-1 Reverse	5’-GCT GCT GGT TTC AAA GTT CAG-3’
Nrf2 Forward	5’-CTC CGT GGA GTC TTC CAT TTA C-3’
Nrf2 Reverse	5’-GCA CTA TCT AGC TCC TCC ATT TC-3’
VEGF-A Forward	5’-CCA CGT CAG AGA GCA ACA TCA-3’
VEGF-A Reverse	5’-TCA TTC TCT CTA TGT GCT GGC TTT-3’
GLUT-1 Forward	5’-ATG GAT CCC AGC AGC AAG-3’
GLUT-1 Reverse	5’-CCA GTG TTA TAG CCG AAC TGC-3’
PGK Forward	5’-GGA AGC GGG TCG TGA TGA-3’
PGK Reverse	5’-GCC TTG ATC CTT TGG TTG TTT G-3’
TRF Forward	5’-TGG AGA CAG ATG CTC CCT CC-3’
TRF Reverse	5’-TTT GTG CTC TGT GTA TGT GGT AAG G-3’
EPO Forward	5’-CAT CTG CGA CAG TCG AGT TCT G-3’
EPO Reverse	5’-CAC AAC CCA TCG TGA CAT TTT C-3’

Table 4.4 Oligonucleotide primers that were used for genomic DNA or quantitative RT-PCR

Chapter V: Summary and Discussion

5.1 Significance

The *in vitro* characterization of claudin-2 functions indicates that claudin-2 forms a cation selective pore (Furuse, Furuse et al. 2001, Amasheh and Meiri et al. 2002). Na^+ transport in renal proximal tubules has been well characterized as well; approximately 60% of glomerulus-filtered Na^+, K^+, and Cl^- ions are reabsorbed in renal proximal tubules, 40% of which are transported through the paracellular pathway. Claudins are a family of tight-junction transmembrane proteins that regulate paracellular ion permeability. Cation-selective claudin-2 is mainly expressed in renal proximal tubules.

Due to the abundance of transporters involved in transcellular transport of Na^+ and other claudin isoforms in renal tubules, the salt wasting phenotypes of claudin knockout mice are usually quite mild (Muto, Hata et al. 2010, Tatum, Zhang et al. 2010). These studies might lead to the misunderstanding that paracellular transport is not important in epithelial transport. However, the fact that renal epithelia have evolved to contain a leaky paracellular pathway has led us to speculate on the evolutionary purpose and significance of tight junctions.

Our work sought to explore the physiological significance of paracellular transport in two ways. First, it explored how the kidney's transcellular Na^+ transport compensated for the loss of claudin-2. Second, we assessed oxygen-utilization efficiency and susceptibility to acute ischemic injury in claudin-2 null mice. We demonstrated that, when the paracellular transport pathway is disrupted in the renal proximal tubule, transcellular transport in the thick ascending limb of the loop of Henle can compensate for its loss. The price for increased transcellular transport is increased oxygen consumption, thereby rendering the tissue more susceptible to ischemic injury.

5.2 Summary of chapter II and chapter III

In the first part of our work, we performed a general characterization of the claudin-2 null

mice that we purchased from Mutant Mouse Regional Resource Centers. We were able to show that the claudin-2 gene was successfully disrupted in the mouse genome. Then, we performed RT-PCR and confirmed the absence of any expression of claudin-2 mRNA and protein. We performed immunofluorescence and confirmed lyonization in heterozygous mice (Cldn2 [+/-]). We performed a 2% saline challenge test in order to confirm the salt wasting phenotype in claudin-2 null mice during a high salt challenge. A thorough characterization of our claudin-2 null mice model provided a solid foundation for subsequent experiments.

We found that the compensation of Na^+ reabsorption was so efficient that claudin-2 null mice exhibited no excessive urine Na^+ loss even when challenged with a sodium-deficient diet. This result surprised us, and we sought to investigate how this compensation occurred. We approached this investigation by measuring changes in both claudin isoforms and transcellular Na^+ transporters. We found no significant difference in claudin isoform expression or localization between WT and claudin-2 KO mice. Following this, we quantitated the protein expression of a majority of the transcellular transporters and found no increase in the amount of protein in the transcellular transporters, NKCC2, NHE3, NCC, or ENaC. These results led us to consider that changes in transcellular transporter activity may occur without changes in protein abundance and its phosphorylation status (Madala Halagappa, Tiwari et al. 2008, Tiwari, Li et al. 2009). In order to test this hypothesis, we performed a diuretic challenge test. When claudin-2 null mice were subjected to a furosemide challenge test, we observed a 40% increase in natriuresis in the knockout compared to WT mice. These results indicated that the loss of paracellular transport in claudin-2 null mice was compensated by an increase in NKCC2 activity in the thick ascending limb of loop of Henle. Although NKCC2 was not upregulated in terms of its protein expression or phosphorylation status, it is known that distal Na^+ delivery to the thick ascending limb can lead to increased NKCC2 activity without changing these parameters. Distal Na^+ delivery increases NKCC2 activity in at least two ways. First, increased Na^+ concentration in the lumen can directly stimulate Na^+ transport by NKCC2 in the thick ascending limb (Morgan and Berliner 1969).

Second, increased Na^+ delivery increases NKCC2 activity by reducing nitric oxide, which is an inhibitor of NKCC2. Na^+ delivery inhibits nitric oxide bioavailability by increasing generation of superoxide (Abe, O'Connor et al. 2006) and nitric oxide inhibits NKCC2 activity by increasing cGMP (Plato, Stoos et al. 1999). An alternative explanation is that NKCC2 activity can be upregulated in response to increased tubular flow rate in thick ascending limb (Burg and Good 1983). Burg proposed that if the capacity for Na^+ reabsorption in the thick ascending limb is sufficiently large that it is not rate-limiting, luminal Na^+ concentration will be lowered until it reaches a limiting concentration or "static head". In claudin-2 KO mice, increased tubular flow rate would simply shift the point at which the static head is attained distally along the thick ascending limb, so that the Na^+ reabsorption will be proportional to the flow rate**.**

5.3 Summary of chapter IV

The work outlined in chapter III established that claudin-2 null mice were able to conserve sodium to the same extent as wild-type mice, even during periods of profound dietary sodium depletion. Subsequent work determined this to be due to the upregulation of transcellular Na-K-2Cl cotransporter activity in the thick ascending limb of Henle. We hypothesized that the primary purpose of paracellular Na^+ transport is to exploit transtubular electrochemical gradients in order to drive passive Na^+ reabsorption and enhance the efficiency of overall renal oxygen consumption. To test this hypothesis, we determined the ratio between whole-kidney Na^+ reabsorption and oxygen consumption in both WT and claudin-2 null mice. As expected, T_{Na}/QO_2 in claudin-2 deficient mice was significantly lower than in WT. We then measured the tissue pO_2 within cortex and medulla of claudin-2-null mice and found that claudin-2-null mice have relative medullary hypoxia. When we treated both WT and claudin-2-null mice with furosemide, the pO_2 increased in the outer medulla of both genotypes. However, as expected, there was a much greater increase in pO_2 in KO as compared to WT mice.

When subjected to bilateral renal ischemia-reperfusion injury, the kidneys of claudin-2-null mice exhibited more severe tubular injury than WT mice. This was shown by higher BUN and creatinine, higher expression of Kidney Injury Molecule-1 and higher histological scoring of injury in claudin-2 null mice. Furosemide pretreatment before ischemic reperfusion injury partially alleviated the injury, presumably by inhibiting NKCC2 and hence increasing pO_2 in outer medulla. It is conceivable that inherited or acquired variations in the proximal tubular paracellular transport pathway in humans might similarly affect the clinical susceptibility to acute ischemic kidney injury.

5.4 Limitations

Several limitations of this dissertation work deserve mention. Because the claudin-2 gene is on the X chromosome, we chose to confine our analysis to male WT and KO mice to simplify the breeding scheme. Also, the claudin-2 coding sequence has been globally deleted in our claudin-2 null mice. Since claudin-2 is expressed in other transporting epithelia and especially in the intestine, it is theoretically possible that absence of claudin-2 in other tissues could explain some of our findings. This is very unlikely, though, because the key experiments, such as assays of oxygen consumption, are specifically confined to the kidney. Moreover, whereas claudin-2 is expressed throughout the intestinal epithelium including the villi in infant mice, it is confined to the crypts in adults (Tamura, Hayashi et al. 2011). Consistent with this, in adult claudin-2 null mice there was little change in the cation permeability of the intestine (25% decrease in PNa compared to WT mice (Tamura, Hayashi et al. 2011)). We therefore believe that in adults claudin-2 likely plays a minor role in intestinal Na^+ absorption. Our interpretation of the results here is also based on the assumption that the renal phenotype of the KO mice is due to loss of proximal tubular claudin-2. However, our lab (Enck, Berger et al. 2001) and others (Kiuchi-Saishin, Gotoh et al. 2002, Lee, Chou et al. 2015) have shown that claudin-2 is also highly expressed in the upper portion of the thin descending limb of long-looped nephrons. The role of this nephron segment is poorly understood, and the implications of claudin-2 deletion here are unknown.

5.4 Future Directions

This dissertation work was able to use claudin-2 null mice to prove that, when paracellular transport is dysfunctional within the proximal tubule of the kidney, transcellular transport will compensate for its loss. This compensation increases energy consumption and susceptibility to ischemic insult. In the future, there are many ways to investigate the wider significance of paracellular transport in the energy efficiency of epithelial transport. There are still questions remaining to be answered. In Chapter III, we found increased NKCC2 activity in the thick ascending limb of claudin-2 null mice. However, we still don't have clear evidence to show how the NKCC2 activity is regulated. We speculate that the increased luminal Na^+ concentration directly stimulates NKCC2 activity. In order to prove this, it would be interesting if we could measure the luminal Na^+ concentration in the thick ascending limb in both WT and claudin-2 KO kidneys in order to determine if there is an increased Na^+ concentration in claudin-2 KO mice. Also, as **Figure 3.8** shows, there is no significant difference in urine Na^+ excretion between WT and claudin-2 KO mice after HCTZ and benzamil treatment. However, we did notice a trend that claudin-2 null mice had more natriuresis after blocking NCC and ENaC with these diuretics. We speculate that it is possible that there is an increase in the activity of NCC and ENaC that our diuretic challenge test was not able to readily demonstrate. Further, it would be interesting to determine the exact percentage of each transporter's contribution to the compensatory salt reabsorption in claudin-2 null mice.

We speculate that our findings in claudin-2 null mice can be also applied to the investigation of other claudin isoforms in the kidney and the other organs. First, we can test a similar hypothesis by investigating the physiological significance of other claudins in the renal tubule. For example, claudin-7 and claudin-10a are both implicated in paracellular NaCl transport in the distal tubule and the proximal tubule, respectively. It would be interesting to perform our oxygen consumption assay and ischemic reperfusion surgery on claudin-7 and claudin-10a KO mice to test the

hypothesis that they also have increased oxygen consumption and susceptibility to ischemic injury.

Second, we can investigate the physiological significance of claudins in other organs. For example, in small intestine, the cation pores, claudin-2 and claudin-15, are believed to mediate the back-leak of Na^+ into the intestinal lumen and facilitate Na^+ dependent glucose and amino acid reabsorption (Wada, Tamura et al. 2013). When claudin-2 and claudin-15 are simultaneously knocked out, mice are not able to reabsorb glucose and amino acids. In this case, transcellular transporter activity may be upregulated in an attempt to absorb these nutrients. It would be interesting to perform an oxygen consumption assay on the claudin-2/claudin-15 double KO small intestine in order to determine if they too have increased oxygen consumption.

References

Abe, M., P. O'Connor, M. Kaldunski, M. Liang, R. J. Roman and A. W. Cowley, Jr. (2006). "Effect of sodium delivery on superoxide and nitric oxide in the medullary thick ascending limb." Am J Physiol Renal Physiol **291**(2): F350-357.

Alexandre, M. D., Q. Lu and Y. H. Chen (2005). "Overexpression of claudin-7 decreases the paracellular Cl- conductance and increases the paracellular Na+ conductance in LLC-PK1 cells." J Cell Sci **118**(Pt 12): 2683-2693.

Amasheh, S., N. Meiri, A. H. Gitter, T. Schoneberg, J. Mankertz, J. D. Schulzke and M. Fromm (2002). "Claudin-2 expression induces cation-selective channels in tight junctions of epithelial cells." J Cell Sci **115**(Pt 24): 4969-4976.

Amasheh, S., S. Milatz, S. M. Krug, M. Bergs, M. Amasheh, J. D. Schulzke and M. Fromm (2009). "Na+ absorption defends from paracellular back-leakage by claudin-8 upregulation." Biochem Biophys Res Commun **378**(1): 45-50.

Anderson, J. M. and C. M. Van Itallie (2009). "Physiology and function of the tight junction." Cold Spring Harb Perspect Biol **1**(2): a002584.

Andreoli, T. E., J. A. Schafer, S. L. Troutman and M. L. Watkins (1979). "Solvent drag component of Cl- flux in superficial proximal straight tubules: evidence for a paracellular component of isotonic fluid absorption." Am J Physiol **237**(6): F455-462.

Angelow, S., R. Ahlstrom and A. S. Yu (2008). "Biology of claudins." Am J Physiol Renal Physiol **295**(4): F867-876.

Angelow, S., R. El-Husseini, S. A. Kanzawa and A. S. Yu (2007). "Renal localization and function of the tight junction protein, claudin-19." Am J Physiol Renal Physiol **293**(1): F166-177.

Barratt, L. J., F. C. Rector, Jr., J. P. Kokko and D. W. Seldin (1974). "Factors governing the transepithelial potential difference across the proximal tubule of the rat kidney." J Clin Invest **53**(2): 454-464.

Berry, C. A., D. G. Warnock and F. C. Rector, Jr. (1978). "Ion selectivity and proximal salt reabsorption." Am J Physiol **235**(3): F234-245.

Bomsztyk, K. (1986). "Chloride transport by rat renal proximal tubule: effects of bicarbonate absorption." Am J Physiol **250**(6 Pt 2): F1046-1054.

Borovac, J., R. S. Barker, J. Rievaj, A. Rasmussen, W. Pan, R. Wevrick and R. T. Alexander (2012). "Claudin-4 forms a paracellular barrier, revealing the interdependence of claudin expression in the loose epithelial cell culture model opossum kidney cells." Am J Physiol Cell Physiol **303**(12): C1278-1291.

Brenner, B. M., J. L. Troy and T. M. Daugharty (1971). "On the mechanism of inhibition in fluid reabsorption by the renal proximal tubule of the volume-expanded rat." J Clin Invest **50**(8): 1596-1602.

Brodwall, E. K. (1964). "The Relation between the Renal Oxygen Consumption and the Transport of Sodium, Clearance of Inulin and the Renal Extraction of Pah." Scand J Clin Lab Invest **16**: 287-291.

Brooks, H. L., A. M. Sorensen, J. Terris, P. J. Schultheis, J. N. Lorenz, G. E. Shull and M. A. Knepper (2001). "Profiling of renal tubule Na+ transporter abundances in NHE3 and NCC null mice using targeted proteomics." J Physiol **530**(Pt 3): 359-366.

Burg, M. and D. Good (1983). "Sodium chloride coupled transport in mammalian nephrons." Annu Rev Physiol **45**: 533-547.

Burg, M. B. (1982). "Thick ascending limb of Henle's loop." Kidney Int **22**(5): 454-464.

Cabral, P. D. and J. L. Garvin (2011). "Luminal flow regulates NO and O2(-) along the nephron." Am J Physiol Renal Physiol **300**(5): F1047-1053.

Colegio, O. R., C. M. Van Itallie, H. J. McCrea, C. Rahner and J. M. Anderson (2002). "Claudins create charge-selective channels in the paracellular pathway between epithelial cells." Am J Physiol Cell Physiol **283**(1): C142-147.

Coyne, C. B., T. M. Gambling, R. C. Boucher, J. L. Carson and L. G. Johnson (2003). "Role of claudin interactions in airway tight junctional permeability." Am J Physiol Lung Cell Mol Physiol **285**(5): L1166-1178.

Crone, C. and O. Christensen (1981). "Electrical resistance of a capillary endothelium." J Gen Physiol **77**(4): 349-371.

Duc, C., N. Farman, C. M. Canessa, J. P. Bonvalet and B. C. Rossier (1994). "Cell-specific expression of epithelial sodium channel alpha, beta, and gamma subunits in aldosterone-

responsive epithelia from the rat: localization by in situ hybridization and immunocytochemistry." J Cell Biol **127**(6 Pt 2): 1907-1921.

Enck, A. H., U. V. Berger and A. S. Yu (2001). "Claudin-2 is selectively expressed in proximal nephron in mouse kidney." Am J Physiol Renal Physiol **281**(5): F966-974.

Ergonul, Z., G. Frindt and L. G. Palmer (2006). "Regulation of maturation and processing of ENaC subunits in the rat kidney." Am J Physiol Renal Physiol **291**(3): F683-693.

Fagerberg, L., K. Jonasson, G. von Heijne, M. Uhlen and L. Berglund (2010). "Prediction of the human membrane proteome." Proteomics **10**(6): 1141-1149.

Farquhar, M. G. and G. E. Palade (1963). "Junctional complexes in various epithelia." J Cell Biol **17**: 375-412.

Flemmer, A. W., I. Gimenez, B. F. Dowd, R. B. Darman and B. Forbush (2002). "Activation of the Na-K-Cl cotransporter NKCC1 detected with a phospho-specific antibody." J Biol Chem **277**(40): 37551-37558.

Furuse, M., K. Furuse, H. Sasaki and S. Tsukita (2001). "Conversion of zonulae occludentes from tight to leaky strand type by introducing claudin-2 into Madin-Darby canine kidney I cells." J Cell Biol **153**(2): 263-272.

Goldfarb, M., C. Rosenberger, Z. Abassi, A. Shina, F. Zilbersat, K. U. Eckardt, S. Rosen and S. N. Heyman (2006). "Acute-on-chronic renal failure in the rat: functional compensation and hypoxia tolerance." Am J Nephrol **26**(1): 22-33.

Han, W. K., V. Bailly, R. Abichandani, R. Thadhani and J. V. Bonventre (2002). "Kidney Injury Molecule-1 (KIM-1): a novel biomarker for human renal proximal tubule injury." Kidney Int **62**(1): 237-244.

Himmerkus, N., Q. Shan, B. Goerke, J. Hou, D. A. Goodenough and M. Bleich (2008). "Salt and acid-base metabolism in claudin-16 knockdown mice: impact for the pathophysiology of FHHNC patients." Am J Physiol Renal Physiol **295**(6): F1641-1647.

Hong, N. J. and J. L. Garvin (2012). "NADPH oxidase 4 mediates flow-induced superoxide production in thick ascending limbs." Am J Physiol Renal Physiol **303**(8): F1151-1156.

Horisberger, J.-D. (2004). "Recent Insights into the Structure and Mechanism of the Sodium pump." Physiology 19:377-387, 2004. .

Hou, J., A. Renigunta, M. Konrad, A. S. Gomes, E. E. Schneeberger, D. L. Paul, S. Waldegger and D. A. Goodenough (2008). "Claudin-16 and claudin-19 interact and form a cation-selective tight junction complex." J Clin Invest **118**(2): 619-628.

Ichikawa, I. and B. M. Brenner (1979). "Mechanism of inhibition of proximal tubule fluid reabsorption after exposure of the rat kidney to the physical effects of expansion of extracellular fluid volume." J Clin Invest **64**(5): 1466-1474.

Jamadarkhana, P., A. Chaudhary, L. Chhipa, A. Dubey, A. Mohanan, R. Gupta and S. Deshpande (2012). "Treatment with a novel hypoxia-inducible factor hydroxylase inhibitor (TRC160334) ameliorates ischemic acute kidney injury." Am J Nephrol **36**(3): 208-218.

Juncos, R. and J. L. Garvin (2005). "Superoxide enhances Na-K-2Cl cotransporter activity in the thick ascending limb." Am J Physiol Renal Physiol **288**(5): F982-987.

Kiil, F., K. Aukland and H. E. Refsum (1961). "Renal sodium transport and oxygen consumption." Am J Physiol **201**: 511-516.

Kiuchi-Saishin, Y., S. Gotoh, M. Furuse, A. Takasuga, Y. Tano and S. Tsukita (2002). "Differential expression patterns of claudins, tight junction membrane proteins, in mouse nephron segments." J Am Soc Nephrol **13**(4): 875-886.

Knox, F. G., J. S. Fleming and D. W. Rennie (1966). "Effects of osmotic diuresis on sodium reabsorption and oxygen consumption of kidney." Am J Physiol **210**(4): 751-759.

Koefoed-Johnsen, V. and H. H. Ussing (1958). "The nature of the frog skin potential." Acta Physiol Scand **42**(3-4): 298-308.

Kokko, J. P. (1973). "Proximal tubule potential difference. Dependence on glucose on glucose, HCO 3 , and amino acids." J Clin Invest **52**(6): 1362-1367.

Kone, B. C. and S. C. Higham (1998). "A novel N-terminal splice variant of the rat H+-K+-ATPase alpha2 subunit. Cloning, functional expression, and renal adaptive response to chronic hypokalemia." J Biol Chem **273**(5): 2543-2552.

Konrad, M., A. Schaller, D. Seelow, A. V. Pandey, S. Waldegger, A. Lesslauer, H. Vitzthum, Y. Suzuki, J. M. Luk, C. Becker, K. P. Schlingmann, M. Schmid, J. Rodriguez-Soriano, G. Ariceta, F. Cano, R. Enriquez, H. Juppner, S. A. Bakkaloglu, M. A. Hediger, S. Gallati, S. C. Neuhauss, P. Nurnberg and S. Weber (2006). "Mutations in the tight-junction gene claudin 19 (CLDN19) are

associated with renal magnesium wasting, renal failure, and severe ocular involvement." Am J Hum Genet **79**(5): 949-957.

Krug, S. M., D. Gunzel, M. P. Conrad, R. Rosenthal, A. Fromm, S. Amasheh, J. D. Schulzke and M. Fromm (2012). "Claudin-17 forms tight junction channels with distinct anion selectivity." Cell Mol Life Sci **69**(16): 2765-2778.

Ladwein, M., U. F. Pape, D. S. Schmidt, M. Schnolzer, S. Fiedler, L. Langbein, W. W. Franke, G. Moldenhauer and M. Zoller (2005). "The cell-cell adhesion molecule EpCAM interacts directly with the tight junction protein claudin-7." Exp Cell Res **309**(2): 345-357.

Landwehr, D. M., R. M. Klose and G. Giebisch (1967). "Renal tubular sodium and water reabsorption in the isotonic sodium chloride-loaded rat." Am J Physiol **212**(6): 1327-1333.

Lee, J. W., C. L. Chou and M. A. Knepper (2015). "Deep Sequencing in Microdissected Renal Tubules Identifies Nephron Segment-Specific Transcriptomes." J Am Soc Nephrol **26**(11): 2669-2677.

Lommel, V. (2003). From Cells to Organs: A Histology Textbook and Atlas.

Lubbers, D. W. and H. Baumgartl (1997). "Heterogeneities and profiles of oxygen pressure in brain and kidney as examples of the pO2 distribution in the living tissue." Kidney Int **51**(2): 372-380.

Lytle, C., J. C. Xu, D. Biemesderfer and B. Forbush, 3rd (1995). "Distribution and diversity of Na-K-Cl cotransport proteins: a study with monoclonal antibodies." Am J Physiol **269**(6 Pt 1): C1496-1505.

Madala Halagappa, V. K., S. Tiwari, S. Riazi, X. Hu and C. M. Ecelbarger (2008). "Chronic candesartan alters expression and activity of NKCC2, NCC, and ENaC in the obese Zucker rat." Am J Physiol Renal Physiol **294**(5): F1222-1231.

Mathisen, O., T. Monclair and F. Kiil (1980). "Oxygen requirement of bicarbonate-dependent sodium reabsorption in the dog kidney." Am J Physiol **238**(3): F175-180.

McDonough, T. S. (2012). "Metabolic Basis of Solute Transport." Brenner and Rector's The Kidney.

Mineta, K., Y. Yamamoto, Y. Yamazaki, H. Tanaka, Y. Tada, K. Saito, A. Tamura, M. Igarashi, T. Endo, K. Takeuchi and S. Tsukita (2011). "Predicted expansion of the claudin multigene family." FEBS Lett **585**(4): 606-612.

Moe OW, Berry CA and J. Rector FC (2000). "Renal transport of glucose, amino acids, sodium, chloride, and water." Brenner and Rector's The Kidney.

Morgan, T. and R. W. Berliner (1969). "A study by continuous microperfusion of water and electrolyte movements in the loop of Henle and distal tubule of the rat." Nephron **6**(3): 388-405.

Muto, S., M. Hata, J. Taniguchi, S. Tsuruoka, K. Moriwaki, M. Saitou, K. Furuse, H. Sasaki, A. Fujimura, M. Imai, E. Kusano, S. Tsukita and M. Furuse (2010). "Claudin-2-deficient mice are

defective in the leaky and cation-selective paracellular permeability properties of renal proximal tubules." Proc Natl Acad Sci U S A **107**(17): 8011-8016.

Najjar, F., H. Zhou, T. Morimoto, J. B. Bruns, H. S. Li, W. Liu, T. R. Kleyman and L. M. Satlin (2005). "Dietary K+ regulates apical membrane expression of maxi-K channels in rabbit cortical collecting duct." Am J Physiol Renal Physiol **289**(4): F922-932.

Nakhoul, N. and V. Batuman (2011). "Role of proximal tubules in the pathogenesis of kidney disease." Contrib Nephrol **169**: 37-50.

Neumann, K. H. and F. C. Rector, Jr. (1976). "Mechanism of NaCl and water reabsorption in the proximal convoluted tubule of rat kidney." J Clin Invest **58**(5): 1110-1118.

Nguyen, M. T., D. H. Lee, E. Delpire and A. A. McDonough (2013). "Differential regulation of Na+ transporters along nephron during ANG II-dependent hypertension: distal stimulation counteracted by proximal inhibition." Am J Physiol Renal Physiol **305**(4): F510-519.

Nguyen, M. T., L. E. Yang, N. K. Fletcher, D. H. Lee, H. Kocinsky, S. Bachmann, E. Delpire and A. A. McDonough (2012). "Effects of K+-deficient diets with and without NaCl supplementation on Na+, K+, and H2O transporters' abundance along the nephron." Am J Physiol Renal Physiol **303**(1): F92-104.

Nitta, T., M. Hata, S. Gotoh, Y. Seo, H. Sasaki, N. Hashimoto, M. Furuse and S. Tsukita (2003). "Size-selective loosening of the blood-brain barrier in claudin-5-deficient mice." J Cell Biol **161**(3): 653-660.

Ortiz, P. A. and J. L. Garvin (2002). "Superoxide stimulates NaCl absorption by the thick ascending limb." Am J Physiol Renal Physiol **283**(5): F957-962.

Picard, N., K. Trompf, C. L. Yang, R. L. Miller, M. Carrel, D. Loffing-Cueni, R. A. Fenton, D. H. Ellison and J. Loffing (2014). "Protein phosphatase 1 inhibitor-1 deficiency reduces phosphorylation of renal NaCl cotransporter and causes arterial hypotension." J Am Soc Nephrol **25**(3): 511-522.

Plato, C. F., B. A. Stoos, D. Wang and J. L. Garvin (1999). "Endogenous nitric oxide inhibits chloride transport in the thick ascending limb." Am J Physiol **276**(1 Pt 2): F159-163.

Powell, D. W. (1981). "Barrier function of epithelia." Am J Physiol **241**(4): G275-288.

Rieg, T., V. Vallon, M. Sausbier, U. Sausbier, B. Kaissling, P. Ruth and H. Osswald (2007). "The role of the BK channel in potassium homeostasis and flow-induced renal potassium excretion." Kidney Int **72**(5): 566-573.

Salceda, S. and J. Caro (1997). "Hypoxia-inducible factor 1alpha (HIF-1alpha) protein is rapidly degraded by the ubiquitin-proteasome system under normoxic conditions. Its stabilization by hypoxia depends on redox-induced changes." J Biol Chem **272**(36): 22642-22647.

Schafer, J. A., C. S. Patlak and T. E. Andreoli (1975). "A component of fluid absorption linked to passive ion flows in the superficial pars recta." J Gen Physiol **66**(4): 445-471.

Schneeberger, E. E. and R. D. Lynch (2004). "The tight junction: a multifunctional complex." Am J Physiol Cell Physiol **286**(6): C1213-1228.

Schneider, C. A., W. S. Rasband and K. W. Eliceiri (2012). "NIH Image to ImageJ: 25 years of image analysis." Nat Methods **9**(7): 671-675.

Schnermann, J., Y. Huang and D. Mizel (2013). "Fluid reabsorption in proximal convoluted tubules of mice with gene deletions of claudin-2 and/or aquaporin1." Am J Physiol Renal Physiol **305**(9): F1352-1364.

Semenza, G. L. (2000). "Surviving ischemia: adaptive responses mediated by hypoxia-inducible factor 1." J Clin Invest **106**(7): 809-812.

Simon, D. B., Y. Lu, K. A. Choate, H. Velazquez, E. Al-Sabban, M. Praga, G. Casari, A. Bettinelli, G. Colussi, J. Rodriguez-Soriano, D. McCredie, D. Milford, S. Sanjad and R. P. Lifton (1999). "Paracellin-1, a renal tight junction protein required for paracellular Mg2+ resorption." Science **285**(5424): 103-106.

Skou, J. C. (2004). "The identification of the sodium pump." Biosci Rep **24**(4-5): 436-451.

Soltoff, S. P. (1986). "ATP and the regulation of renal cell function." Annu Rev Physiol **48**: 9-31.

Stephenson, J. L., R. P. Tewarson and R. Mejia (1974). "Quantitative analysis of mass and energy balance in non-ideal models of the renal counterflow system." Proc Natl Acad Sci U S A **71**(5): 1618-1622.

Suzuki, H., T. Nishizawa, K. Tani, Y. Yamazaki, A. Tamura, R. Ishitani, N. Dohmae, S. Tsukita, O. Nureki and Y. Fujiyoshi (2014). "Crystal structure of a claudin provides insight into the architecture of tight junctions." Science **344**(6181): 304-307.

Tamura, A., H. Hayashi, M. Imasato, Y. Yamazaki, A. Hagiwara, M. Wada, T. Noda, M. Watanabe, Y. Suzuki and S. Tsukita (2011). "Loss of claudin-15, but not claudin-2, causes Na+ deficiency and glucose malabsorption in mouse small intestine." Gastroenterology **140**(3): 913-923.

Tamura, A., Y. Kitano, M. Hata, T. Katsuno, K. Moriwaki, H. Sasaki, H. Hayashi, Y. Suzuki, T. Noda, M. Furuse, S. Tsukita and S. Tsukita (2008). "Megaintestine in claudin-15-deficient mice." Gastroenterology **134**(2): 523-534.

Tatum, R., Y. Zhang, Q. Lu, K. Kim, B. G. Jeansonne and Y. H. Chen (2007). "WNK4 phosphorylates ser(206) of claudin-7 and promotes paracellular Cl(-) permeability." FEBS Lett **581**(20): 3887-3891.

Tatum, R., Y. Zhang, K. Salleng, Z. Lu, J. J. Lin, Q. Lu, B. G. Jeansonne, L. Ding and Y. H. Chen (2010). "Renal salt wasting and chronic dehydration in claudin-7-deficient mice." Am J Physiol Renal Physiol **298**(1): F24-34.

Thurau, K. (1961). "Renal Na-reabsorption and O2-uptake in dogs during hypoxia and hydrochlorothiazide infusion." Proc Soc Exp Biol Med **106**: 714-717.

Tiwari, S., L. Li, S. Riazi, V. K. Halagappa and C. M. Ecelbarger (2009). "Sex and age result in differential regulation of the renal thiazide-sensitive NaCl cotransporter and the epithelial sodium channel in angiotensin II-infused mice." Am J Nephrol **30**(6): 554-562.

Torelli, G., E. Milla, A. Faelli and S. Costantini (1966). "Energy requirement for sodium reabsorption in the in vivo rabbit kidney." Am J Physiol **211**(3): 576-580.

Uhlen, M., P. Oksvold, L. Fagerberg, E. Lundberg, K. Jonasson, M. Forsberg, M. Zwahlen, C. Kampf, K. Wester, S. Hober, H. Wernerus, L. Bjorling and F. Ponten (2010). "Towards a knowledge-based Human Protein Atlas." Nat Biotechnol **28**(12): 1248-1250.

Ussing, H. H. and K. Zerahn (1951). "Active transport of sodium as the source of electric current in the short-circuited isolated frog skin." Acta Physiol Scand **23**(2-3): 110-127.

Van Itallie, C., C. Rahner and J. M. Anderson (2001). "Regulated expression of claudin-4 decreases paracellular conductance through a selective decrease in sodium permeability." J Clin Invest **107**(10): 1319-1327.

Van Itallie, C. M., S. Rogan, A. Yu, L. S. Vidal, J. Holmes and J. M. Anderson (2006). "Two splice variants of claudin-10 in the kidney create paracellular pores with different ion selectivities." Am J Physiol Renal Physiol **291**(6): F1288-1299.

Waanders, F., M. M. van Timmeren, C. A. Stegeman, S. J. Bakker and H. van Goor (2010). "Kidney injury molecule-1 in renal disease." J Pathol **220**(1): 7-16.

Wada, M., A. Tamura, N. Takahashi and S. Tsukita (2013). "Loss of claudins 2 and 15 from mice causes defects in paracellular Na+ flow and nutrient transport in gut and leads to death from malnutrition." Gastroenterology **144**(2): 369-380.

Wang, G. L. and G. L. Semenza (1993). "Characterization of hypoxia-inducible factor 1 and regulation of DNA binding activity by hypoxia." J Biol Chem **268**(29): 21513-21518.

Warnock, D. G. and M. B. Burg (1977). "Urinary acidification: CO2 transport by the rabbit proximal straight tubule." Am J Physiol **232**(1): F20-25.

Weber, S., L. Schneider, M. Peters, J. Misselwitz, G. Ronnefarth, M. Boswald, K. E. Bonzel, T. Seeman, T. Sulakova, E. Kuwertz-Broking, A. Gregoric, J. B. Palcoux, V. Tasic, F. Manz, K. Scharer, H. W. Seyberth and M. Konrad (2001). "Novel paracellin-1 mutations in 25 families with familial hypomagnesemia with hypercalciuria and nephrocalcinosis." J Am Soc Nephrol **12**(9): 1872-1881.

Wei, Q. and Z. Dong (2012). "Mouse model of ischemic acute kidney injury: technical notes and tricks." Am J Physiol Renal Physiol **303**(11): F1487-1494.

Weinberg, J. M. (2011). "Mitochondrial biogenesis in kidney disease." J Am Soc Nephrol **22**(3): 431-436.

Weinstein, S. W., R. Klose and J. Szyjewicz (1984). "Proximal tubular Na, Cl, and HCO3 reabsorption and renal oxygen consumption." Am J Physiol **247**(1 Pt 2): F151-157.

Welch, W. J., H. Baumgartl, D. Lubbers and C. S. Wilcox (2003). "Renal oxygenation defects in the spontaneously hypertensive rat: role of AT1 receptors." Kidney Int **63**(1): 202-208.

Welch, W. J., J. Blau, H. Xie, T. Chabrashvili and C. S. Wilcox (2005). "Angiotensin-induced defects in renal oxygenation: role of oxidative stress." Am J Physiol Heart Circ Physiol **288**(1): H22-28.

Welch, W. J., M. Mendonca, S. Aslam and C. S. Wilcox (2003). "Roles of oxidative stress and AT1 receptors in renal hemodynamics and oxygenation in the postclipped 2K,1C kidney." Hypertension **41**(3 Pt 2): 692-696.

Whittembury, G. and F. A. Rawlins (1971). "Evidence of a paracellular pathway for ion flow in the kidney proximal tubule. Electromicroscopic demonstration of lanthanum precipitate in the tight junction." Pflugers Arch **330**(4): 302-309.

Windhager, E. E. and G. Giebisch (1961). "Micropuncture study of renal tubular transfer of sodium chloride in the rat." Am J Physiol **200**: 581-590.

Yamazaki, Y., K. Okawa, T. Yano, S. Tsukita and S. Tsukita (2008). "Optimized proteomic analysis on gels of cell-cell adhering junctional membrane proteins." Biochemistry **47**(19): 5378-5386.

Zhang, S., R. Gillihan, N. He, T. Fields, S. Liu, T. Green and J. R. Stubbs (2013). "Dietary phosphate restriction suppresses phosphaturia but does not prevent FGF23 elevation in a mouse model of chronic kidney disease." Kidney Int **84**(4): 713-721.

Zhou, H., A. Kato, T. Miyaji, H. Yasuda, Y. Fujigaki, T. Yamamoto, K. Yonemura, S. Takebayashi, H. Mineta and A. Hishida (2006). "Urinary marker for oxidative stress in kidneys in cisplatin-induced acute renal failure in rats." Nephrol Dial Transplant **21**(3): 616-623.

Appendix I: List of license agreements for copyrighted materials

License agreement for chapter I figure 1.1

Lei Pei

From: Brown, Carol <brown@cshl.edu>
Sent: Tuesday, May 31, 2016 10:42 AM
To: Lei Pei
Cc: Mazzullo, Mala
Subject: RE: CSHL Press Reprint Permission Request Form

Hello Lei,

I have located the figure on p. 2 of the article. You have our permission to use it in your PhD thesis only. Please cite this article as Cold Spring Harb Perspect Biol 2009;1:a002584, with copyright to Cold Spring Harbor Laboratory Press.

Best wishes for success with your thesis.

Carol C. Brown
Books Development, Marketing and Sales
Cold Spring Harbor Laboratory Press
500 Sunnyside Blvd
Woodbury, New York 11797
516 422 4038 ph.
516 422 4095 fx.
brown@cshl.edu

-----Original Message-----
From: Lei Pei [mailto:lpei@kumc.edu]
Sent: Tuesday, May 31, 2016 11:36 AM
To: Brown, Carol
Subject: RE: CSHL Press Reprint Permission Request Form

Title of CSHLP Journal/Book:

Title of Article/Chapter:Physiology and Function of the Tight Junction

CSHL Authors/Editors:James M. Anderson and Christina M. Van Itallie

Page Numbers:

Figure Numbers:figure1

Figure Page Numbers:

Copyright Date:

I really don't know the page numbers, is there any way I can know the page numbers?

From: Brown, Carol [brown@cshl.edu]

1

License agreement for Chapter IV figure 4.1

License agreement for Chapter IV figure 1.2

Copyright Clearance Center RightsLink®

Home | Create Account | Help | Live Chat

Title: Biology of claudins
Author: Susanne Angelow,Robert Ahlstrom,Alan S. L. Yu
Publication: Am J Physiol-Renal Physiology
Publisher: The American Physiological Society
Date: Oct 1, 2008
Copyright © 2008, Copyright © 2008 the American Physiological Society

LOGIN
If you're a copyright.com user, you can login to RightsLink using your copyright.com credentials. Already a RightsLink user or want to learn more?

Welcome to RightsLink

American Physiological Society has partnered with Copyright Clearance Center's RightsLink service to offer a variety of options for reusing American Physiological Society content. Select the "I would like to ..." drop-down menu to view the many reuse options available to you.

I would like to... make a selection

Copyright © 2016 Copyright Clearance Center, Inc. All Rights Reserved. Privacy statement. Terms and Conditions.
Comments? We would like to hear from you. E-mail us at customercare@copyright.com

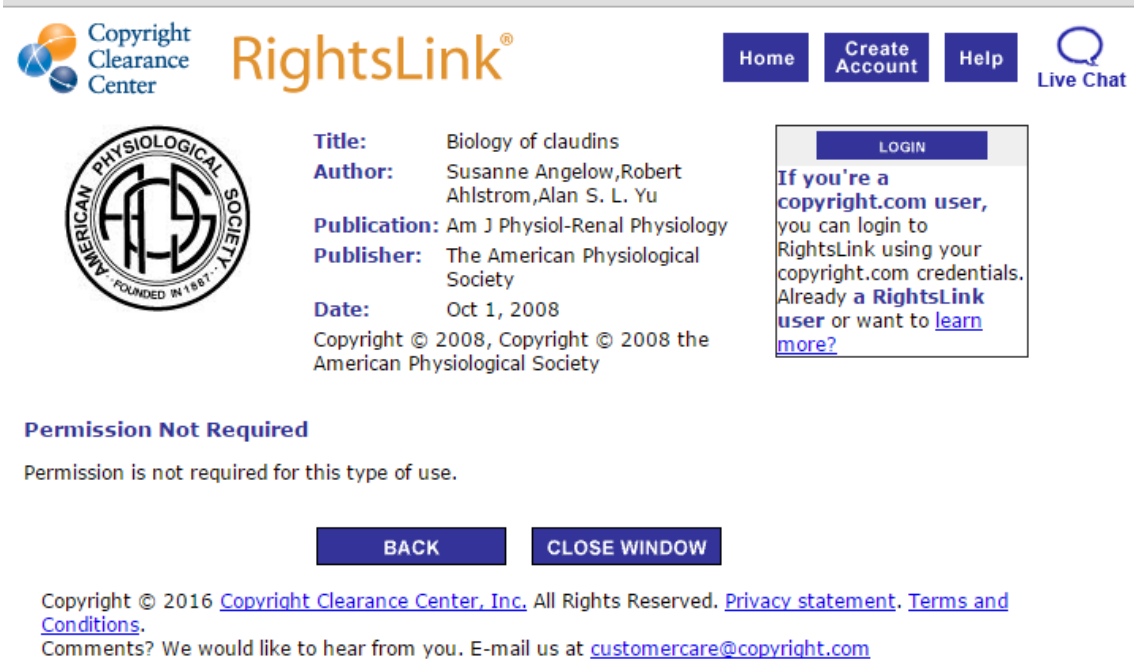

Copyright Clearance Center RightsLink®

Home | Create Account | Help | Live Chat

Title: Biology of claudins
Author: Susanne Angelow,Robert Ahlstrom,Alan S. L. Yu
Publication: Am J Physiol-Renal Physiology
Publisher: The American Physiological Society
Date: Oct 1, 2008
Copyright © 2008, Copyright © 2008 the American Physiological Society

LOGIN
If you're a copyright.com user, you can login to RightsLink using your copyright.com credentials. Already a RightsLink user or want to learn more?

Permission Not Required

Permission is not required for this type of use.

BACK | CLOSE WINDOW

Copyright © 2016 Copyright Clearance Center, Inc. All Rights Reserved. Privacy statement. Terms and Conditions.
Comments? We would like to hear from you. E-mail us at customercare@copyright.com